An investigation of the mechanics of tapered roller bearings

R. H. Leaver

U N I V E R S I T Y O F D U R H A M

AN INVESTIGATION OF THE MECHANICS OF TAPERED ROLLER BEARINGS.

Thesis submitted for the Degree of
Master of Science in the Faculty
of Engineering Science,

by

R. H. LEAVER. B.Sc. (Eng.)

March, 1969.

PLATE 1.

Abstract.

This investigation is concerned with the performance of tapered roller bearings under a pure thrust load.

The design and development of a suitable test rig is described in some detail and the results of friction torque and film thickness measurements are compared with values predicted using recent elasto-hydrodynamic theory.

It is shown that the reaction torque on the outer race may be ascribed to two principal sources. Firstly, to viscous rolling friction depending upon the product of speed and viscosity, and secondly to metallic hysteresis depending upon the load.

If the maldistribution of load due to small dimensional differences in the rollers, is taken into consideration close agreement is obtained between the experimental and theoretical values of friction torque for a wide range of loads and speeds. At higher loads a third source becomes significant due to sliding between the ends of rollers and the lip of the inner race.

A further important effect of the uneven loading of rollers is its influence on the life of a bearing. It is suggested that improved roller matching would result in an increase in bearing life.

Measurements of race and cage speeds, taken throughout the investigation failed to detect any cage slip.

Electrical resistance measurements made across the races confirm the presence of a lubricant film of a thickness which is consistent with theory. A visual display of the voltage drop indicated that the degree of asperity contact depended upon the surface finish and the thickness of the oil film.

An analysis of the dynamics of the tapered roller bearing showed that although the geometry leads to a gyroscopic couple acting on the rollers, its magnitude is small and of little practical importance.

Acknowledgements.

The work was carried out in the Engineering Laboratories of Constantine College and was generously sponsored by the Teesside Education Authority.

The author wishes to thank Professor G.R. Higginson, B.Sc., Ph.D., who supervised the work, for his advice, encouragement and time spent in valuable discussion.

Thanks are also due to Mr. G.B. Weatherley, C.G.L.I., Senior Technician in the Laboratories of Constantine College, for his painstaking work in the manufacture of the rig and assistance in the subsequent experimentation.

Contents

Notation.

ω	Roller speed, rad/s.
ω^1	Roller speed relative to cage, rad/s.
ω_c	Cage speed, rad/s.
Ω_i	Inner race speed, rad/s.
Ω_o	Outer race speed, rad/s.
Ω_x, Ω_y and Ω_z	Frame velocities about x, y and z axes, rad/s.
ω_y and ω_z	Body velocities about y and z axes, rad/s.
I_x, I_y and I_z	Moments of inertia of roller about x, y and z axes.
h_x h_y and h_z	Angular momentum about x, y and z axes.
M_x, M_y and M_z	External moments about x, y and z axes.
m	Mass of a roller.
α	Semi-apex angle of roller centre line.
β	Semi-apex angle of a roller.
R	Distance from apex to centre of gravity of roller.
F_c	Centrifugal force on a roller.
V	Reaction force at outer race due to inertia forces only.
F	Reaction force at lip due to inertia forces only.

P_i	Reaction force at inner race due to external load only.
P_o	Reaction force at outer race due to external load only.
P_L	Reaction force at lip due to external load only.
P_J	Journal load.
T	Thrust load.
V	$\frac{\text{Time average voltage}}{\text{applied voltage}}$
ν	Rate of contact interruption.
R_1 and R_2	Series and parallel resistors.
R_3	Resistance of contact.
R_e	Effective radius of solids in contact
R_{eo} and R_{ei}	Effective radii at outer and inner races respectively.
u	Entraining velocity.
H*	$= \frac{h}{R_e}$
h	Film thickness.
G	Materials parameter ($\propto E'$)
U	Speed parameter $\left(\frac{\eta_o u}{E' R_e}\right)$
W	Load parameter $\left(\frac{w}{R E'}\right)$

E'	$\frac{E}{1-\sigma^2}$ where E is Young's modulus and σ is Poisson's ratio.
η_o	Inlet viscosity at atmospheric pressure.
w	Load per unit length of roller.
	Length of roller contact.
N	Inner race speed, R.P.M.
τ	Viscous stress.
F_r	Viscous force per unit width of roller, due to rolling only.
T_v	Torque due to viscous rolling forces only.
F_s	Viscous force due to sliding only.
T_e	Torque due to elastic hysteresis only.
2b	Hertzian width.
v	Relative velocity of sliding.
K	Elastic constant $\frac{2}{\pi E'}$
δ	Deflection of roller and associated races.
T_i	Hysteresis torque for an individual roller.
L	Thrust on an individual roller.

CHAPTER 1.

1.1. Introduction.

This thesis is concerned with tapered roller bearings under a pure thrust load and investigates the friction torque and lubricant film over a practical range of loads and running speeds.

There exists a weight of experimental evidence in support of the more recent theoretical assessments of film thickness and pressure distribution in an elastohydrodynamic situation (1). In the main, this has been gained on disc machines; it would now seem timely to extend the work to relevant practical applications where the results may be of direct interest to the designer.

One obvious field for study, involving surfaces of low conformity, is that of rolling bearings. Garnell and Higginson (2) and Garnell (3), have reported experimental work with parallel roller bearings and were able to account for the measured friction torque using the theoretical solution of the elastohydrodynamic problem of Dowson and Higginson (4).

With parallel roller bearings the analysis is complicated because of the uneven loading of the rollers as they change their position relative to the radial load, and also by the effects of clearance. In the case of the tapered roller

bearing subjected to a thrust load only, both these effects are absent. However, new difficulties arise due to dimensional differences within the manufacturing tolerances. Small differences in the diameters of the rollers, compared at some chosen distance from the machined end, cause uneven loading. This, in turn, has a profound effect upon the friction torque.

The geometry of tapered roller bearings introduces a number of interesting dynamic effects which do not occur with parallel rollers. These have been explored in some detail by Frenkel (5), who was principally concerned with finding the optimum shape for a roller and with its motion under steady and accelerating conditions. In this thesis, the dynamic forces on a roller are analysed to determine if they are significant compared with the forces due to the externally applied loads.

Tapered roller bearings find a wide range of application involving both thrust and journal loads. For a given size, their capacity compares very favourably with any other type of bearing arrangement and hence, are of great practical interest.

CHAPTER 2. DESIGN AND DEVELOPMENT OF TEST-RIG.

2.1. Design of the Rig.

The basic design specification of the rig was that known thrust loads, of up to 2 tonf, could be imposed on the test bearing whilst running at speeds from as near zero as practicable up to 4000 r.p.m. and that the friction torque, the speeds of the inner race and cage, the electrical resistance across the bearing and the temperature at a number of points in both the inner and outer race could all be measured.

Two general arrangements were considered. The first used a single test bearing and required an oil bearing to support the load on the free race through which the friction torque must be measured. The design was rejected because of the complication involved. An alternative scheme using two test bearings running back-to-back, seemed to offer the most practical solution and was finally adopted. In this design the thrust could be applied to the rotating inner race of the front bearing whilst the outer races were left free and accessible for the measurement of the friction torque reaction. The scheme has the merit of testing two bearings at once, hence, half the measured torque is the mean from a sample of two nominally identical bearings; it does however, suffer from the disadvantage that the running

temperature of the races may differ in the two bearings. The choice of test-bearings dictated the capacity of the rig; these were selected from a popular commercial range which included two different race angles for a given inner bore diameter of 2.25 in. Also, the sizes and capacities were roughly comparable with those of the parallel roller bearings used by Garnell and Higginson (2), (3).

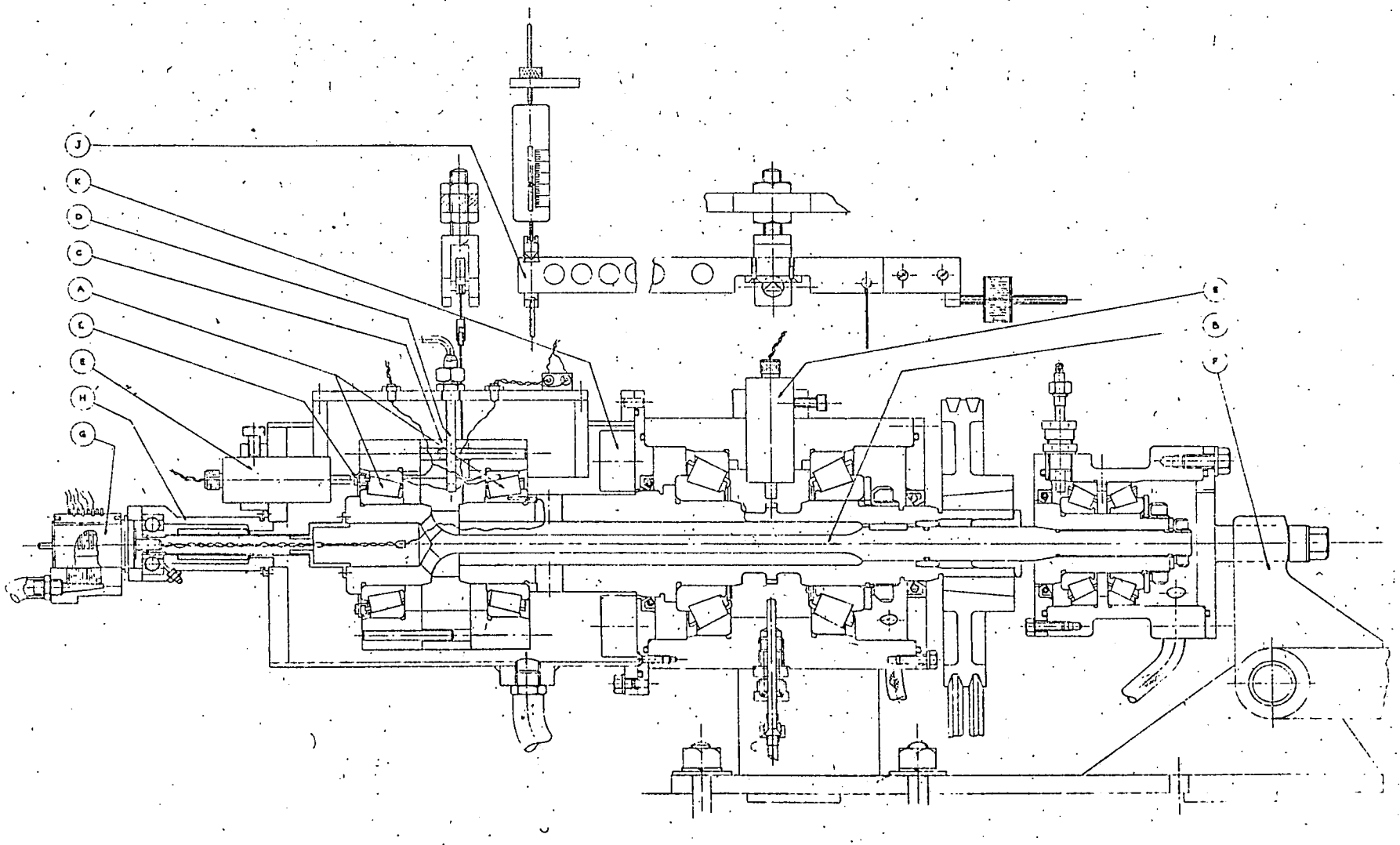

CROSS SECTION OF TEST RIG.

FIGURE 1.

A cross-section of the main body of the rig is shown in Figure 1, and a simplified diagrammatic section is shown in Figure 2. The thrust load was applied to the inner race of the front bearing by means of the slender shaft (B) running through the centre of the rig which was made as long and flexible as was considered safe; a pessimistic estimate of its whirling speed, assuming no inhibiting end moments or helpful effect from the tensile load, was well above the maximum running speed envisaged. The shaft was driven by a loosely fitting key and the diameter at the driving end was free to slide longitudinally in its bore. Lubricant could penetrate from the test-cell to the bore but no positive feed was provided. Some frettage occured at this point but was considered acceptable over the duration of test running.

The inner race of the rear bearing was pressed onto and located by its carrier, whilst the two outer races and the spacer were fully floating. The important feature of the design was that the flexibility of the drive shaft allowed the front inner race to take up a central position giving even loading to the rollers in both the front and rear bearings.

The two outer races were carried in thick steel housings

and were separated and electrically insulated from each other by a Tufnol spacer (C), suitably machined to allow the thermo-couples and electrical connections to pass from the outer races to the upper perspex cover of the test-cell. The friction torque reaction was measured by holding the outer race assembly by a light cable which passed through the cover to a simple balance arm (J). Care was taken to ensure that both the inner and outer races were backed by equal thickness of material. Although the thrust load was unlikely to cause any creep, the races were given interference fits in their housings. Whilst with parallel roller bearings the fit of the races and clearance are interdependent, with tapered roller bearings this is not so.

The test-cell was arranged so that the test bearings could be removed without disturbing the main rig bearing assembly.

A feature of the layout adopted was that one of each pair of bearings carried the full thrust load. The rig bearings were selected on the basis of a constant 2 tonf load for a life of 10^3 hours at a running speed of 2000 r.p.m. Steep angled bearings were used in the rear loading unit to minimise weight and overhang.

An adequate range of speeds could be covered by using a Kopp-variator coupled to a two-speed, three-phase, 5 h.p. electric

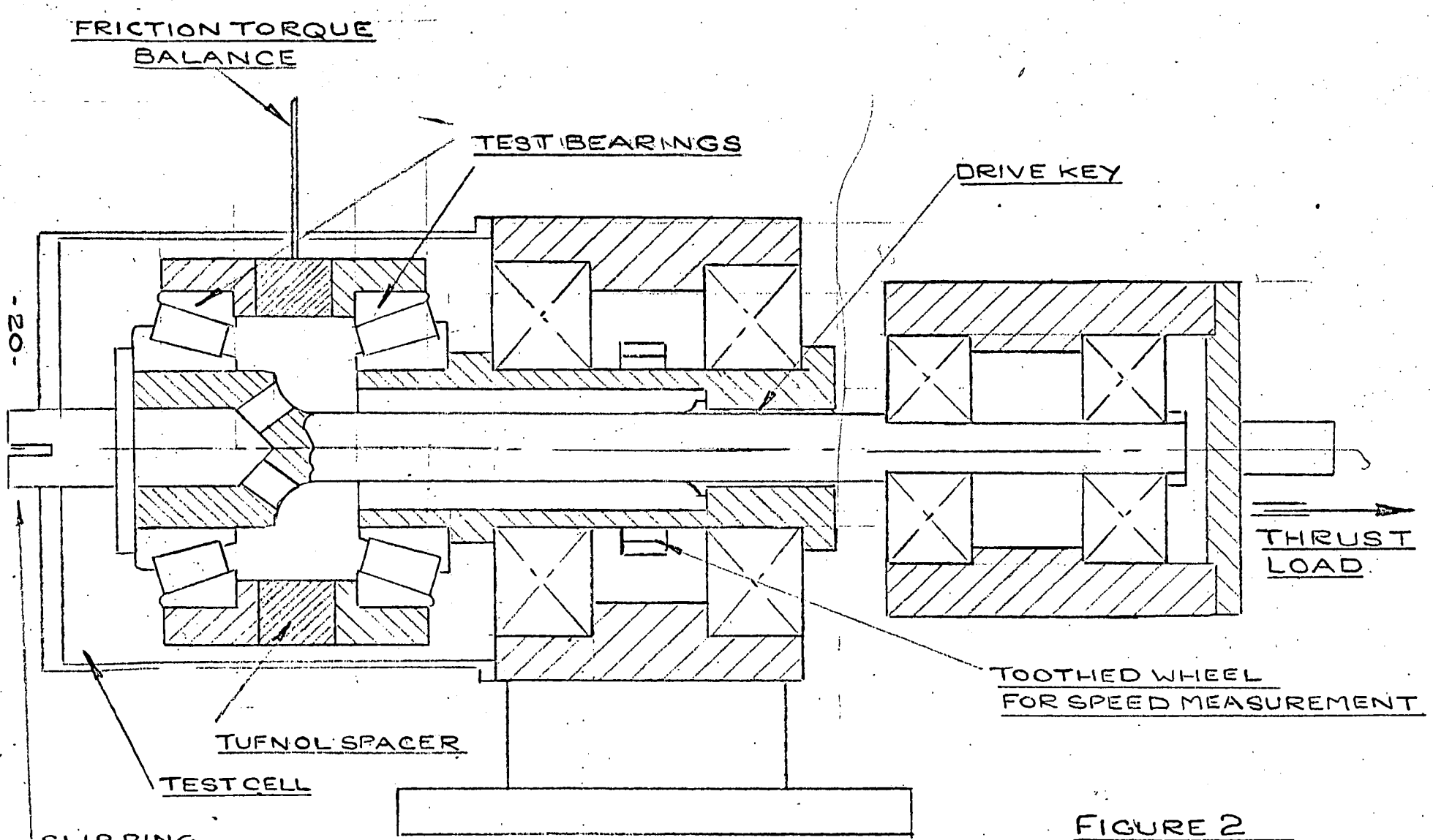

FIGURE 2

DIAGRAMMATIC SECTION OF TEST RIG

motor, together with a range of pulleys and vee-belts. A lay-shaft was found to be necessary to keep the belt lengths within reasonable bounds and to facilitate belt changes. The maximum motor speeds in the two ranges were nominally 750 and 1500 r.p.m., the variator gave ratios from 1/3 to 3, and the belt drive was arranged to give further ratios of $\frac{1}{2}$ and 1, so that rig speeds from 125 to 4500 r.p.m. were available. Fenner Taper-lock cones were used so that pulleys could easily be changed.

Jet lubrication was used for both the rig and test bearings. Two independent Tecalemit supply units, each having its own sump, gauge, filter, electric motor and pump, gave a maximum flow of approximately 200 cc/min at a maximum pressure of 180 p.s.i. The flow in each supply line could be controlled by an adjustable relief valve and was passed through a 25 micron pressure filter before being fed to the bearings. A Bourdon pressure gauge was mounted in the line to the test bearings so that the jet could be flow calibrated. Adequate oil drains were provided from both the rig and the test-cell, but in the case of the former the drains were arranged so that a pool of oil would be retained in the housings to be available immediately on starting. All stationary seals were made with 0.319 rubber O-rings and garter seals running on plunge ground diameters were used for rotating

parts; all seals could be assembled without damage over 15° tapers.

No provision was made for either oil cooling or for cooling the rig, it was decided to confine test running to a range of loads and speeds limited by an upper bearing temperature of approximately 100°C.

The thrust load was applied through a lever system using 50 lbf dead weights acting against an adjustable difference Salter spring scale. The weight of the beam was fully counterbalanced. Needle roller bearings on hardened steel pins were used at all pivot points and the mechanical advantage of the system was 32:1. The main bearing housing and the support for the bell-crank lever (F) were made as an integral unit so that the cast iron bed was unstressed by the loading forces. The upper limb of the bell-crank was machined to ensure that an axial load only was applied to the hardened steel bridge on the rear cover of the loading unit. The position of the bridge piece could be adjusted, by means of shims, to bring the main loading beam horizontal at no load.

The friction torque reaction was measured by means of weights on a steel arm (J). A light adjustable difference balance was used to cover intervals of 0.1 lbf. The balance

points of the steel arm were hardened and accurately ground and the centre pivot was arranged to be above the mass centre of the system as a whole. The arrangement proved satisfactory without additional damping.

Induction pick-ups (E) were used to measure the speed of the inner races and of the cage of the front bearing. A wheel with 24 teeth was machined integrally with the rear bearing inner race carrier and its pick-up was mounted in the main bearing housing.. The pick-up for the cage speed was mounted in the front face of the test-cell cover and a special toothed disc (L) was designed to clip on to the bearing cage.

Temperature measurements could be made using thermocouples embedded into the rear inner and two outer races. The leads from the outer race couples were brought directly up through the perspex cover, whilst those from the inner race were lead through the centre of the front bearing and out to a slip-ring unit (G) mounted on a turret (H) at the front of the test-cell.

The arrangements made for the measurement of the variables will be discussed in detail under the heading of Instrumentation.

2.2. Manufacture and development of the Rig.

In general the initial design proved to be satisfactory and little development work was required.

The most time consuming difficulty was encountered during the manufacturing stage. The design called for 0.021 in. diameter holes to be sunk into the bearing races for the thermocouples. These were to be produced on a Wickman Erodomatic machine. Several types of electrode material were tried, some solid and some tubular; different flushing arrangements were developed and although techniques improved, consistent results were never achieved. No difficulties were experienced down to depths of about 0.2 in, but beyond this it was extremely difficult to prevent arcing round the sides of the wire and impossible to rely on a constant rate of electrode wear. Satisfactory holes were eventually produced, the best results being obtained with plain brass wire well supported in a fixture just above the top of the holes, but the process was tedious and called for much skill and patience on the part of the machine operator.

During preliminary running, difficulty was experienced in counting the small notches cut into the cage of the outer bearing. The pick-up could not differentiate between the notches, the

bearing extraction grooves on the end of the shaft and the bearing rollers. The problem was solved by covering the extraction slots with a complete steel ring and designing a disc with 36 radial slots machined on to its surface, to clip over the cage. Care was taken to ensure that it was clear of both races and the rollers.

The neck of the bell-crank lever in the loading system was highly stressed in bending and the original design yielded under a load of 3500 lbf. A modification increasing the depth of the section proved effective and loads of up to 3 tonf were carried without further embarrassment.

The principal difficulties arose in measuring the temperature of the inner race through slip-rings. The subject will be fully discussed in the section on instrumentation. Initially, the slip-ring unit was mounted directly on the front face of the test-cell; after the first series of runs a turret was designed to remove the unit away from the heat of the test-cell and in addition the wiring and assembly arrangements were improved. The slip-ring unit itself was modified to take thermocouple wire right up to the contacts, thus eliminating the short lengths of copper wire originally used. The thermocouples proved to be very fragile and several

modifications to the clipping arrangements were made to relieve the potted ends of the cables from accidental strain.

Attempts were made to control the oil flow to each test bearing so as to keep the two outer races at the same temperature, this proved difficult. Between the runs with the Standard and the Steep-angled bearings, a fibre board 1 in. thick was fixed to the front of the rig bearing housing to reduce the radiation to the rear outer race of the test bearing which generally ran hotter than the front outer.

CHAPTER 3. RIGID MECHANICS OF TAPERED ROLLER BEARINGS.

3.1 Kinematics

Figure 4 shows a cross-section of a tapered roller bearing. R is the distance from the apex O to the centre of gravity of a roller G, β is the semi-apex angle of a roller and α the semi-apex angle of the roller centre line.

If the outer race is fixed and no slip occurs, the line OB is an instantaneous axis of velocity. The linear velocity of point G in a roller, measured with respect to the line OB, is given by:-

$$\omega R \tan \beta$$

The linear velocity of a coincident point G on the cage, measured with respect to the centre line of the bearing, is:-

$$\omega_c R \sin \alpha$$

Equating,

$$\omega_c = \omega \frac{\tan \beta}{\sin \alpha} \qquad 3.1$$

Similarly, the linear velocity of point A on a roller, measured with respect to the axis OB is given by:-

$$2 \omega R \tan \beta$$

and the linear velocity of a coincident point A on the inner

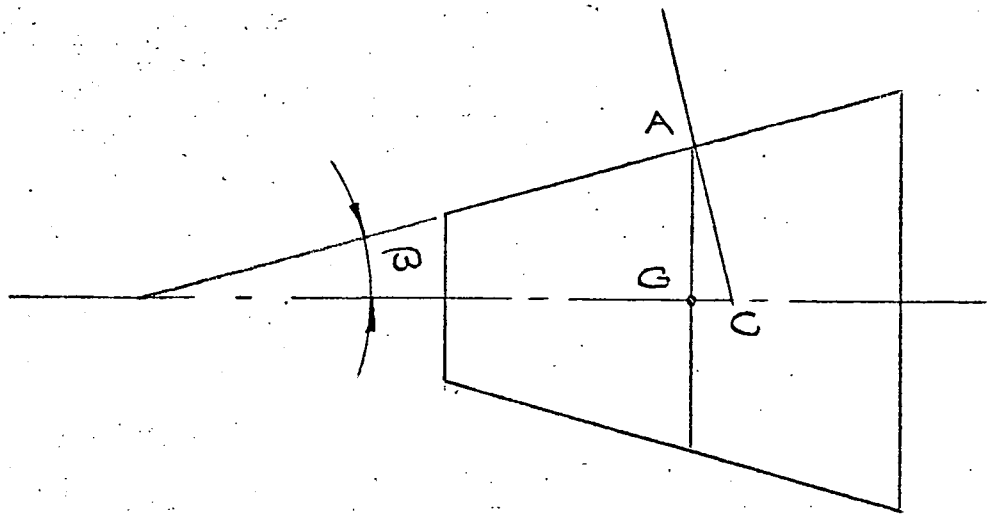

FIGURE 3

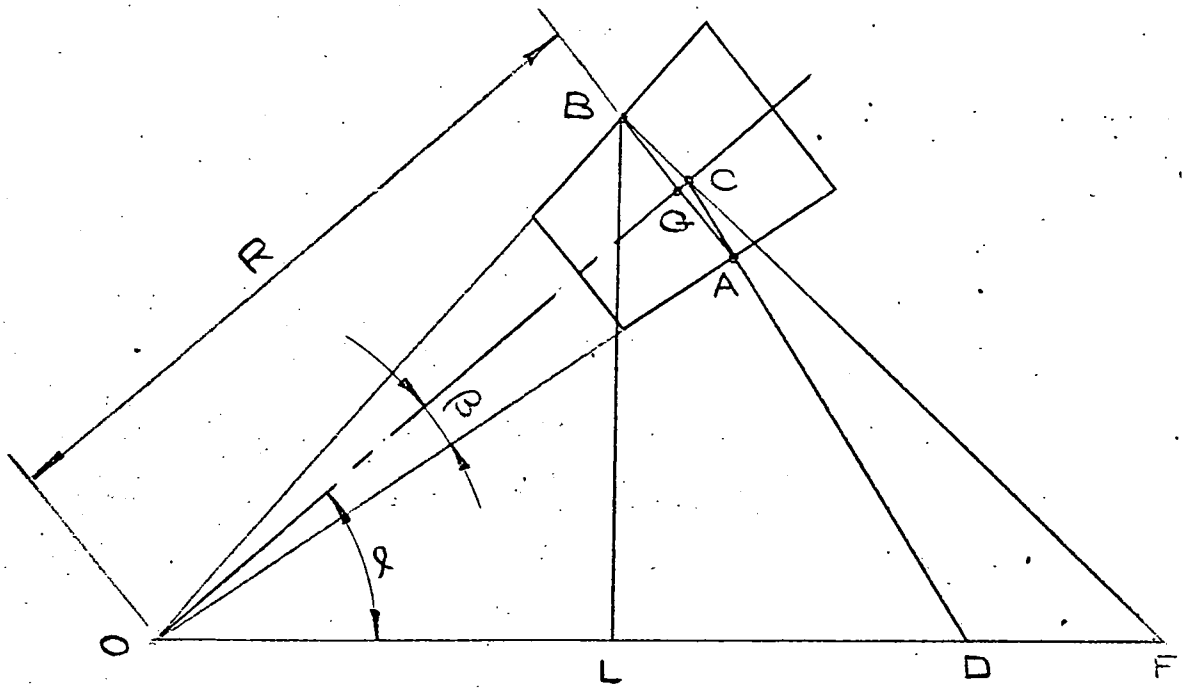

FIGURE 4

race, measured with respect to the centre line of the bearing, is :-

$$\Omega_i \quad OA \sin (\alpha - \beta)$$

Equating and noting that,

$$OA = OB = \frac{R}{\cos \beta}$$

$$2 \omega R \tan \beta = \Omega_i \frac{R}{\cos \beta} \sin (\alpha - \beta) \qquad 3.2$$

Substituting from 3.1 in 3.2 gives :-

$$\omega_c = \frac{\Omega_i}{2} \left(1 - \frac{\tan \beta}{\tan \alpha}\right) \qquad 3.3$$

If the inner race is fixed and the outer race rotates without slip, the line OA becomes an instantaneous axis of velocity. The linear velocity of point G on the roller and cage, measured with respect to the axes OA and the centre line of the bearing respectively, may be equated giving :-

$$2\omega R \tan \beta = \Omega_o \frac{R}{\cos \beta} \sin (\alpha + \beta) \qquad 3.4$$

Substituting from 3.1 in 3.4 we get :-

$$\omega_c = \frac{\Omega_o}{2} \left(1 + \frac{\tan \beta}{\tan \alpha}\right) \qquad 3.5$$

If both the inner and outer races rotate independantly and in the same sense, the general expression for cage velocity is given by the superposition of 3.3 and 3.5.

$$\omega_c = \frac{\Omega_o}{2}\left(1 + \frac{\tan\beta}{\tan\alpha}\right) + \frac{\Omega_i}{2}\left(1 \mp \frac{\tan\beta}{\tan\alpha}\right) \qquad 3.6$$

An expression for ω, the angular velocity of a roller in terms of Ω_o and Ω_i may be obtained directly by substituting 3.6 into 3.1 and taking due account of signs :-

$$\omega = \frac{\Omega_o}{2}\left(\frac{\sin\alpha}{\tan\beta} + \cos\alpha\right) - \frac{\Omega_i}{2}\left(\frac{\sin\alpha}{\tan\beta} - \cos\alpha\right)$$

It is interesting to note that if the bearing rotates as a solid body, i.e. $\Omega_i = \Omega_o = \Omega$ the roller has an angular velocity about its own axis equal to the component of Ω resolved along its axis.

In the rig used in this research, the outer race was fixed, hence the epicyclic velocity of the cage was given by equation 3.3.

If slip occurs then :-

$$\text{cage slip \%} = \left\{1 - \frac{2\,\omega_c}{\Omega_i\left(1 - \frac{\tan\beta}{\tan\alpha}\right)}\right\} \times 100$$

where ω_c is the measured cage velocity.

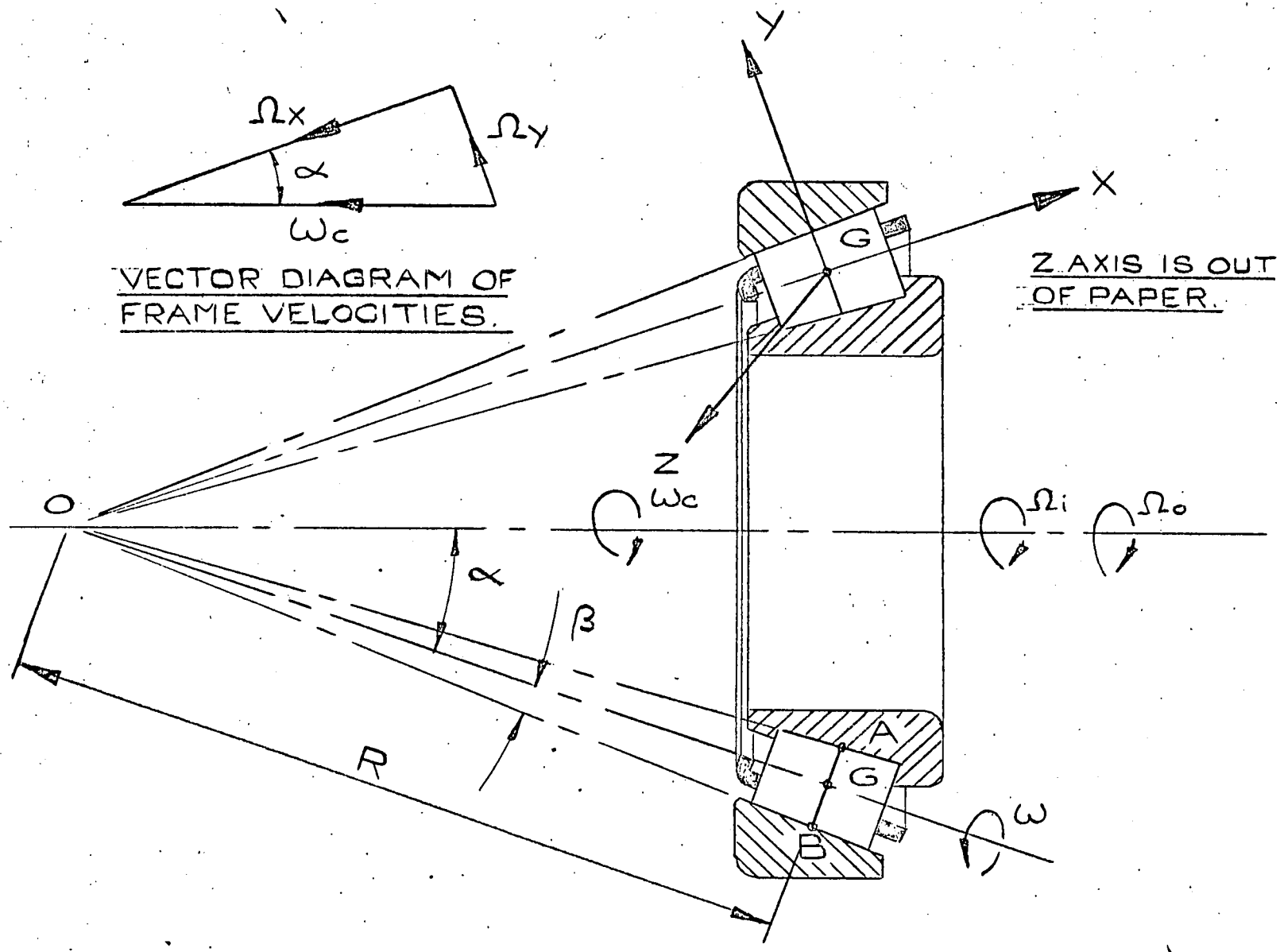
Ωx
Ωy
α
ωc
VECTOR DIAGRAM OF FRAME VELOCITIES.
Y
X
Z
G
Z AXIS IS OUT OF PAPER.
O
ωc
Ωi
Ωo
α
β
R
A
G
B
ω

FIGURE 5

3.2. Body moments and forces.

The right handed set of axes shown in Figure 5 have their origin at G, the centre of gravity of a roller, and are fixed to the cage and move with it. The angular velocities of the frame are Ω_x, Ω_y and Ω_z, taken positive according to the right hand screw rule. If ω, the angular velocity of a roller, is arbitrarily taken as positive; then,

$$\Omega_x = -\omega_c \cos \alpha$$

$$\Omega_y = +\omega_c \sin \alpha$$

$$\Omega_z = 0$$

The body velocities of a roller, ω, ω_y and ω_z are,

$$\omega = (\omega^1 - \omega_c \cos \alpha)$$

$$\omega_y = +\omega_c \sin \alpha$$

$$\omega_z = 0$$

where ω is the velocity of spin of a roller and ω^1 is its velocity relative to the cage.

The axes X, Y and Z are Principal Axes and if I_x, I_y and I_z are the moments of inertia of a roller about these axes respectively, the angular momentum about each axis, h_x, h_y and h_z is given simply by,

$$h_x = I_x \omega$$

$$h_y = I_y \omega_c \sin \alpha$$

$$h_z = 0$$

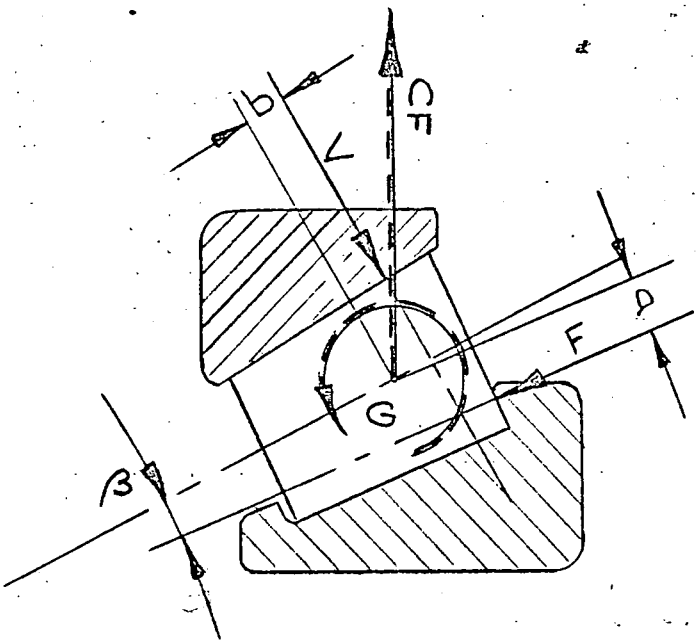

BODY FORCES SHOWN IN BROKEN LINE. REACTIONS DUE TO BODY FORCES ONLY SHOWN IN FULL.

FIGURE 6

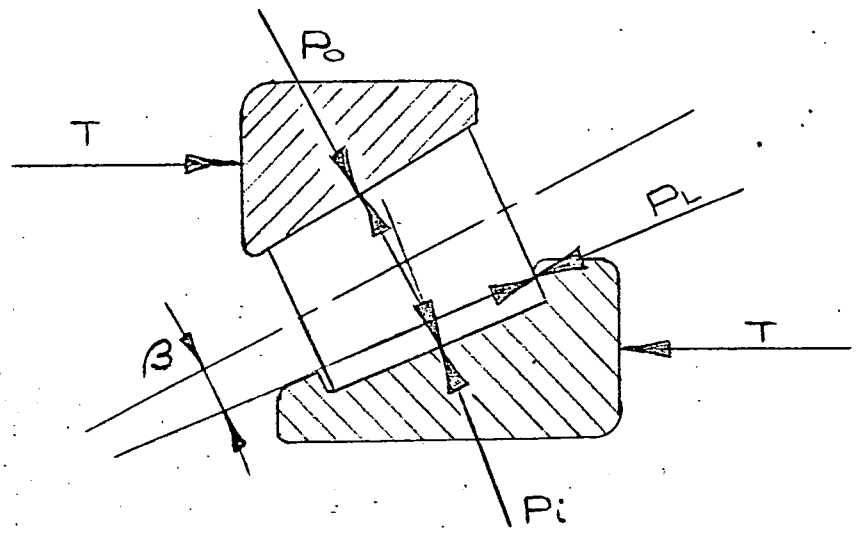

REACTIONS DUE TO EXTERNAL LOAD ONLY.

FIGURE 7

The externally applied moments M_x, M_y and M_z may be equated to the rate of change of angular momentum about each of the axes.

For a rigid bearing running in the steady state,

$$\frac{dh_x}{dt} = \frac{dh_y}{dt} = \frac{dh_z}{dt} = 0$$

and as $\omega_z = \Omega_z = 0$.

$$M_x = M_y = 0$$

The remaining equation is,

$$M_z = -h_x \Omega_y + h_y \Omega_x$$

or

$$M_z = -I_x \omega \omega_c \sin \alpha - I_y \omega_c^2 \sin \alpha \cos \alpha \quad 3.7$$

Substituting in 3.7 for ω and ω_c from 3.1 and 3.3 gives,

$$M_z = -\frac{\Omega_i^2}{4} \left(1 - \frac{\tan \beta}{\tan \alpha}\right)^2 \sin \alpha \left(I_x \sin \alpha \cot \beta + I_y \cos \alpha\right)$$

Note, the external moment required about the Z axis is independent of R.

In addition to the gyroscopic moment about the centre of gravity, a centrifugal force F_c will act through G and will be equal to,

$$F_c = m \omega_c^2 R \sin \alpha \quad 3.8$$

where m is the mass of a roller.

3.3. Reaction forces.

The reactive forces on a roller must be in equilibrium with the body forces. Figure 6, shows the centrifugal force and the gyroscopic moment in dotted lines and the reactions V and F acting at the outer race and the lip of the bearing respectively. a is the perpendicular distance from G to the line of action of F and b the perpendicular distance from G to the line of action of V.

Equating the components of the forces perpendicular to the surface of the inner race to zero gives,

$$F \cos(\alpha - \beta) - V \cos 2\beta = 0 \qquad 3.9$$

Similarly, equating the components parallel to the surface of the inner race to zero,

$$F \sin(\alpha - \beta) + V \sin 2\beta - F = 0 \qquad 3.10$$

and finally equating the moments about G to zero,

$$M_z - Fa - Vb = 0 \qquad 3.11$$

from 3.8 and 3.9

$$V = m\omega_c^2 \frac{R \sin\alpha \cos(\alpha - \beta)}{\cos 2\beta}$$

and from 3.8 and 3.10

$$F = m\omega_c^2 R \sin\alpha \,(\sin(\alpha - \beta) + \cos(\alpha - \beta) \tan 2\beta)$$

The distance b is fixed by the design of the bearing; the distance a may be found from equation 3.10.

3.4. External forces.

The reactions at the contact surfaces, due to an external thrust load may be found by considering the equilibrium of the inner and outer races and of a roller. If P_i, P_o and P_L are the reactions at the inner and outer races and at the lip respectively, as shown in Figure 7; then,

$$P_i = \frac{T \cos 2\beta}{n \sin(\alpha+\beta)} \qquad 3.12$$

$$P_o = \frac{T}{n \sin(\alpha+\beta)} \qquad 3.13$$

$$P_L = \frac{T \sin 2\beta}{n \sin(\alpha+\beta)} \qquad 3.14$$

where n is the number of rollers in the bearing. The total reaction forces on a roller will be given by the superposition of the forces due to the thrust load and those due to the inertia loads.

If a journal load P_J is carried by a tapered roller bearing a thrust load is induced which must be resisted by a second bearing. The magnitude of the thrust load is given by,

$$P_J \tan(\alpha+\beta)$$

3.5. Inertia forces and moments for test bearings.

The inertia forces and moments for the rollers of the test bearings have been calculated for an arbitrary inner race speed of 10,000 r/m. This, of course, is higher than normally used or recommended by the manufacturer.

The inertia moment M_z, the centrifugal force F_c and the reaction forces at the outer race V and at the lip F, are listed for each of the two bearings.

	Standard bearing	Steep angled bearing
M_z	1.13 lbf in	3.86 lbf in
F_c	36.6 lbf	51.3 lbf
V	32.9 lbf	49.6 lbf
F	7.70 lbf	19.9 lbf

It is evident that the gyroscopic effect is negligible, even in the case of the steep angled bearing.

The centrifugal force for both bearings is significant. Its magnitude may best be gauged by thinking in terms of an equivalent external thrust load required on the bearing to produce on all rollers a load equal to that due to centrifugal force. Such equivalent loads would be 128 lbf and 308 lbf in the case of the standard and the steep angled bearing respectively. These loads are small compared with the thrust capacity of the bearings.

The lip forces, due to inertia effects only, represent a considerable increase over those due to external loads, mainly because the lip takes so little of the external load. For example, it would require external thrust loads of 532 lbf and 1093 lbf on the standard and the steep angled bearing respectively, to produce the lip loads due to inertia effects at 10,000 r/m.

The off-set of the reaction at the outer race due to inertia effects, i.e. the value of b, is small, being 0.023 in. in the case of the standard bearing and 0.058 in for the steep angled bearing.

Manufacturers are usually reluctant to quote general figures for maximum speeds for tapered roller bearings. There appears to be little reason, judging by the above calculations why bearings with modest taper should not be satisfactory at speeds similar to those allowed for parallel roller bearings of comparable size. It is clear that the lip loading may be a limiting factor; however, as will be seen later, a film of lubricant is usually present at the lip under most running conditions.

Smith (6) has referred to the difficulty of preventing slip, particularly under accelerating and decelerating conditions in lightly loaded, intershaft roller bearings used

in multi-rotor aircraft propulsion engines. In such applications speeds of 15,000 r/m are not uncommon; both races generally rotate in the same sense and roller pitch diameters may be 8 in or more. The problem grows more difficult as engines become larger, more sophisticated and the diameters of the bearings required increases.

It is interesting to speculate on the possibility of using thoughtfully designed preloaded tapered roller bearings for this type of duty. The preload might be provided by means of a suitable spring, allowing lateral movement for expansion in a controlled manner. It is obvious that a redesign of the soft steel type of cage would be necessary, but should not prove difficult.

CHAPTER 4. INSTRUMENTATION.

4.1. Temperature measurement.

Both film thickness and friction torque are very dependent upon the viscosity of the lubricant in the contact zone. It is clearly of the utmost importance that an accurate assessment of film temperature be made so that the viscosity at the inlet to the contact may be estimated. Archard and Kirk (7) have shown that the temperature of the oil film in circumstances similar to those in rolling bearings is effectively that of the surfaces in contact; hence, the problem becomes one of finding the surface temperature of the races.

Thermocouples were embedded in spark eroded holes in the races with their ends generally at perpendicular depths of 0.05, 0.10 and 0.15 in under the centre of the roller track, as shown in Figure 8. The surface temperature of the race was found by extrapolating the readings from the three thermocouples. The temperature gradient across the thermocouples varied but was in the range 1° - 2° C at the higher speeds and loads.

Pyrotenex nickel-chromium/nickel-aluminium couples in 0.021 in diameter insulated sheaths were used with a Honeywell printing recorder and an external ice cold-junction. The recorder was essentially a servo-balanced bridge milli-voltmeter, arranged

to give a full-scale deflection of 10 in for an input of 5 mv. As the sensitivity of the couples was about 4 mv/100°C, temperatures of up to 125°C could be recorded.

The outer race couples were connected directly to the recorder and presented no problem; those from the rear inner race were passed through slip-rings to the recorder and a considerable amount of development work was required before satisfactory readings were obtained. The slip-ring unit was basically an I.D.M. design using silver rings and silver-graphite brushes on beryllium-copper cantilever springs. The springs were by-passed by short silver wires running directly from the brushes to the terminals. The rotating connections to the rings were of Ni/Cr and Ni/Al as appropriate. In the final arrangement the unit was mounted on a thermally insulated turret in an attempt to isolate it from the heat of the test-cell. After the first series of tests air cooling was introduced, a jet of air being directed at each brush contact to reduce the thermal contact voltage to a minimum. The thermal emf, assumed to be the difference between the reading with and without air cooling, varied with speed but not according to any simple law. At 100 rpm it was negligible, rising to 0.5 mv at 1300 rpm leading to a temperature error of 12°C.

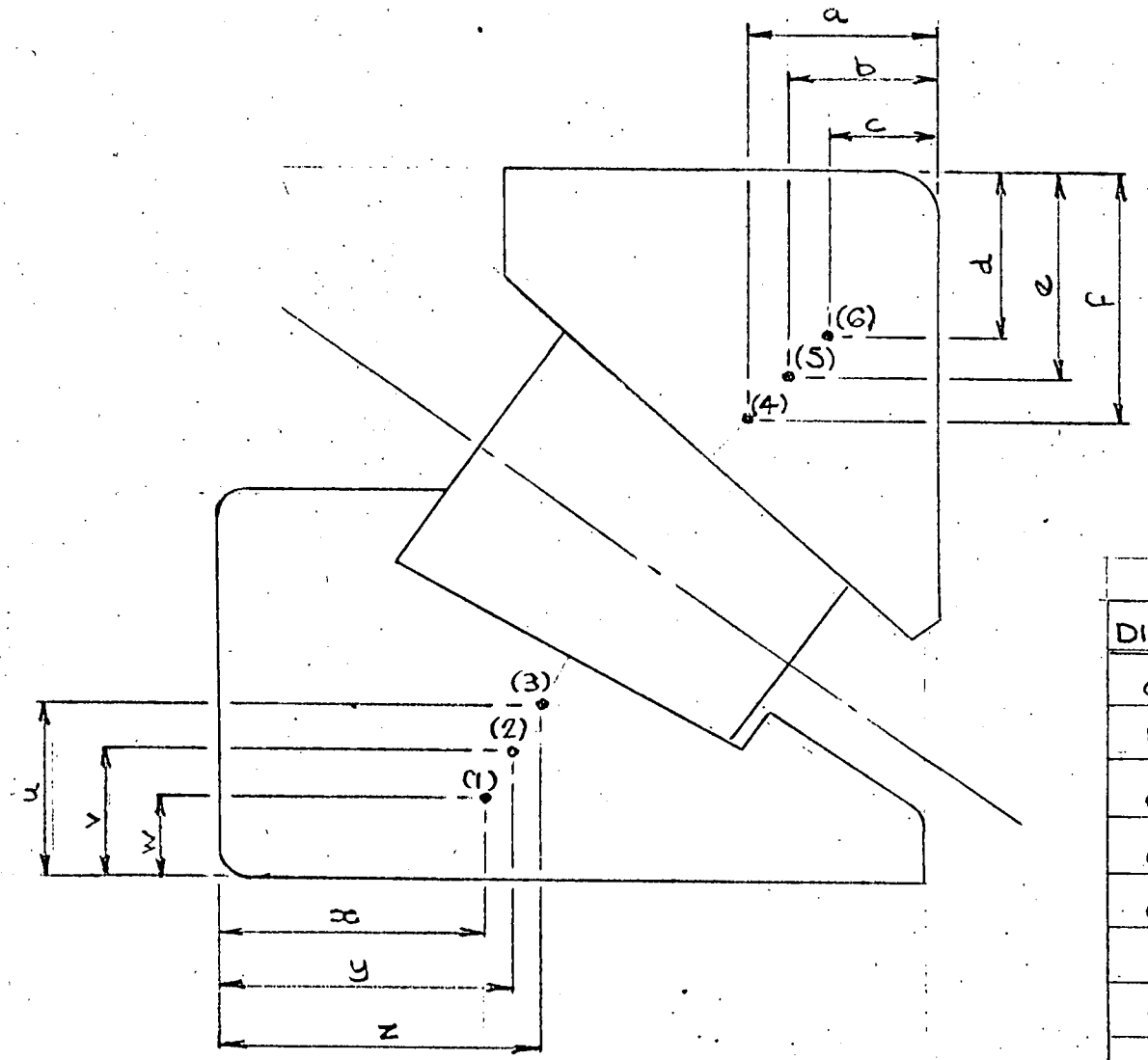

	BEARING.	
DIM'N	STANDARD	STEEP ANGLE.
a	0·463"	0·3807"
b	0·452"	0·3614"
c	0·441"	0·3422"
d	0·095"	0·2459"
e	0·1435"	0·292"
f	0·1925"	0·3382"
u	0·1453"	0·2896"
v	0·096"	0·2416"
w	0·0467"	0·1936"
x	0·601"	0·4582"
y	0·609"	0·4721"
z	0·617"	0·4861"

DETAILS OF THERMOCOUPLE POSITIONS

FIGURE 8

The temperatures of the two outer races were not necessarily equal. In the tests with the Standard bearing, the difference though small at low loads and speeds, increased to almost 10°C at 4000 rpm but was generally 2° - 5°C at 2000 rpm. A heat shield on the rear wall of the test-cell, introduced before commencing tests with Steep angled bearings, proved to be most effective and reduced the difference to rather less than 2% at the highest temperature recorded. The inner race of the rear test bearing and presumably also of the front bearing, invariably run cooler than the outer races.

The test programme covered the commercial range of loads and speeds for the bearings, up to an arbitarily selected upper temperature limit of 100°C measured in the test bearings. No cooling was provided and the rig bearings ran at roughly the same temperature as the test bearings.

According to the manufacturer, the recorder was accurate to .04% at its calibration temperature 85°F. The smallest division on the chart was 0.025 mv but discrimination was about half this, 0.01 mv or 0.25°C. The thermocouples were checked at one point only and found to agree with the makers calibration, giving 4.1 mv/100°C. It seems reasonable to assume that the surface temperatures of the outer races were correct to within

$\pm$ 1°C. Those of the inner race were probably less reliable because of the slip-rings but on the other hand were less important and were not used in the subsequent analysis.

4.2. Speed measurement.

It was decided to measure the rotational speed of the inner race and cage as accurately as practicable so that any departure from true epicyclic motion could be detected.

An inductive probe, mounted on the main body of the rig, was used to count the teeth on a 24 toothed wheel machined integrally with the rear inner race carrier. A second probe, mounted on the front face of the test-cell, was used to count the teeth on a specially designed 36 toothed ring which clipped onto the cage of the front bearing. Each of the Airmec N392 probes contained a small transistorised amplifier powered by an external 5 volt stabilised D.C. supply. The amplified output pulses were fed to Advance SCI, five decade counters. The two counters and an accurate electrical chronometer were started and stopped simultaneously by a single switch. The chronometer scale was divided into 0.01 s intervals and counts were usually made over 3 minute periods. The time measurements were used to calculate the speed of the inner races and the two counter readings to calculate the cage slip. Very small amounts of mean slip would be detectable.

The true epicyclic speed of the cage was calculated from the measured bearing dimensions and checked by running at low

speed under moderate load, where slip would not be expected to occur.

The accuracy of the count was $\pm$ 1, so that in 3 minutes the error could only be $\pm$ 1 in 7200 for the inner race, even at a low speed of 100 rpm. The chronometer was as accurate as the mains frequency, so that the overall accuracy of the speed figures was limited only by the numerical division, which in all cases was performed on a desk top calculating machine to seven significant figures.

In order to get a spot check on the accuracy of the speed and slip measurements a sample of eleven sets of readings were taken at a nominal speed of 1550 r/m with all the external variables held constant. Conditions were allowed to settle over a long period. A statistical analysis of the results gave a mean speed of 1588 r/m $\pm$ 0.2050 rpm to 95% confidence limits. A similar analysis on the slip figures gave 0.41878 $\pm$ 3.3124×10^{-4}, again to 95% confidence limits. This compares with the calculated epicyclic ratio of 0.419 and represents zero slip.

4.3. Friction torque measurement.

The friction torque on the two outer races was balanced by means of a steel-arm using weights in increments of 0.1 lbf against a sensitive and adjustable difference spring balance calibrated in 0.01 lbf intervals. The lever ratio of the arm was 5:1, hence, the friction torque for the two bearings was given by 12.5 W lbf.in where W was the total load on the arm. The pivot points on the arm were hardened and accurately ground and the arm carefully balanced. Damping was not provided nor found necessary. The arm was always adjusted to the horizontal position before a reading was taken. A discrimination of rather better than $\pm$ 0.1 lbf.in was achieved for steady readings.

4.4. Load measurement.

The load was applied by hanging 50 lbf weights on to the loading beam. An upward force, acting against the dead load, could be applied to the end of the beam through a spring balance by adjusting the threaded hanger by means of a handwheel. The balance had a full scale of 100 lbf which was divided into 0.5 lbf intervals. All the pivots of the level system, which had a mechanical advantage of 32, were hardened steel pins in greased needle roller bearings. The whole system was carefully balanced before running. The tension shaft running through the centre of the rig and forming the carrier for the inner race of the front bearing, was a free sliding fit in its bore as was the driving key in its keyway. Under steady running conditions the friction forces were minimal. Although, as theory shows, there was no necessity for very accurate measurement of the load, in fact it could easily be controlled to better than 0.5 lbf at the loading end of the beam even at the highest loads, that is to 16 lbf at the bearing at loads of up to 3 tons.

4.5. Oil film measurements.

The problem of measuring film thickness has received considerable attention in recent years and many ingenious and successful experimental techniques have been developed. These are described in detail elsewhere (1) (8). Most of the methods, whilst satisfactory for use with disc and ball machines, are not directly applicable to rolling bearings.

In the present work, a low voltage resistance method, similar to that first used by Furey (9) and subsequently by Tallian et al (10) and others, was employed to assess the degree of contact taking place between the rollers and races. No attempt was made to relate a calculated contact resistance to mean film thickness; to have done so would have required a knowledge of the resistivity of the lubricant under the unusual physical conditions obtaining in the contact zone, together with an assumption of film shape. It may be noted, in passing, that a capacitance method was also considered, but again the shape of the film and the dielectric properties of the lubricant would have been required for the film thickness to be calculated.

Measurements were made of the voltage drop across each of the test bearings using the arrangement shown in Figure 9.

The circuit consisted of a low voltage, low impedence D.C. source, a series resistor R_1 of 200KΩ, and in parallel with the bearing, a resistor R_2 of 1KΩ, an oscilloscope and a milli-voltmeter.

The outer races of the two bearings were insulated by a Tufnol spacer, so that the voltage drop across each bearing could be measured independently. The electrical connections to the races were made by insulated wires secured in spark eroded holes. Those from the inner races passed to the slip-ring unit.

The oscilloscope had a differential amplifier input which reduced extraneous noise whilst achieving a suitable gain of 10 mv/cm with a 400 Kc cut-off and an input impedence of 1MΩ. Rapid changes of voltage could be recorded on film with a Polaroid oscilloscope camera. Typical photographs are shown in Figure 12, and will be discussed in detail later.

The milli-voltmeter had a mechanical pointer, hence its time constant was large. Readings were assumed to represent the time average voltage across the contact. The instrument had a full scale range of 10mv with an input impedance of 1MΩ.

When the bearing ran under conditions resulting in near metal-to-metal contact, the resistance and voltage drop across

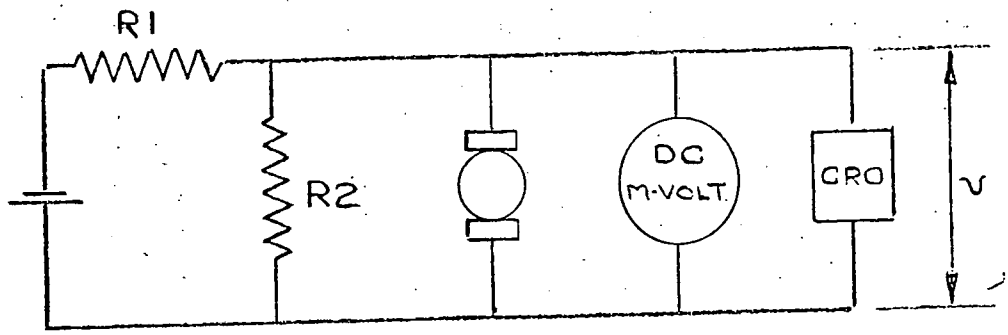

FIGURE 9

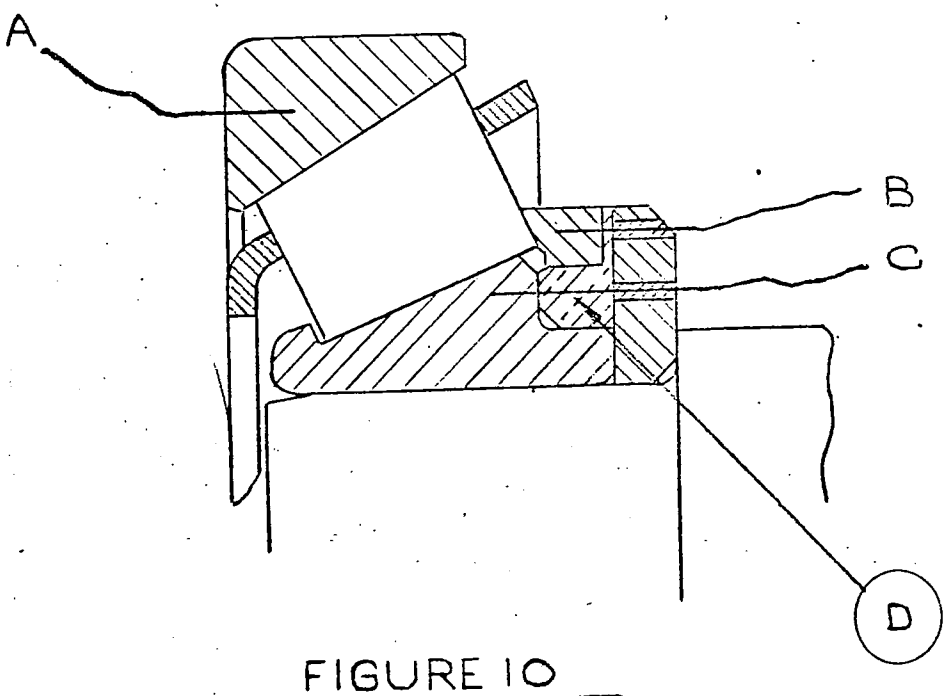

FIGURE 10

the bearing approached zero and the current passing was limited by the series resistor R_1, to 10μ amps. This minimised the risk of a discharge occurring and being sustained across the thin film. When the bearing ran under full elastohydrodynamic conditions, the circuit was open and the recorded voltage 10mv. At intermediate conditions, the reading on the milli-voltmeter represented the time-average voltage where some contact of asperities occurred followed by periods of no contact.

The circuit was essentially an "on - off" device and Figure 11a shows an over simplified representation of the voltage changes which occurred as contact between asperities were made and broken. Using this interpretation, it is clear that the time average recorded voltage is directly proportional to the "no-contact" time. However, the contact and circuit was not purely resistive but included some capacitance which when contact was broken, had to be charged through the series resistor R_1. A more appropriate model would seem to be that illustrated in Figure 11b. Here the assumptions are similar to those made by Chiu (11) and later by Tallian et al (12). Firstly, the pulses are vertical at contact followed by an exponential rise according to the law of an R.C. circuit, and secondly, the electrical contact resistance between asperities is small

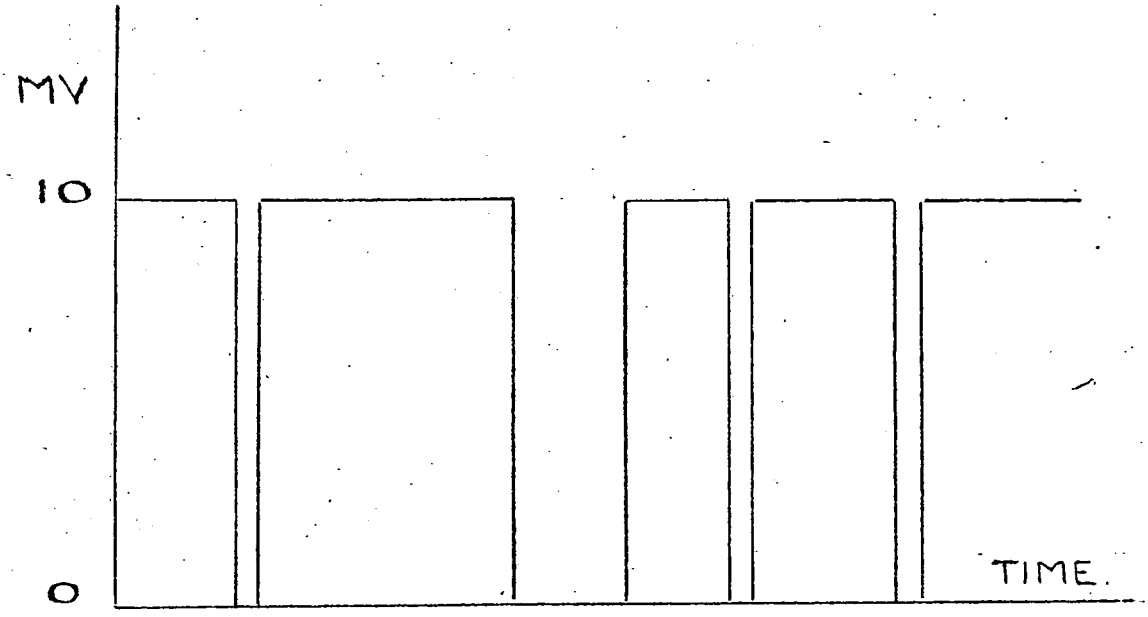

FIGURE 11a

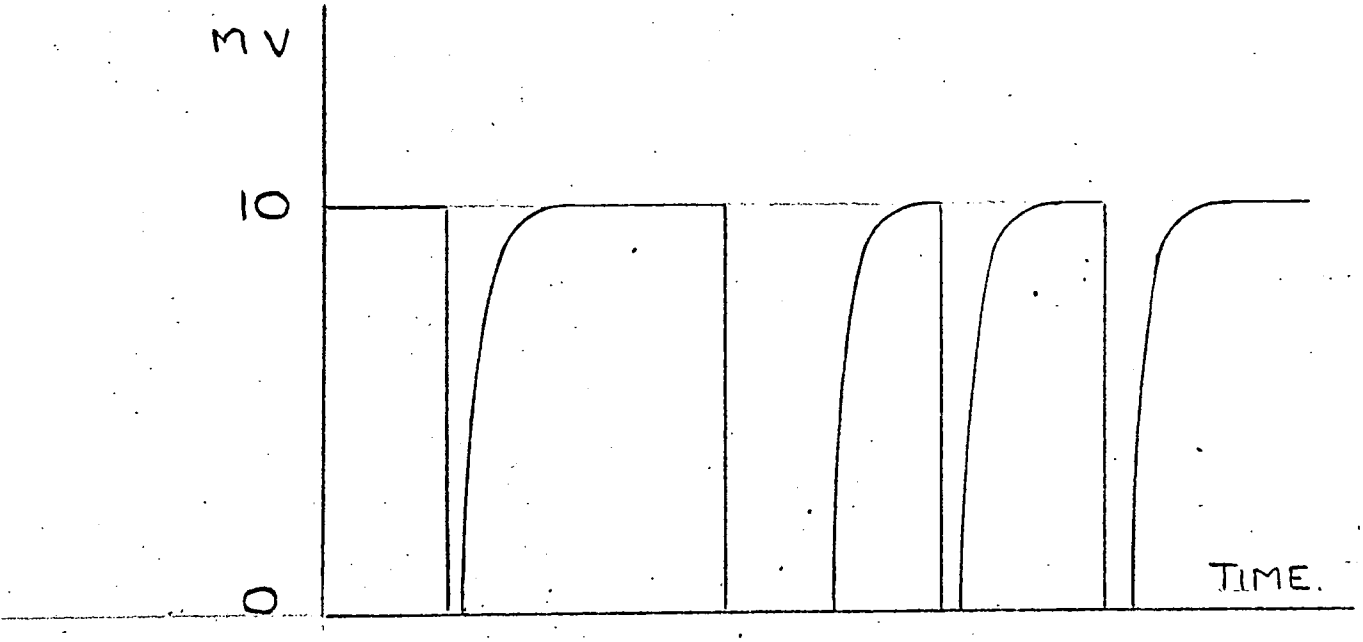

FIGURE 11b

compared with the series resistor. The photograph in Figure 12d, taken from the oscilliscope using an extended time scale, clearly shows the rapid drop in voltage at contact followed by an exponential rise as the circuit is opened. In this example the measured time constant is 0.08 ms, which with a series resistor of 200 KΩ, gives a contact capacitance of 400 pf; the theoretical film thickness being 11 μ in.

If the model is accepted, then as was shown by Chiu,

$$V = \frac{T^2}{(\nu CR + T)} \qquad 4.1.$$

where V is the ratio of the time average voltage to applied voltage, T is the proportion of no contact time, R and C are the series resistance and contact capacitance respectively and ν the rate of contact interruption. If ν and the time constant are small, the relationship approaches.

$$V = T$$

and the time average voltage drop may be taken as a measure of the no-contact time. When ν and C are not small, a correction may be made. If two tests are run under identical conditions, but with different values of R_1, ν and C may be determined from the resulting two equations.

The applied voltage throughout this research was maintained

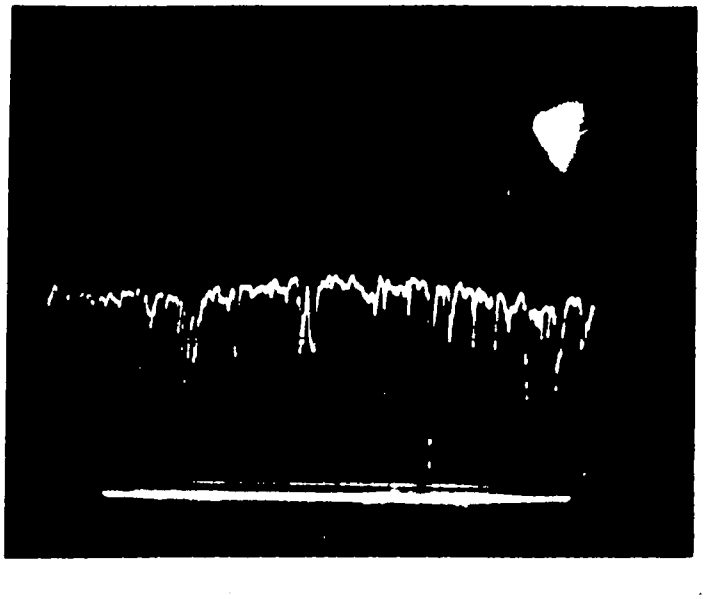

a. Load 3200 lbf N 200 Mean Volts 7.3 mv
Standard Bearing Oil HVI 165

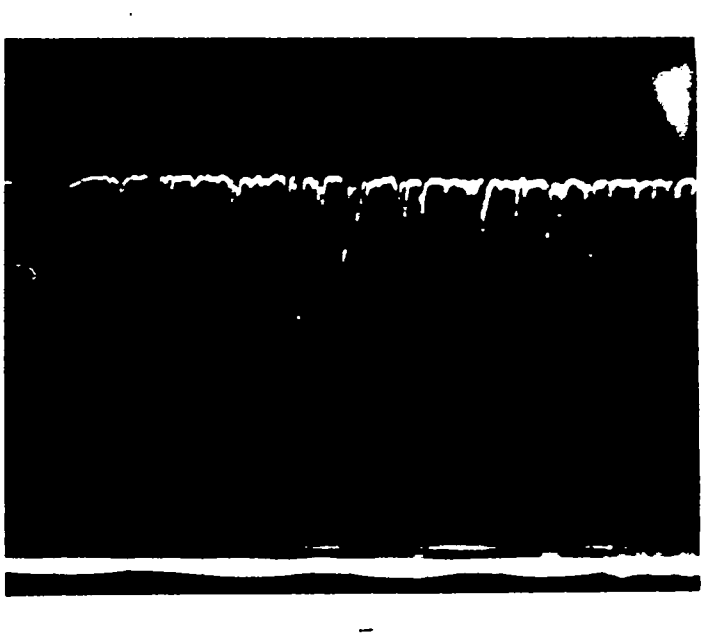

b. Load 640 lbf N 326.6 Mean Volts 9.8 mv
Steep-angled bearing Oil HVI 165

Figure 12

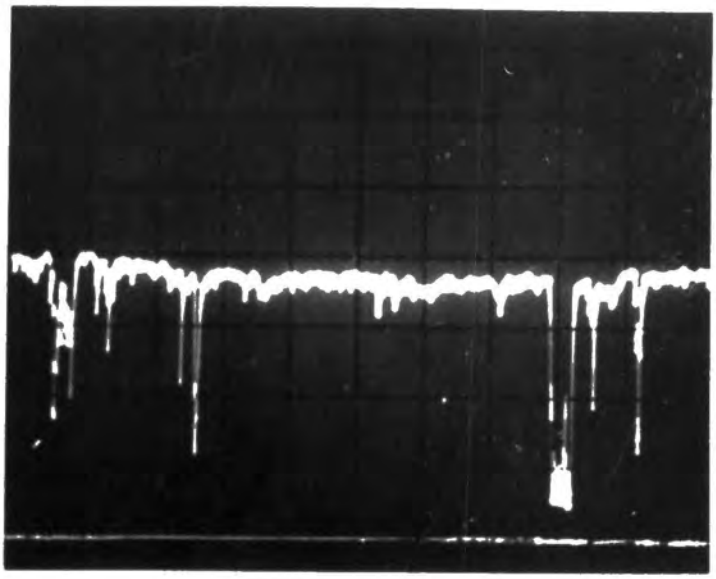

c. Load 1920 lbf N 32.8 Mean Volts 7.0 mv
Standard Bearing Oil HVI 55

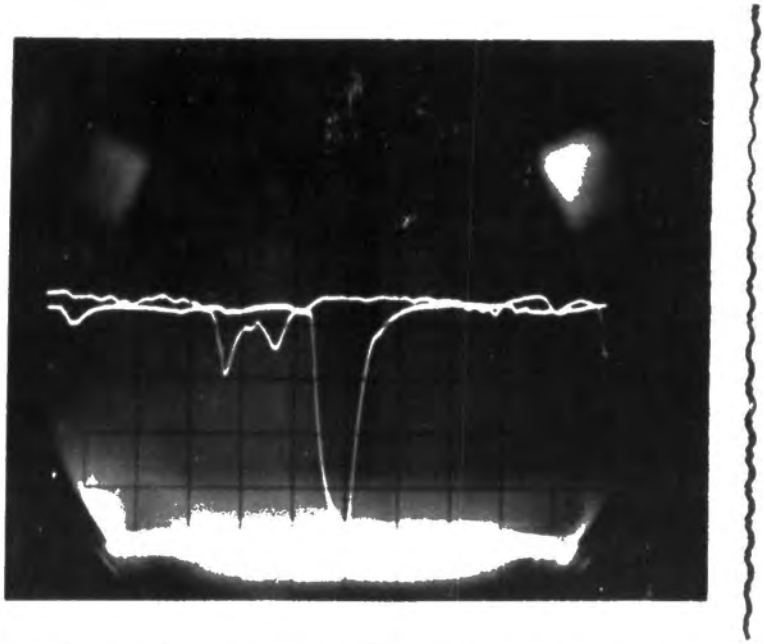

d. Load 1600 lbf N 230 Mean Volts 9.2 mv
Standard Bearing Oil HVI 165
Rise Time Constant 0.08 ms

Figure 12 (continued)

at 10 mv. Attention is drawn to the fact that the no-contact time is not independent of the applied voltage but tends to decrease as the voltage increases. Also it was noted that all pulses did not extend between the limiting voltages. As may be seen in the photographs in Figure 12, it is quite possible for contact to be remade or rebroken before a pulse has reached its extreme.

It is of interest to note that Tallian et. al. (10), using a ball machine, found that a degree of correlation existed between the no-contact time, determined in the manner described above, and the count of asperity contacts in given intervals of time using a level discriminator. Also, both methods gave results which could be related to the amount of wear.

4.6. Lip contact measurements.

Whilst pure rolling was found to exist at the races, the lip contact was subjected to a sliding motion. It was decided to investigate the film conditions at the lip in order to get an indication of its contribution to the friction torque of the bearing as a whole.

A series of tests were carried out using a bearing which had the end lip removed and replaced insulated from the inner and outer races by a hard Tufnol spacer. The original geometry of the bearing was preserved. A cross-section of the bearing is shown in Figure 10. Measurements of voltage drop were made between (a) the inner and outer races, (b) the inner race and the lip, and (c) the outer race and the lip.

4.7. Oil flow measurements.

The test bearings were lubricated by means of two jets supplied through filters from a pressure pump and arranged to impinge on the larger ends of the rollers, between the races and against the direction of rotation. A Bourdon pressure gauge was installed in the supply line so that the quantity of lubricant delivered could be approximately assessed. Different sized orifices were used with HVI 55 and HVI 165. The supply of HVI 55 was of the order of 0.25 pt/min in total to both bearings and remained fairly constant, whereas when HVI 165 was used the supply varied in the range 0.25 to 0.05 pt/min. The bore of the oil piping was small, hence the supply was regulated rather by the temperature-dependent piping losses than by the orifices or relief valve.

CHAPTER 5. DETAILS OF TEST BEARING AND LUBRICANTS.

5.1. Details of Test Bearings.

Two types of tapered roller bearing were used. The first, referred to throughout this thesis as the Standard Bearing, was chosen from a commercial range intended for applications where a combination of radial and thrust load exists. The second, referred to as the Steep Angled Bearing, was from a range designed for applications where the applied load is predominantly thrust. Both bearings had a bore diameter of 2.250 in.

The manufacturers recommended range of thrust load against inner race speed for both bearings is shown in Figure 13. The curves are drawn on the basis of 3000 hr and 5000 hr life, defined as the time during which not more than 10% of the bearings may be expected to fail due to surface fatigue. These particular periods were chosen as representative for heavy automotive duties where no allowance has been made for shock loads. The curves may be extended to cover other life spans by means of the Palmgren formula (13),

$$\text{Life} = \frac{\text{Constant}}{\text{Speed} \times (\text{Load})^{3.33}}$$

It may also be noted that, according to Palmgren, the average life of a bearing is five times the 10% life.

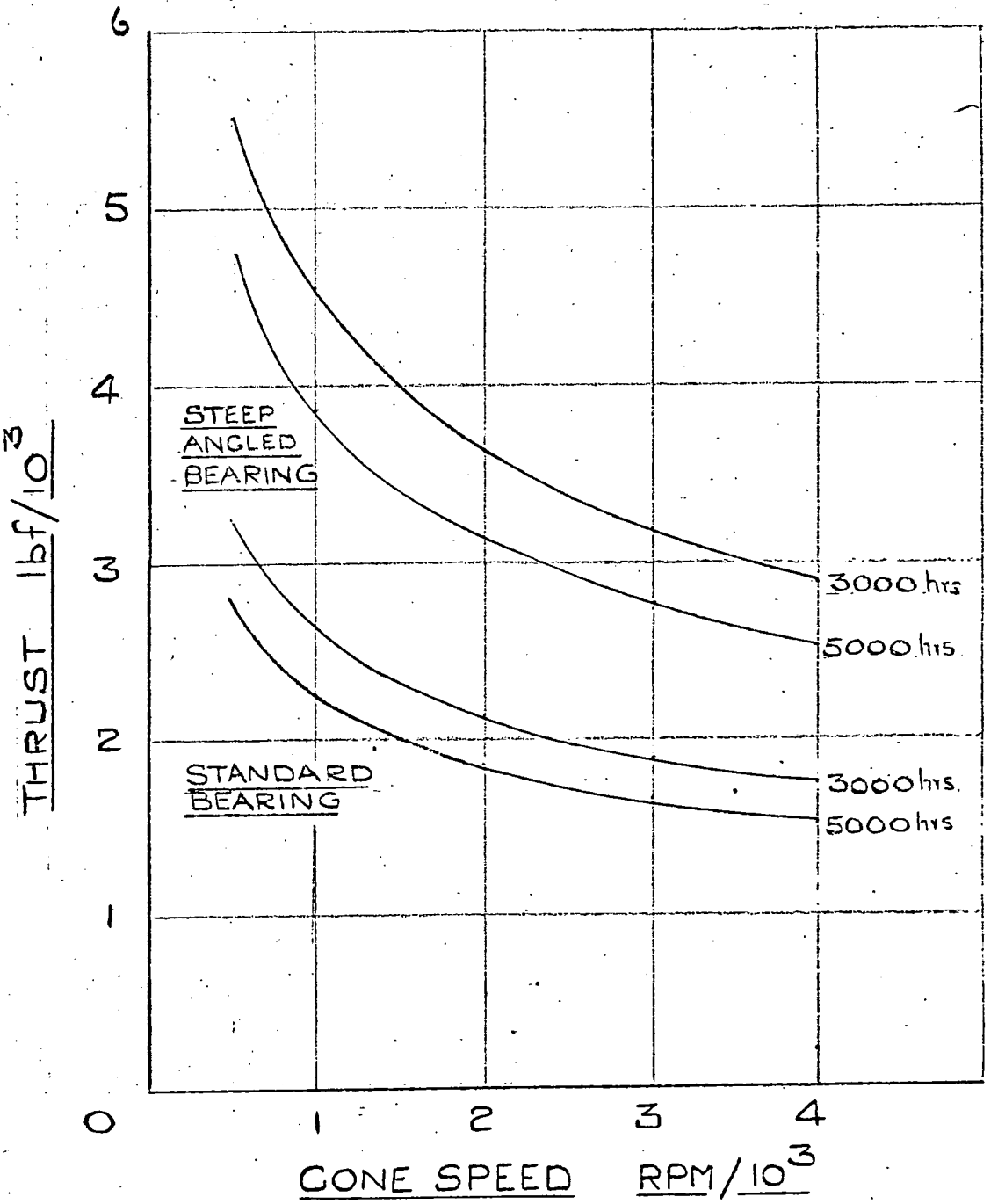
6
5
4
3
2
1
0
THRUST lbf/10³
STEEP ANGLED BEARING
STANDARD BEARING
3000 hrs
5000 hrs
3000 hrs.
5000 hrs
1
2
3
4
CONE SPEED RPM/10³

FIGURE 13.

Figures 14 and 15, show the principal dimensions of the two bearings, the details are also listed in Table 1. Manufacturers drawings of the internal bearing geometry were not available so that the angles of the races had to be calculated from coordinate measurements made with a S.I.P. Universal Measuring Machine. The contact lengths were measured on a shadowgraph. It was noted that no particular attention had been paid to the blend of the roller end radii. The position of the centre of gravity of the rollers was found by suspending them on a thread on a sensitive Oertling balance and taking moments. The same balance was used to find the weights of the rollers.

Measurements of surface finish were made using a portable Talysurf machine. The figures given below shows the results of tests on the outer races and rollers of the bearings before running. It was not possible to measure the finish on the inner race without destroying the assembly. One spot check was made on a stripped Steep Angled Bearing similar to those used in the test. Finishes were also measured after running but no significant changes were observed.

DETAILS OF STANDARD BEARING.

(NOT TO SCALE)

ROLLER WEIGHT = 0·044 LBf

No. ROLLERS = 18

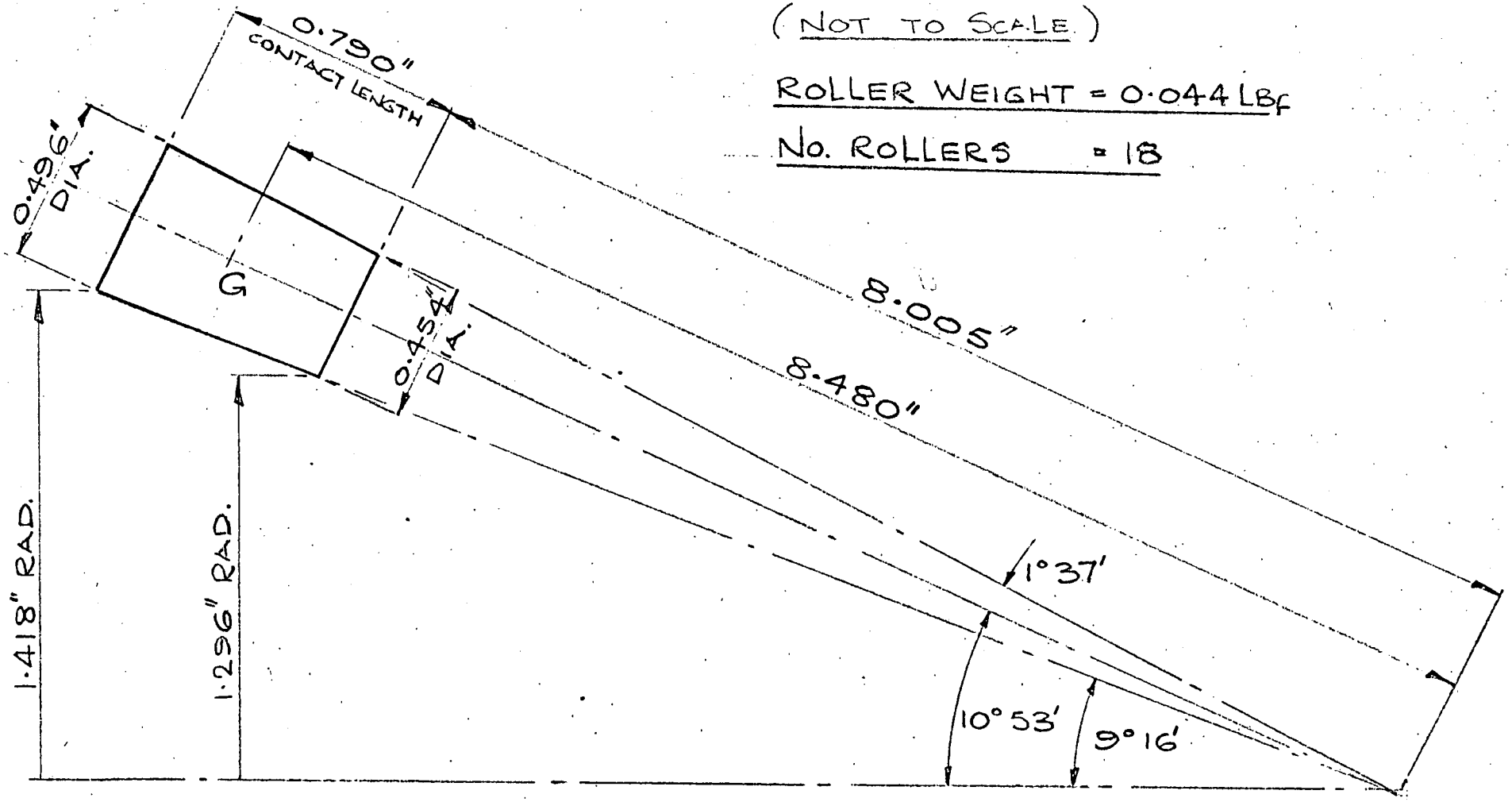

FIGURE 14.

DETAILS OF STEEP ANGLE BEARING

(NOT TO SCALE)

ROLLER WEIGHT = 0·060 LBf

No. ROLLERS = 16

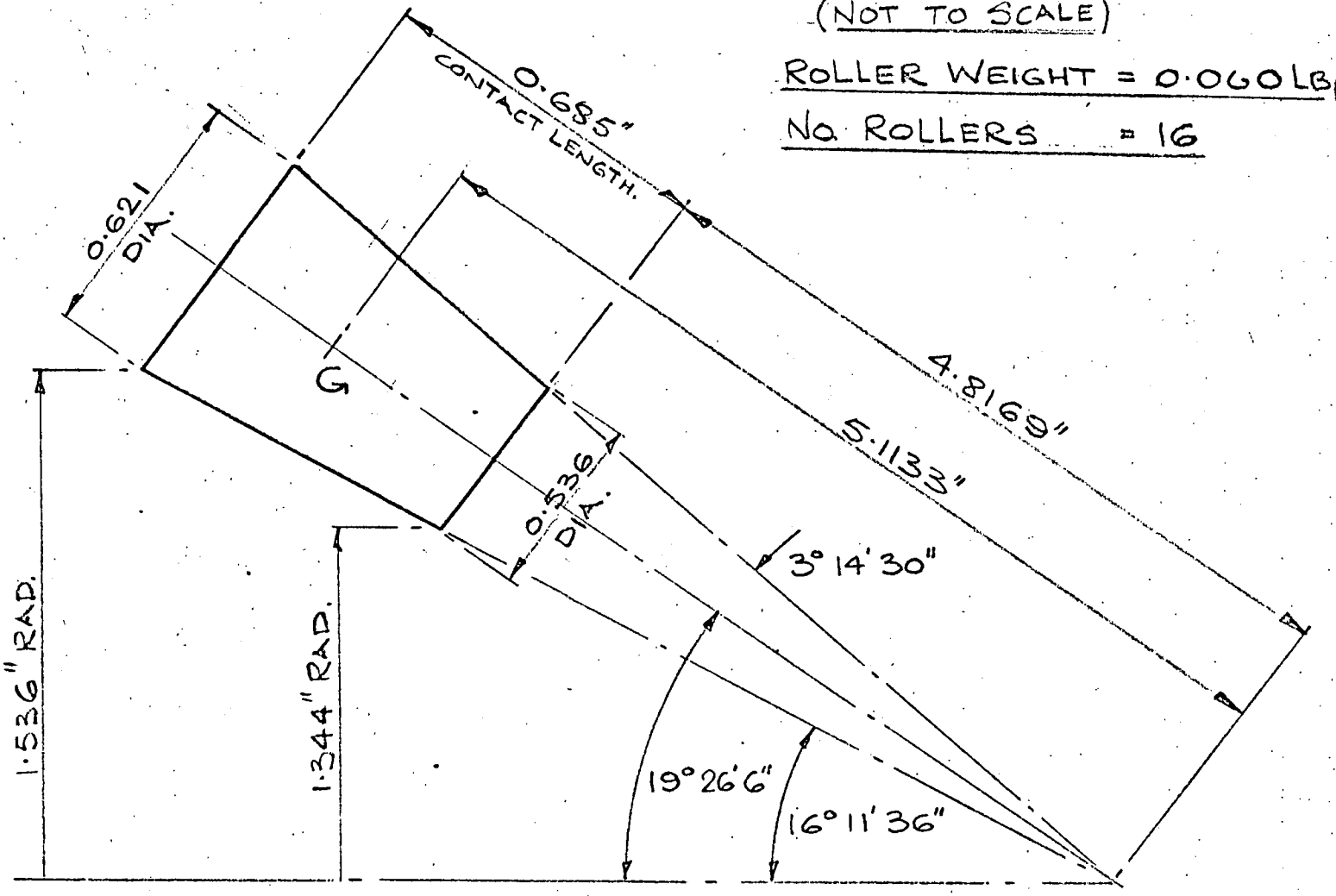

FIGURE 15

Standard Bearing. (new bearing)	C.L.A. figures.
Inner	Not measured
Outer	8μ in (mean of 12 readings)
Rollers	6μ in (mean of 18 readings)

Steep Angled Bearing. (new bearing)	C.L.A. figures.
Inner	8μ in (mean of 12 readings)
Outer	7μ in (mean of 12 readings)
Rollers	5μ in (mean of 16 readings)

A check was made on the dimensional consistency of the rollers from a Standard Bearing. The diameters were measured at a specified distance from the ground face at the large end. These were found to be within a tolerance range of 87×10^{-6} in.

The races of the bearings were made from case hardened steel and the rollers from through hardened stock. The cages were soft steel pressings.

Leading Details of Test Bearings.

	Standard Bearing	Steep Angled Bearing
R	8.480 in	5.113 in
α	10° - 53'	19° - 26'
β	1° - 37'	3° - 14'

	Standard Bearing	Steep Angled Bearing.
N	18	16
m	0.044 lb	0.060 lb
I_x	0.00123 lb in^2	0.00318 lb in^2
$I_y = I_z$	0.00350 lb in^2	0.00463 lb in^2
Length of Contact l	0.790 in	0.685 in

TABLE 1.

5.2. Test Oils.

Three straight mineral oils containing no additives were supplied by Shell. These were known as HVI 650, HVI 165 and HVI 55. The first was found to be too heavy for the lubricating system of the rig and was abandoned after early tests. Figure 16 shows the viscosity of the oils against temperature. The figures were obtained using a Ferranti rotating cylinder viscometer in a temperature controlled bath and compared closely with data supplied by Shell.

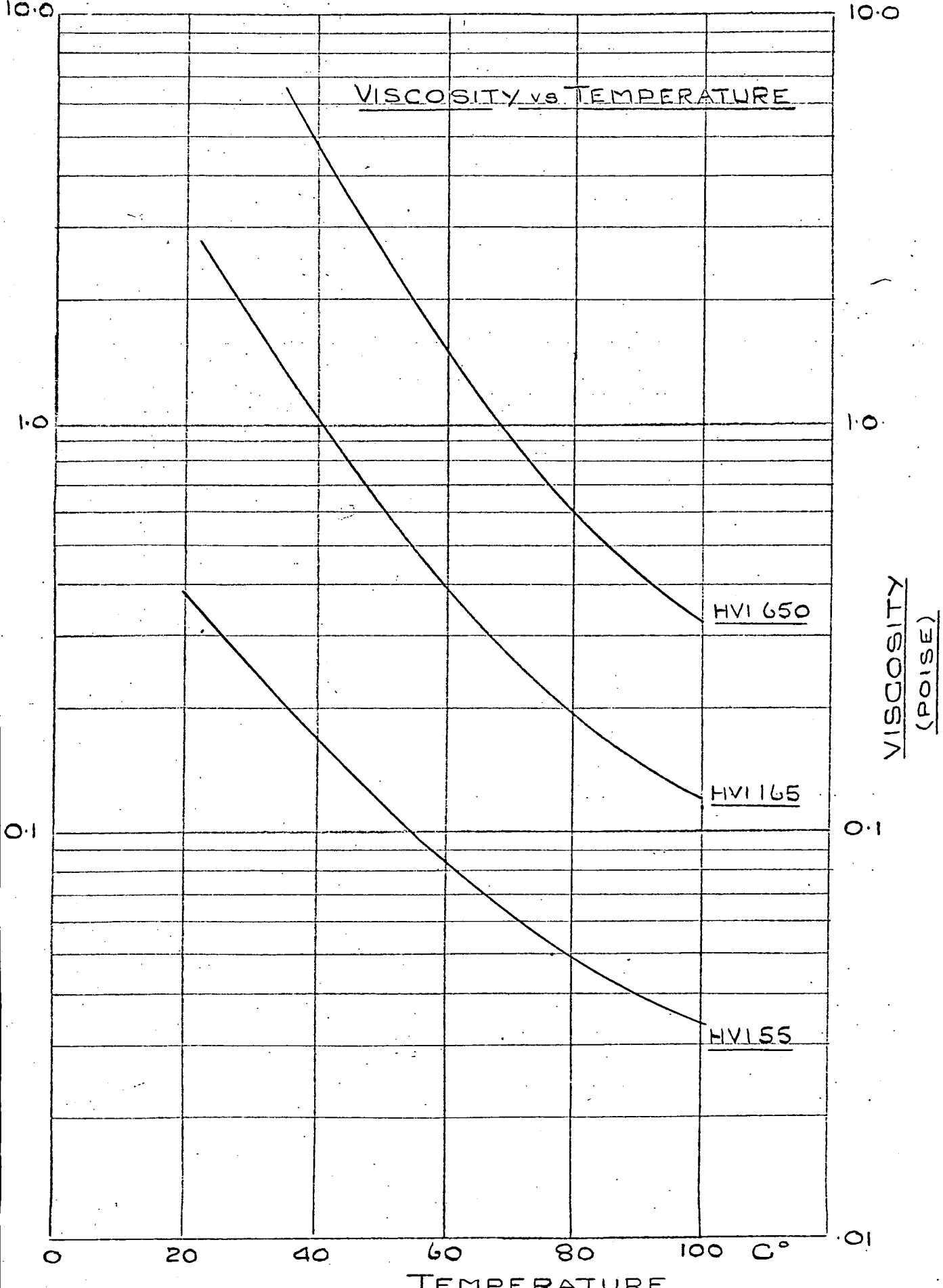
VISCOSITY vs TEMPERATURE
10·0
1·0
0·1
·01
HVI 650
HVI 165
HVI 55
VISCOSITY (POISE)
0
20
40
60
80
100
C°
TEMPERATURE

FIGURE 16

CHAPTER 6. THEORETICAL FILM THICKNESS.

6.1. Equivalent Radius at a contact.

The magnitude and distribution of stress, both in the dry and elastohydrodynamic cases, depends, in part, upon the geometry of the bodies in the region of contact. It is analytically convenient to replace the actual bodies by an equivalent cylinder acting against a plane. In the case of tapered roller bearings, where two of the principal radii of curvature at the contact are infinite and contact takes place along a line, a suitable equivalent body is a cylinder having a radius R_e given by,

$$\frac{1}{R_e} = \frac{1}{R_1} + \frac{1}{R_2}$$

where R_1 and R_2 are the two remaining principal radii of curvature of the original undeformed bodies.

These radii may be determined directly using Meusnier's theorem.

Figure 3 shows a cross-section of a single roller, AG is the radius in a plane perpendicular to the centre-line through the centre of gravity G. The principal radius of curvature R_a at A, is given by,

$$R_a = \frac{AG}{\cos \beta}$$

where β is the semi-vertex angle of the cone.

Hence,

$$R_a = AC$$

Figure 4 shows the geometry of a roller in its races.

$$OG = R$$

and,

$$OA = OB = \frac{R}{\cos \beta} \qquad 6.1$$

The principal radii of curvature, R_i, R_o and R_r, of the inner and outer races and of the roller at A and B are given by,

$$R_i = DA$$

$$R_o = BF$$

$$R_r = AC = BC$$

Using 6.1, these radii may be expressed in terms of the known bearing dimensions.

$$R_i = \frac{R \tan (\alpha - \beta)}{\cos \beta} \qquad 6.2$$

$$R_o = \frac{R \tan (\alpha + \beta)}{\cos \beta}$$

$$R_r = \frac{R \tan \beta}{\cos \beta}$$

The Equivalent radius R_{eo}, at point B on the outer track is given by,

$$R_{eo} = \frac{R_o R_r}{R_o - R_r} \qquad 6.3$$

substituting in 6.3 from 6.2 gives,

$$R_{eo} = \frac{R}{\cos\beta \ (\cot\beta - \cot(\alpha + \beta))}$$

Similarly, for the point A at the inner track, noting the change in sign in the denominator, the Equivalent radius R_{ei} is given by,

$$R_{ei} = \frac{R_l \, R_r}{R_l + R_r}$$

Hence,

$$R_{ei} = \frac{R}{\cos\beta \ (\cot\beta + \cot(\alpha - \beta))}$$

6.2. Entraining velocity at contact.

Before attempting to calculate the theoretical film thickness, it is necessary to know the mean velocity of the lubricant flow through the contact zone; that is to say, the entraining velocity. For thin films this may be assumed to be equal to the mean of the velocities of the two surfaces at the contact. If a bearing is running without slip, the entraining velocity and the surface velocities relative to the contact, will, of course, be equal.

Consider point B in Figure 4, which is close to the centre of the contact trapezium on the outer race. If the cage is assumed to be held stationary by giving the whole bearing a rotational velocity of $-\omega_c$, the velocity of point B on the outer race, relative to the stationary roller centre, will be the entraining velocity and is given by,

$$u = \omega_c \quad BL \qquad 6.4$$

$$\text{and } BL = R \frac{\sin(\alpha + \beta)}{\cos \beta}$$

when substituting in 6.4 for BL and for ω_c from 3.3

$$u = \frac{\Omega_1}{2} R \sin\alpha \left[1 - \left(\frac{\tan \beta}{\tan \alpha}\right)^2\right] \qquad 6.5$$

6.3. Calculation of theoretical film thickness.

Dowson and Whitaker (14) have defined three distinct phases of contact lubrication. In the first, which applies at very small loads, the bodies may be considered rigid and the lubricant incompressible and isoviscous. Under these conditions, a close approximation to the film thickness is given by the Martin formula: this in dimensionless form may be stated as,

$$H^* = 4.9 \frac{U}{W}$$

In the second or intermediate phase, the bodies may again be considered rigid but the effect of pressure upon the viscosity of the lubricant becomes important. Finally, in the third phase, lubrication is completely elastohydrodynamic. Dowson and Higginson (8) have shown that the minimum film thickness in an elastohydrodynamic contact, as given by their theoretical isothermal solution, may be fairly accurately represented by the formula,

$$H^* = 1.6 \frac{G^{0.6} U^{0.7}}{W^{0.13}} \qquad 6.6$$

where $H^* = \frac{h}{R_e}$ and h is the film thickness.

G, U and W are convenient numerics which will now be considered individually in forms suitable for application to the outer race of a tapered roller bearing.

The voltage drops were taken across both races and across the two oil films; the film at the outer race is expected to be larger than at the inner race, and the resistance method only detected the establishment of the first film to be formed. Further, the outer film is of greater interest as the reaction was measured on the outer race.

Load parameter, W

The load parameter is defined in general terms as,

$$W = \frac{w}{R_e E'} \qquad 6.7$$

where w is the load per unit length of contact and E', the materials of the race and rollers being similar, is given by,

$$E' = \frac{E}{1 - \sigma^2}$$

σ being Poisson's ratio.

Substituting in 6.7 for w from 3.13 gives,

$$W = \frac{T}{R_{eo} E \; l \; n \sin(\alpha + \beta)}$$

n is the number of rollers and l the length of contact.

Inertia effects have been neglected.

Speed parameter, U

The speed parameter is given by,

$$U = \frac{\eta_o \; u}{E' \; R_{eo}}$$

η_0 is the viscosity of the lubricant at the entry to the contact zone and is usually taken at the surface temperature of the race. u is the entraining velocity of the lubricant and for conditions of zero slip is given by 6.5.

Materials parameter, G.

The materials parameter is defined as,

$$G = \alpha E'$$

where α is obtained from the pressure viscosity relationship for the lubricant which is assumed to be of exponential form,

$$\eta = \eta_0 e^{\alpha p}$$

For mineral oils α lies within a narrow range; hence, for combinations of steel and steel with mineral oil as the lubricant, G varies little and has usually been taken as 5000.

Examining equation 6.6, it is clear that both G and U have a large effect on film thickness, whereas the effect of load is small. As G is practically constant, the predominant variable is speed viscosity.

In the paper by Dowson and Whitaker referred to earlier, the authors included a chart which is reproduced in Figure 17. This indicates the regions, in terms of U, W and H*, in which the three types of lubrication occur. The area outlined on the chart

encloses the range of parameters used in the present investigation. It follows that the elastohydrodynamic formula may justifiably be used to estimate the theoretical film thickness for the test bearings. It may also be noted, that as no measurable slip occurred throughout the tests, the assumption of isothermal conditions within the film is reasonable. It is of interest to observe from the chart that the use of the Martin formula would seriously underestimate the film thickness in the intermediate and elastohydrodynamic ranges.

Equation 6.6 may now be recast into forms suitable for application to the outer races of the two test bearings.

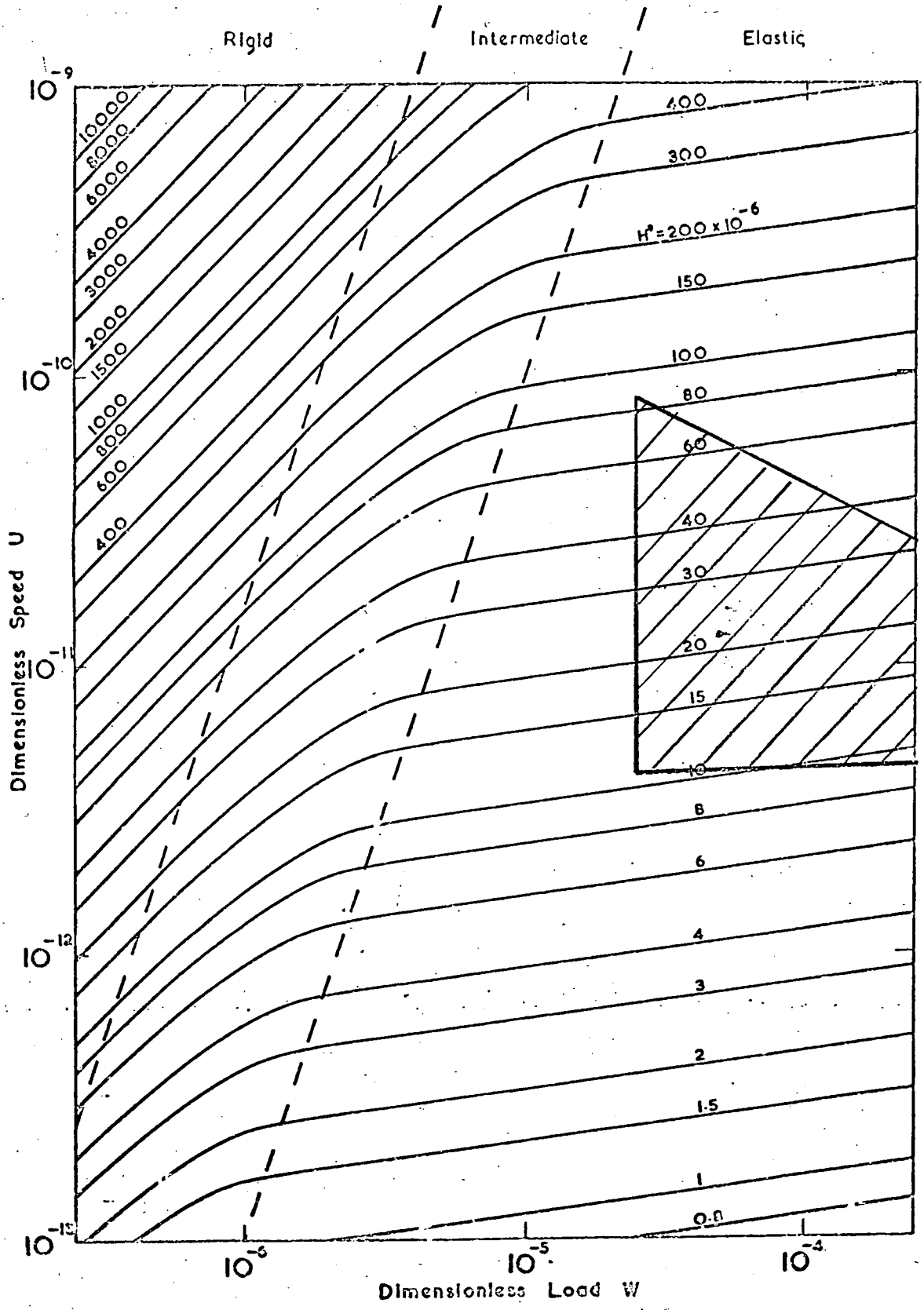
Rigid
Intermediate
Elastic
Dimensionless Speed U
Dimensionless Load W
10^{-9}
10^{-10}
10^{-11}
10^{-12}
10^{-13}
10^{-6}
10^{-5}
10^{-4}
$H^o = 200 \times 10^{-6}$
10000
8000
6000
4000
3000
2000
1500
1000
800
600
400
400
300
150
100
80
60
40
30
20
15
10
8
6
4
3
2
1.5
1
0.8

FIGURE 17

6.4. Elastohydrodynamic parameters and film thickness for test bearings.

Standard Bearing.

$$R_{eo} = 0.2748 \text{ in}$$

$$u = 0.082\ N \text{ in/s}$$

$$U = \frac{0.1298}{10^{12}} \eta_o\ N$$

$$W = \frac{3.590\ T}{10^8}$$

$$h = 0.6519 \frac{(\eta_o N)^{0.7}}{T^{0.13}} \mu \text{ in} \qquad 6.8$$

Steep-angled Bearing.

$$R_{eo} = 0.3359 \text{ in}$$

$$u = 0.087\ N \text{ in/s}$$

$$U = \frac{0.1123}{10^{12}} \eta_o\ N$$

$$W = \frac{2.135\ T}{10^8}$$

$$h = 0.7575 \frac{(\eta_o N)^{0.7}}{T^{0.13}} \mu \text{ in} \qquad 6.9$$

Standard Bearing with 9 rollers.

$$h = 0.5959 \frac{(\eta_o N)^{0.7}}{T^{0.13}} \mu \text{ in} \qquad 6.10$$

A comparison of equations 6.8 and 6.10 further emphasises the characteristic of elastohydrodynamic lubrication, the film thickness is only slightly dependent upon load.

The theoretical film thickness λ_{es} for the test bearings have been calculated using equations 6.8, 6.9 and 6.10, and are plotted in Figures 18, 19, and 20, over the relevant ranges of the variables.

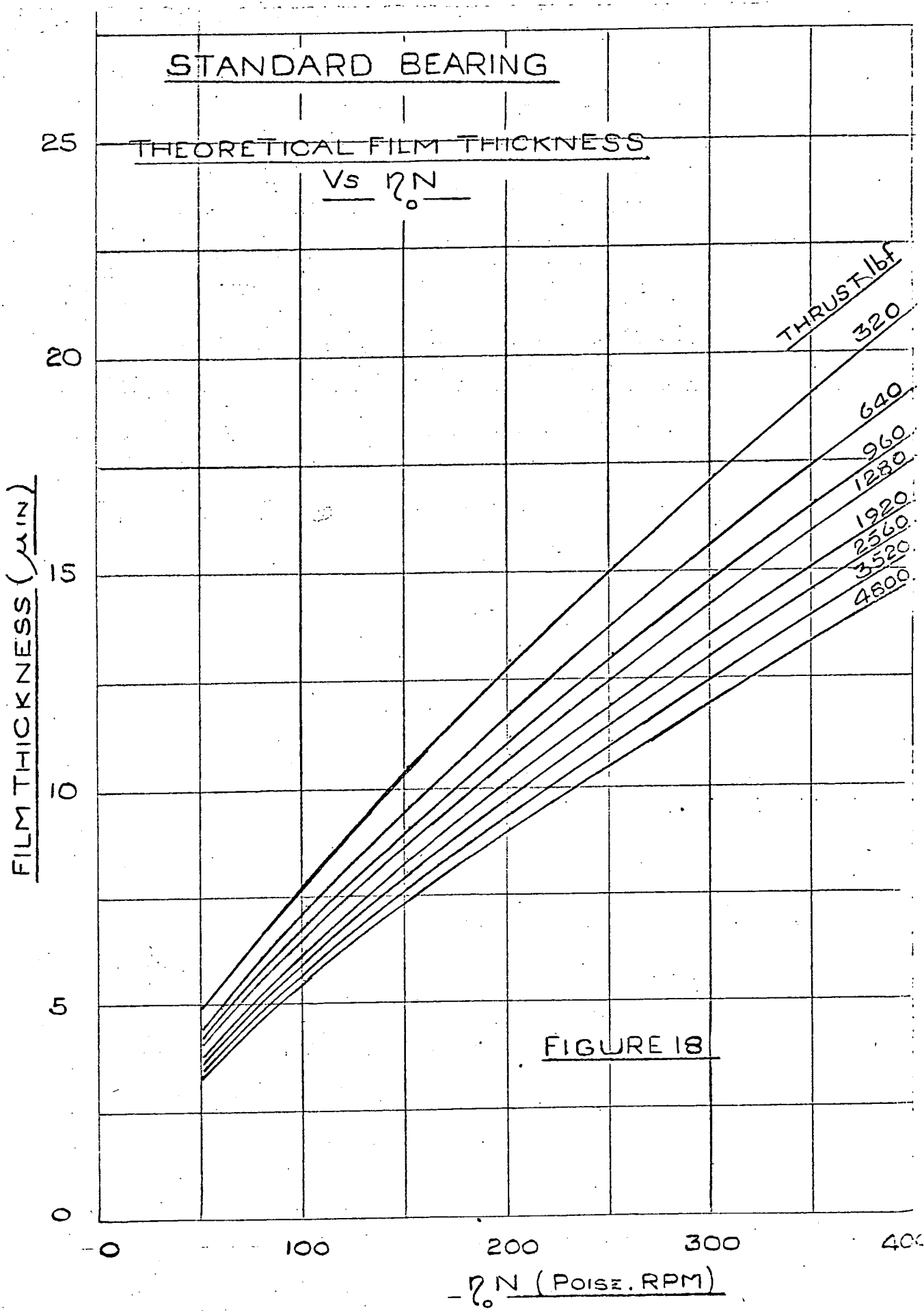
STANDARD BEARING
THEORETICAL FILM THICKNESS
Vs $\eta_o N$
THRUST lbf
320
640
960
1280
1920
2560
3520
4600
FILM THICKNESS (μIN)
0
5
10
15
20
25
0
100
200
300
400
$\eta_o N$ (POISE. RPM)

FIGURE 18

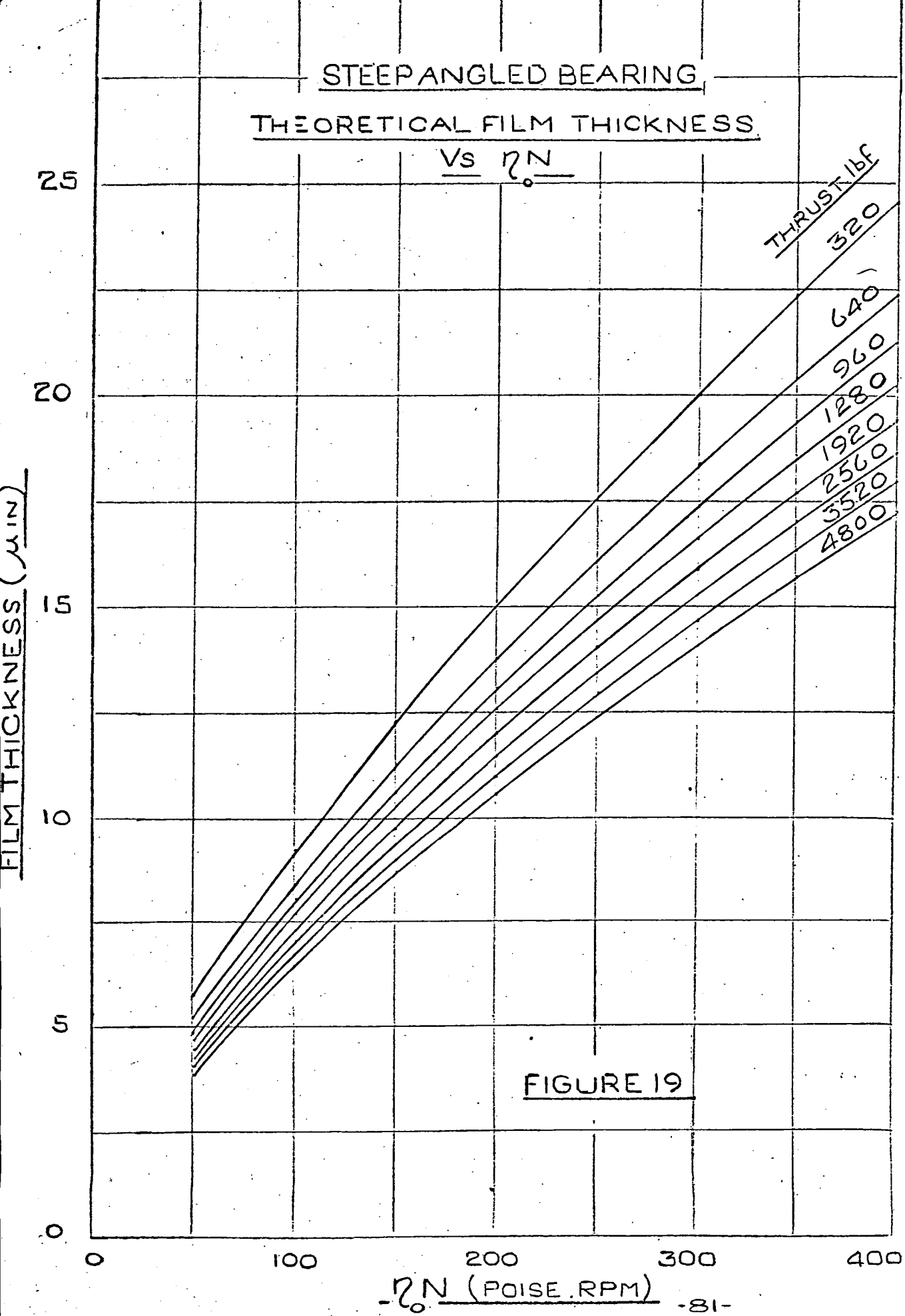
STEEP ANGLED BEARING
THEORETICAL FILM THICKNESS
Vs $\eta_o N$
THRUST lbf
320
640
960
1280
1920
2560
3520
4800
FILM THICKNESS (μin)
0
5
10
15
20
25
0
100
200
300
400
$\eta_o N$ (POISE.RPM)

FIGURE 19

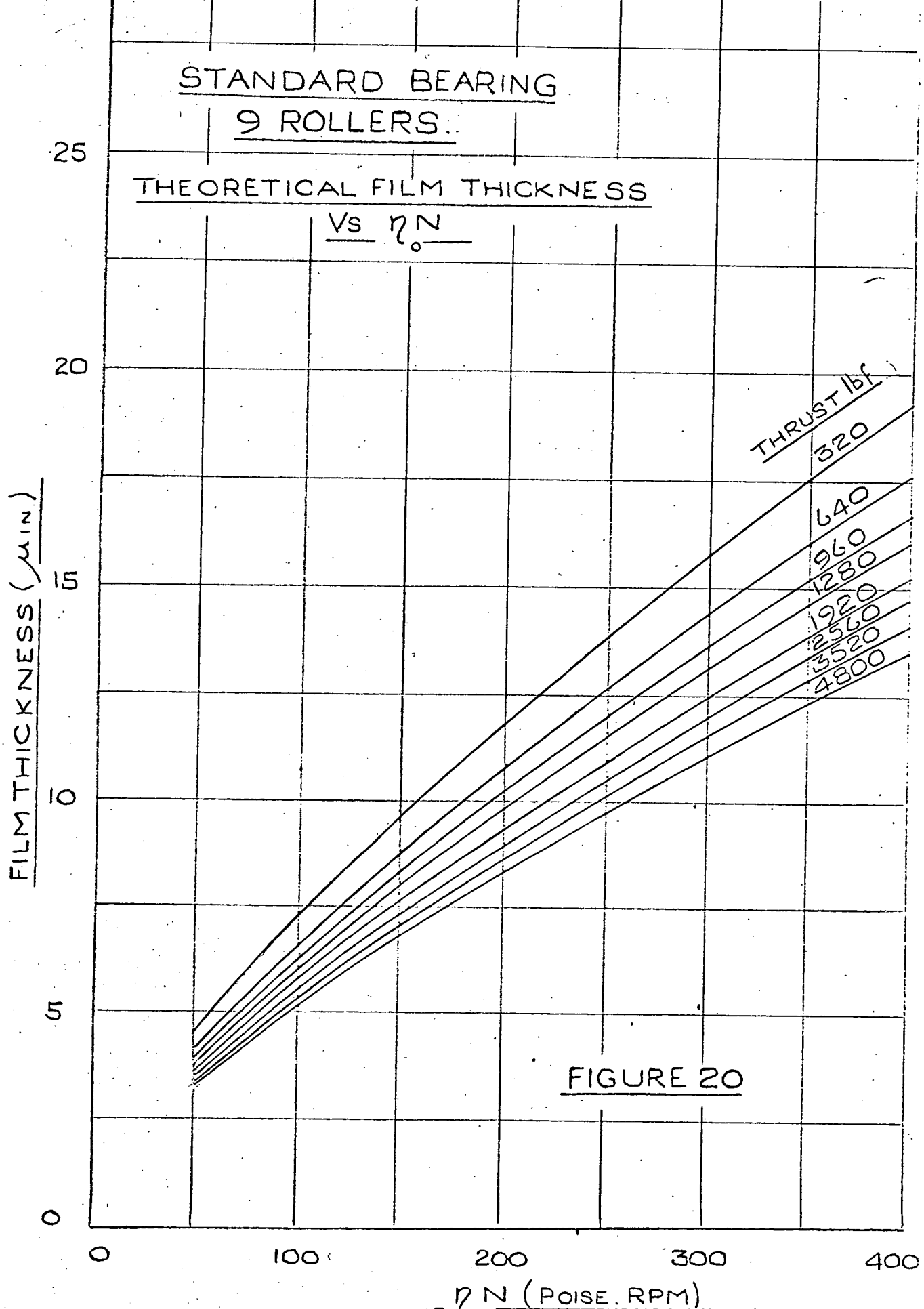
STANDARD BEARING
9 ROLLERS.
THEORETICAL FILM THICKNESS
Vs $\eta_o N$
THRUST lbf
320
640
960
1280
1920
2560
3520
4800
FILM THICKNESS (μIN)
0
5
10
15
20
25
0
100
200
300
400
$\eta_o N$ (POISE. RPM)

FIGURE 20

CHAPTER 7. THEORETICAL FRICTION TORQUE

7.1. Viscous forces in a contact film.

Figure 21 represents an elemental volume of fluid within the contact film. The velocities of the volume in the directions X, Y and Z are u, v and w respectively. If inertia and body forces are neglected, the pressure and viscous forces are in equilibrium, then by Pai (15), the Reynolds equation reduces to :

$$\frac{\partial p}{\partial x} = \frac{2}{3}\frac{\partial}{\partial x}\eta\left(\frac{\partial u}{\partial x} - \frac{\partial w}{\partial z}\right) + \frac{2}{3}\frac{\partial}{\partial x}\eta\left(\frac{\partial u}{\partial x} - \frac{\partial v}{\partial y}\right) + \frac{\partial}{\partial y}\eta\left(\frac{\partial u}{\partial y} + \frac{\partial v}{\partial x}\right)$$

$$+ \frac{\partial}{\partial z}\eta\left(\frac{\partial w}{\partial x} + \frac{\partial u}{\partial z}\right) \qquad 7.1$$

Similar expressions may be formed for the Y and Z directions. However, since the pressure gradient across the film is small and as we are concerned with a long roller and hence may neglect end leakage, neither $\frac{\partial p}{\partial z}$ nor $\frac{\partial p}{\partial y}$ is of interest. Further, as the derivative of u with respect to y is large compared with the others, equation 7.1 may be reduced to the two dimensional case,

$$\frac{\partial p}{\partial x} = \frac{\partial}{\partial y}\eta\left(\frac{\partial u}{\partial y}\right)$$

This equation may be solved using the boundary conditions,

at $y = 0$ $\qquad u = u_1$

and at $y = h$ $\qquad u = u_2$

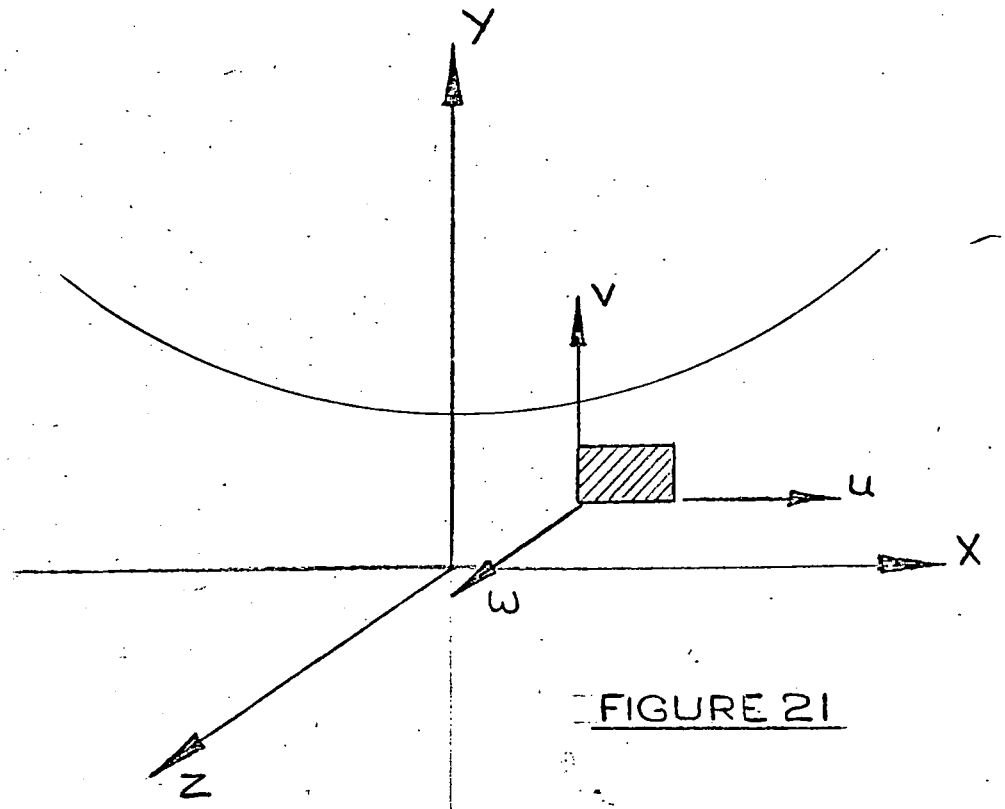

FIGURE 21

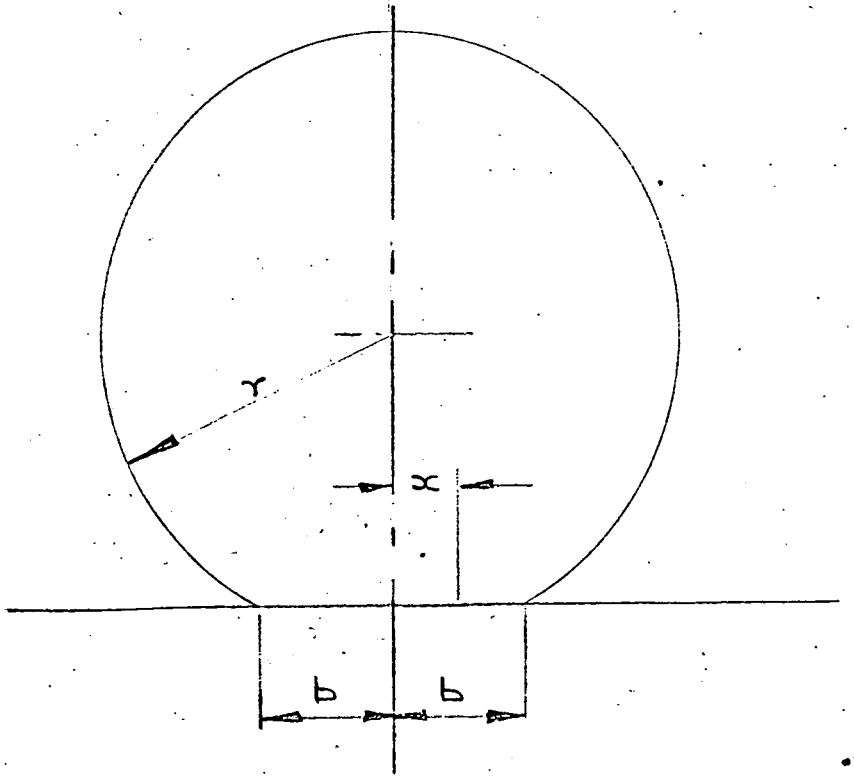

FIGURE 22

giving,

$$u = u_1 \left(1 - \frac{y}{h}\right) + u_2 \frac{y}{h} - \left(y \frac{(y - h)}{2\eta}\right) \frac{\partial p}{\partial x}$$

Hence,

$$\frac{\partial u}{\partial y} = \frac{1}{h} (u_2 - u_1) - \left(\frac{h - 2y}{2\eta}\right) \frac{\partial p}{\partial x}$$

The stress Γ_2 at y = h is given by,

$$\Gamma_2 = \frac{\eta}{h} (u_2 - u_1) + \frac{h}{2} \frac{\partial p}{\partial x} \qquad 7.2$$

and the stress Γ_1 at y = 0, by,

$$\Gamma_1 = (u_2 - u_1) - \frac{h}{2} \frac{\partial p}{\partial x} \qquad 7.3$$

The first terms in equations 7.2 and 7.3 represent the sliding components and reduce to zero for the case of pure rolling, where $u_2 = u_1$.

Hence, numerically

$$\Gamma_1 = \Gamma_2 = \frac{h}{2} \frac{\partial p}{\partial x}$$

If p is assumed to vary only with x, we may write,

$$\Gamma_1 = \Gamma_2 = \frac{h}{2} \frac{dp}{dx}$$

The force per unit width of roller F_r, is then given by,

$$F_r = \int_1^0 \frac{h}{2} \, dp$$

where the limits i and o refer to the inlet and outlet of the lubricant film.

Dowson, Higginson and Whitaker (16) have noted that the rolling friction force is almost independent of load over the range $W = 3 \times 10^{-5}$ to 3×10^{-4} and have evaluated $P'x$ for the isothermal elastohydrodynamic case treating it as a function of $\bar{U}$ only. Their results are given in graphical form in Figure 23.

The relationship between F_r and the non-dimensional $P'x$ is,

$$F_r = P'x \frac{E'Re}{2} \qquad 7.4$$

The computation assumes the viscosity-pressure relationship $\eta = \eta_o e^{\alpha p}$ where,

$$P'x = \frac{p}{E'Re}$$

G has been taken as 5000 and E' as 33×10^6 lbf/in^2

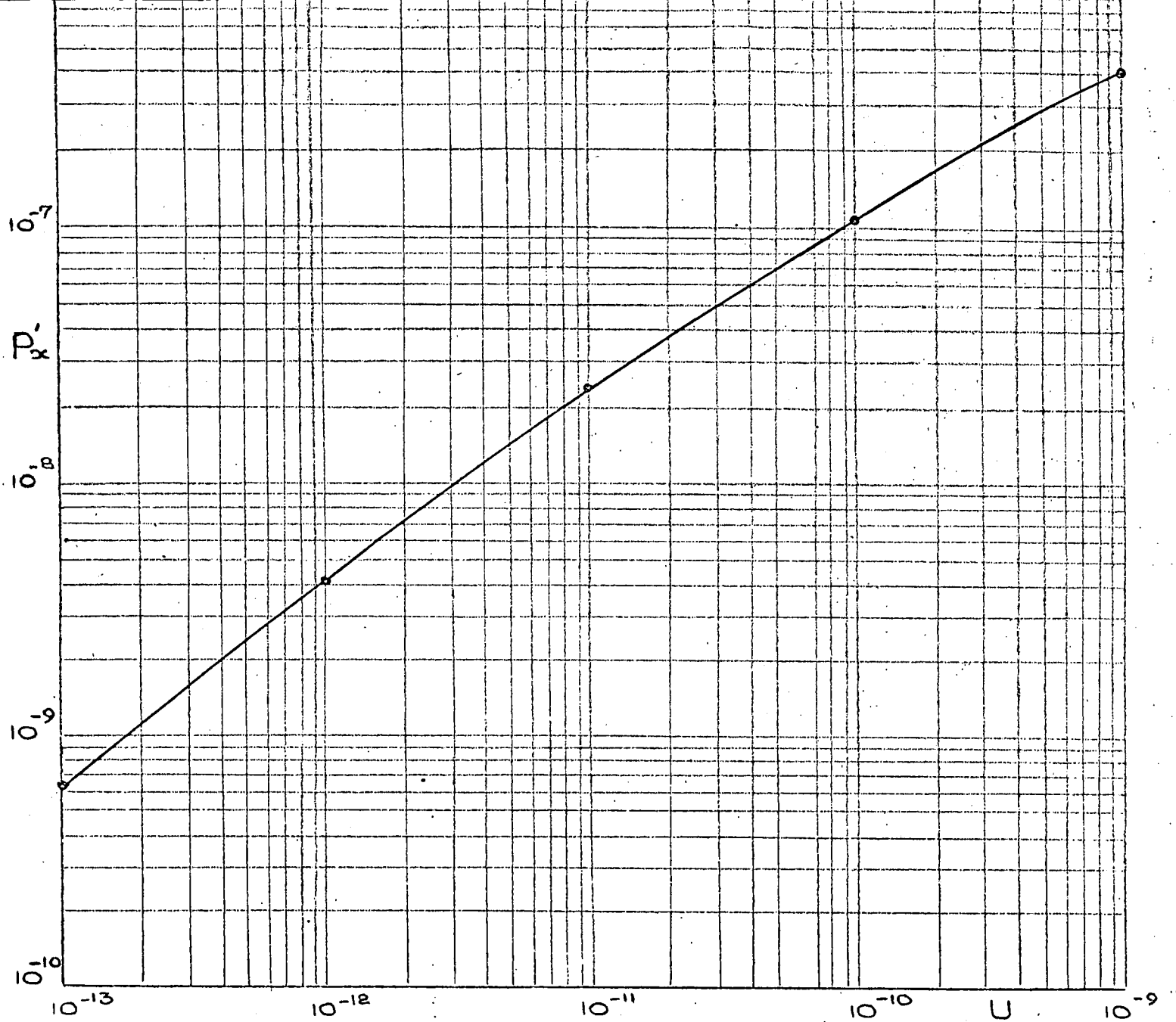

FIGURE 23

7.2. Calculation of viscous friction torque in test bearings, due to rolling only.

The loading of the three bearings varied within the following limits

Standard bearing

W varied from 1.15×10^{-5} to 1.15×10^{-4}

Steep angled bearing

W varied from 1.36×10^{-5} to 9.56×10^{-5}

Standard bearing with 9 rollers

W varied from 3.30×10^{-5} to 1.15×10^{-4}

Although at low loads the value of W falls below 3×10^{-5}, it has already been shown in Figure 17 that all test points are well within the elastohydrodynamic range. Values of P'x may be taken directly from Figure 23 for calculated values of $\bar{U}$. Values of F_r may then be found directly from Equation 7.4. Viscous friction torque T_V is given by the equation,

$$T_V = \eta \, l \, (BL) \, F_r \qquad 7.5$$

where n is the number of rollers, l the length of roller contact and, from Figure 4, BL is the mean radius of the outer race.

Tabulated below are calculated values of torque for the three test bearings over a suitable range of values of ηN.

Table of calculated viscous friction torques due to pure rolling assuming that each roller takes an equal share of the load.

Torque lbf.in (T_V)			
η N	Standard Bearing	9 Roller Bearing	Steep Angled Bearing
50	2.1	1.0	1.9
100	3.4	1.7	3.2
200	5.6	2.8	5.2
300	7.2	3.6	6.9
400	8.9	4.5	8.3
500	10.4	5.2	9.6

It may be noted that the viscous torque for the 9 roller bearing is half that for the Standard 18 roller bearing.

7.3. Calculation of sliding friction forces.

The first terms in equations 7.2 and 7.3, represent sliding components and will have a value of $u_1 \neq u_2$.

If Fs is the tangential force at the surface due to sliding then,

$$Fs = (u_1 - u_2) \int_{i}^{o} \frac{\eta}{h} \, dx \qquad 7.6$$

It is convenient to write the equation in non-dimensional form.

Let $(u_1 - u_2) = v$

and $V = \frac{v \eta_o}{E'Re}$

also let

$$\bar{\eta} = \frac{\eta}{\eta_o} \quad \text{and} \quad \bar{x} = \frac{x}{b}$$

where b is half the Hertzian width.

Substituting in equation 7.6 gives,

$$\frac{Fs}{E'Re} = V \left(\frac{Re}{h}\right) \left(\frac{b}{Re}\right) \int_{-1}^{+1} \bar{\eta} \, d\bar{x}$$

Let $J = \left(\frac{b}{Re}\right) \int_{-1}^{+1} \bar{\eta} \, d\bar{x}$

Then $\frac{Fs}{E\,Re} = V \left(\frac{Re}{h}\right) \left(\frac{b}{Re}\right) J \qquad 7.7$

The integral J has been evaluated by Garnell and Higginson for a range of values of W, using a Hertzian pressure distribution and an expression for viscosity provided by Dowson and Whitaker. Their solution is given in graphical form in Figure 24.

Fs may be evaluated using these values of J. W and the film thickness h may be calculated using the formula in Section 6.4.

The significance of sliding friction will be discussed later when considering the experimental results.

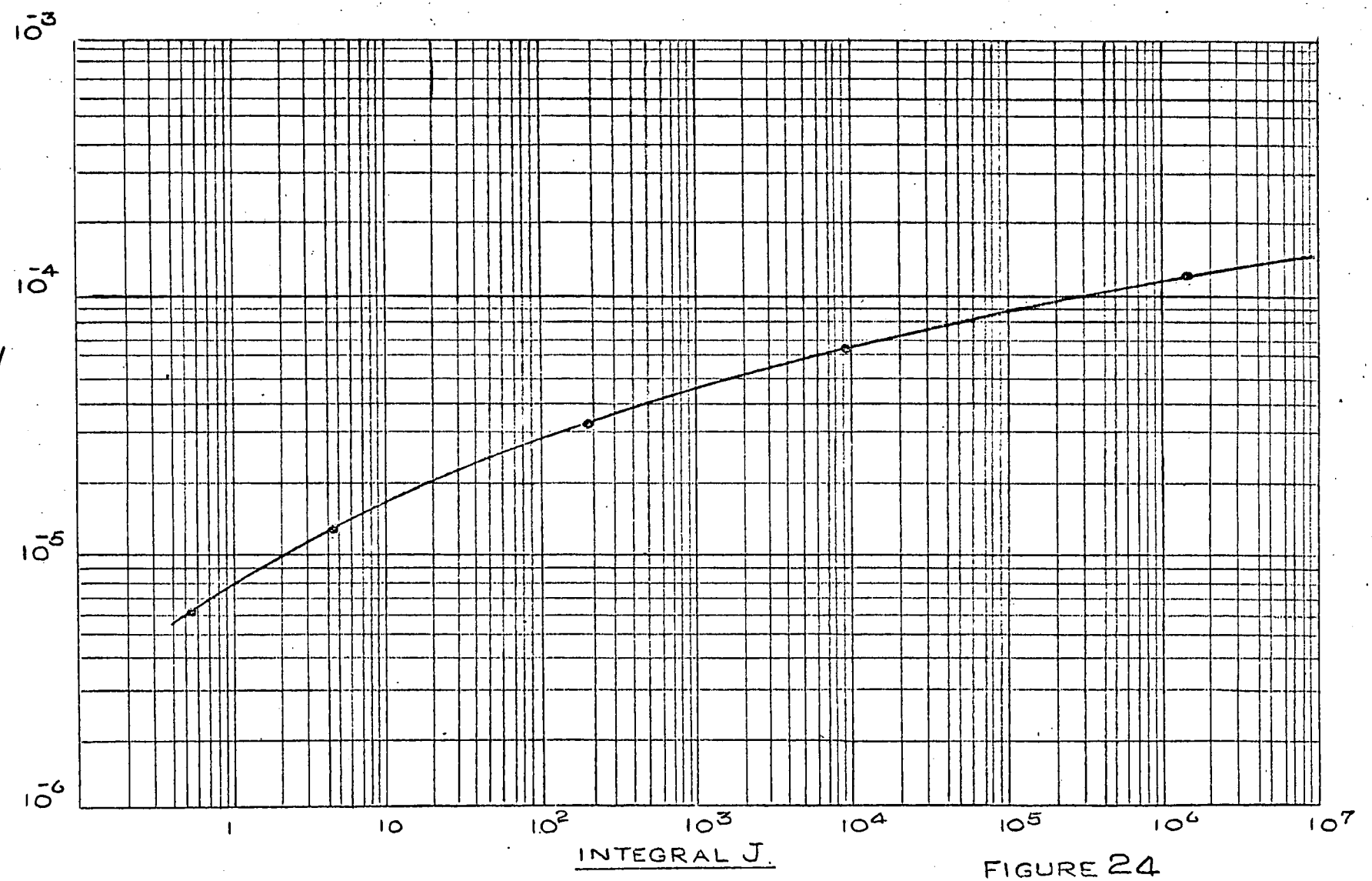

FIGURE 24

7.4. Torque due to elastic hysteresis.

The Hertzian band width for a cylinder against a plane surface is equal to 2b, and is given by

$$b = 4 \left(\frac{w\,Re}{2\pi E'} \right)^{\frac{1}{2}} \qquad 7.8$$

where w is the load per unit length of contact.

The dry static pressure distribution over the band is given by,

$$p = p_o \left(1 + \left(\frac{x}{b} \right)^2 \right)^{\frac{1}{2}}$$

where p_o is the maximum pressure at the centre of the band and,

$$p_o = \frac{2\,w}{\pi\,b}$$

x is the distance coordinate measured from the centre-line of the contact zone as shown in Figure 22. If the couple exerted by the front half of the band width is G.

$$G = \int_o^b p\,x.dx$$

$$\therefore \quad G = \frac{2\,w\,b}{3\,\pi} \qquad 7.9$$

If ρ is the work done against this couple in rolling unit distance, then,

$$\rho = \frac{G}{r}$$

and substituting for G from equation 7.9 gives,

$$p = \frac{2\,w\,b}{3\,\pi\,r}$$

Bowden and Tabor (17) suggest that the energy loss due to hysteresis, E_L, may be expressed as a simple fraction of the input energy. Greenwood (18) has shown that the loss is given by,

$$E_L = 3.5\,\alpha\,\phi \qquad 7.10$$

Where α is the fractional loss due to static loading and unloading, and the factor 3.5 accounts for the complex changing stress pattern due to rolling.

Garnell (3) quotes a lower limit for α, due to K.L. Johnson of 0.5%.

Substituting in 7.10 for p and using equation 7.8 for b, gives,

$$E_L = 3.5\,\alpha \left(\frac{8\,w}{3\pi r} \sqrt{\frac{w\,Re}{2\pi E'}} \right)$$

As this is the energy loss per unit distances, the coefficient of friction μ is obtained simply by dividing by W.

$$\mu = \frac{28\alpha}{3\pi r} \left(\frac{w\,Re}{2\pi E'} \right)^{\frac{1}{2}}$$

Hence, the torque loss due to elastic hysteresis T_E, for a tapered roller bearing is given by,

$$T_E = \frac{28\alpha}{3\pi r} \left(\frac{w\,Re}{2\pi E'} \right)^{\frac{1}{2}} (BL)\ w\ l\ n \qquad 7.11$$

where, w for the outer race is,

$$w = \frac{P_o}{l} = \frac{T}{n\, l \sin(\alpha + \beta)}$$

7.5. Friction torque due to elastic hysteresis in test bearings assuming that each roller takes an equal share of the load

Applying equation 7.11 to the test bearings results in the following formula,

Standard bearing

$$T_E = \frac{1.09}{10^5} T^{\frac{3}{2}} \text{ lbf.in}$$

Standard bearing with nine rollers

$$T_E = \frac{1.54}{10^5} T^{\frac{3}{2}} \text{ lbf.in}$$

Steep angled bearing

$$T_E = \frac{0.52}{10^5} T^{\frac{3}{2}} \text{ lbf.in}$$

It is interesting to note that the hysteresis torque for the nine roller bearing is $\sqrt{2.}$ that for the Standard eighteen roller bearing.

CHAPTER 8. EXPERIMENTAL RESULTS.

8.1. Friction Torque.

Friction torque has been plotted against $\eta_o N$ (poise x R.P.M.) for the three test bearings.

The same increments of load were used in each case, starting at 320 lbf thrust up to 4480 lbf for the Steep angled bearing, 3200 lbf for the Standard bearing and 1600 lbf for the Standard bearing with 9 rollers. The results for the Steep angled bearing are plotted on two sheets (Figures 25 and 26) for the sake of clarity. Similarly, those for the Standard bearing are shown in Figures 27 and 28 whilst the results for the 9 roller bearing are given in Figure 29. The abscissa used in each case was the product $\eta_o N$ (poise x r.p.m.), η_o and N being taken as being directly interchangeable, as suggested by the non-dimensional speed parameter U.

As no cooling system was provided on the rig, the range of $\eta_o N$ was limited by the safe running temperature of the test and rig bearings. In general this was taken as 100°C, however, in some high speed runs it was impossible to achieve steady torque measurements or to stabilise the rig at temperatures in excess of 80°C.

The viscosity of the oil was not under control but varied

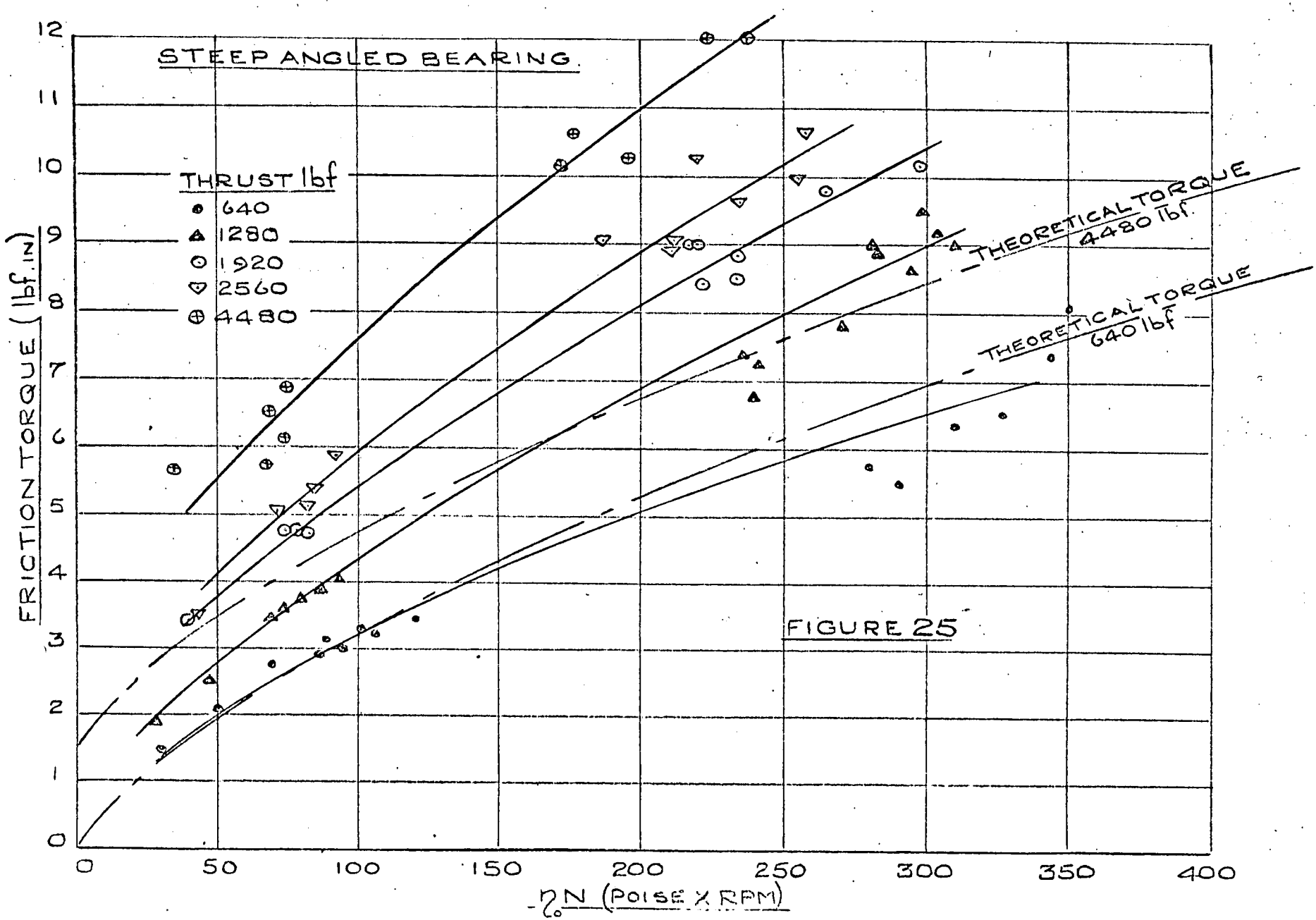
STEEP ANGLED BEARING
THRUST lbf
640
1280
1920
2560
4480
THEORETICAL TORQUE 4480 lbf
THEORETICAL TORQUE 640 lbf
FRICTION TORQUE (lbf.in)
η N (POISE X RPM)
0
1
2
3
4
5
6
7
8
9
10
11
12
0
50
100
150
200
250
300
350
400

FIGURE 25

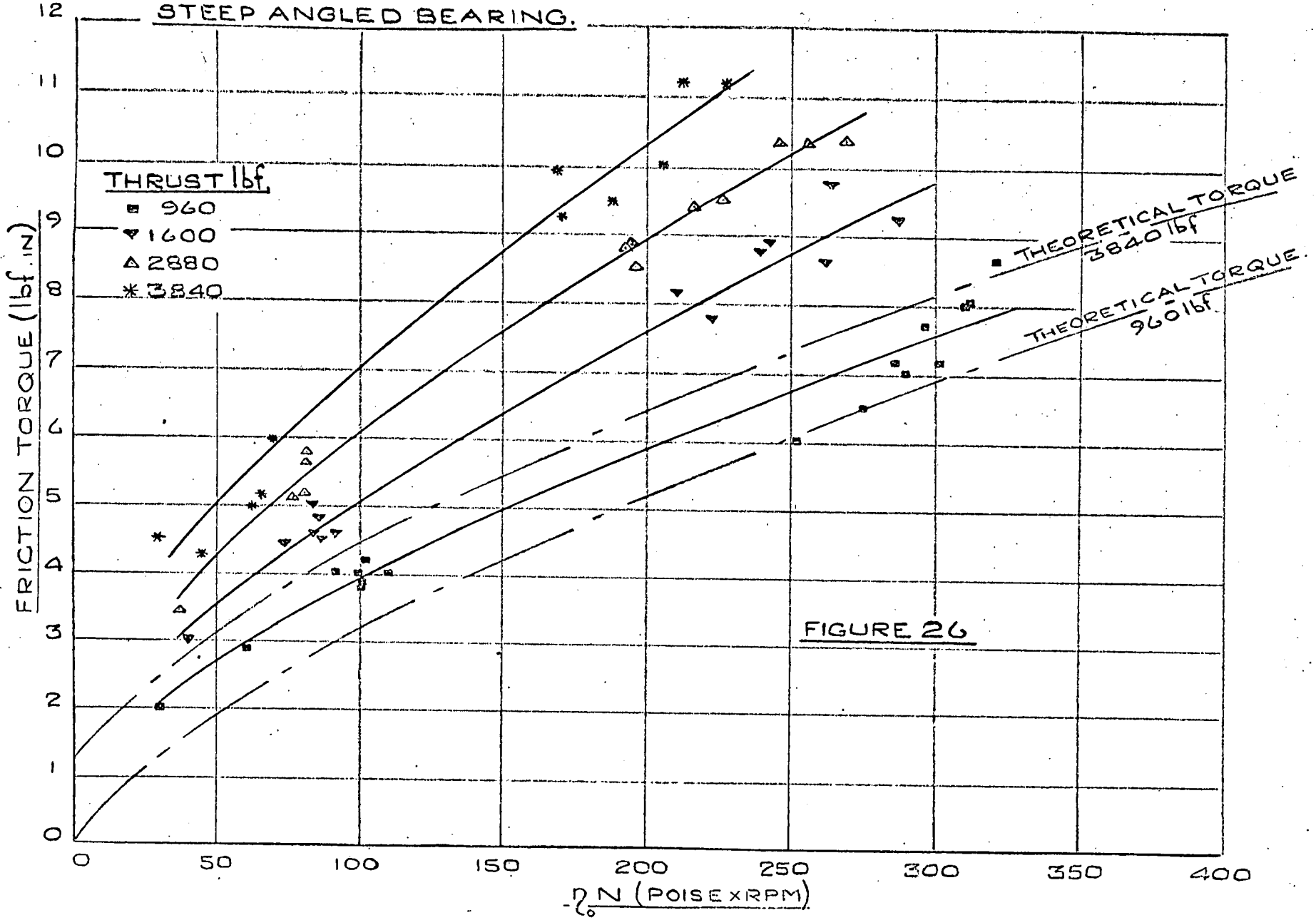
STEEP ANGLED BEARING.
THRUST lbf.
960
1600
2880
3840
THEORETICAL TORQUE 3840 lbf
THEORETICAL TORQUE 960 lbf
FRICTION TORQUE (lbf.in)
$\eta_o N$ (POISE x RPM)
0
1
2
3
4
5
6
7
8
9
10
11
12
0
50
100
150
200
250
300
350
400

FIGURE 26

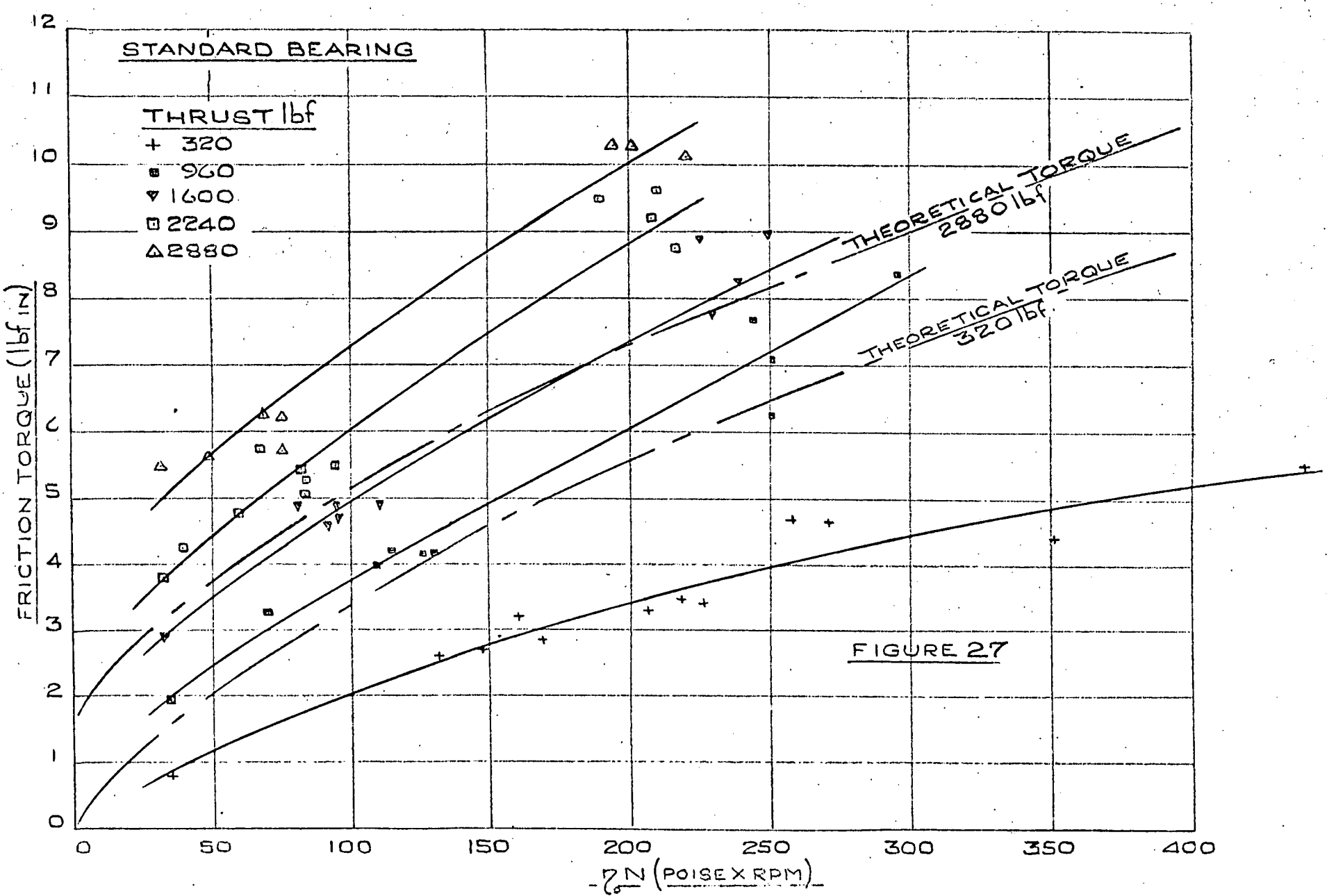
STANDARD BEARING
THRUST lbf
+ 320
960
1600
2240
2880
THEORETICAL TORQUE 2880 lbf
THEORETICAL TORQUE 320 lbf
FRICTION TORQUE (lbf in)
0
1
2
3
4
5
6
7
8
9
10
11
12
0
50
100
150
200
250
300
350
400
ηN (POISE X RPM)

FIGURE 27

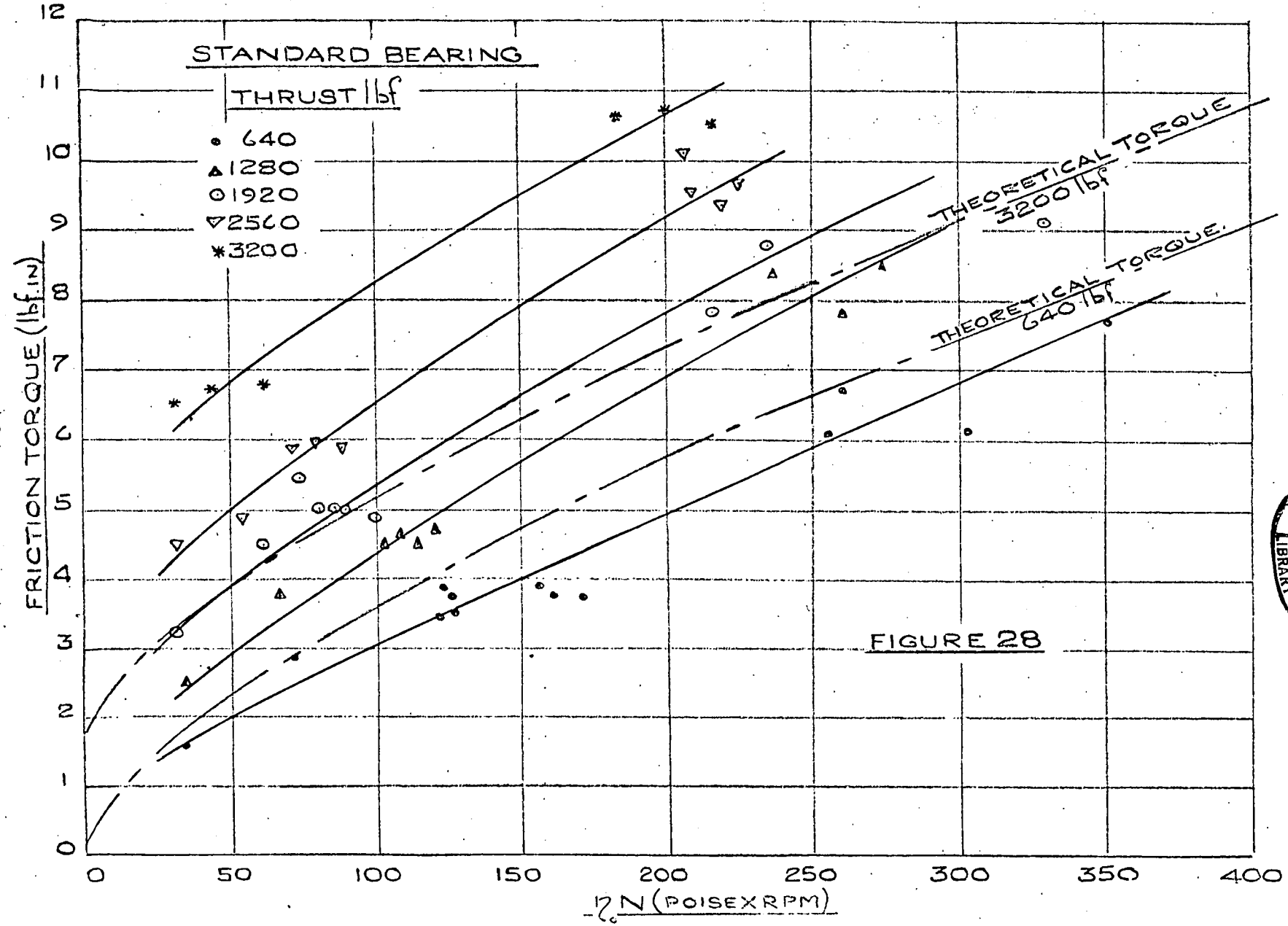

FIGURE 28

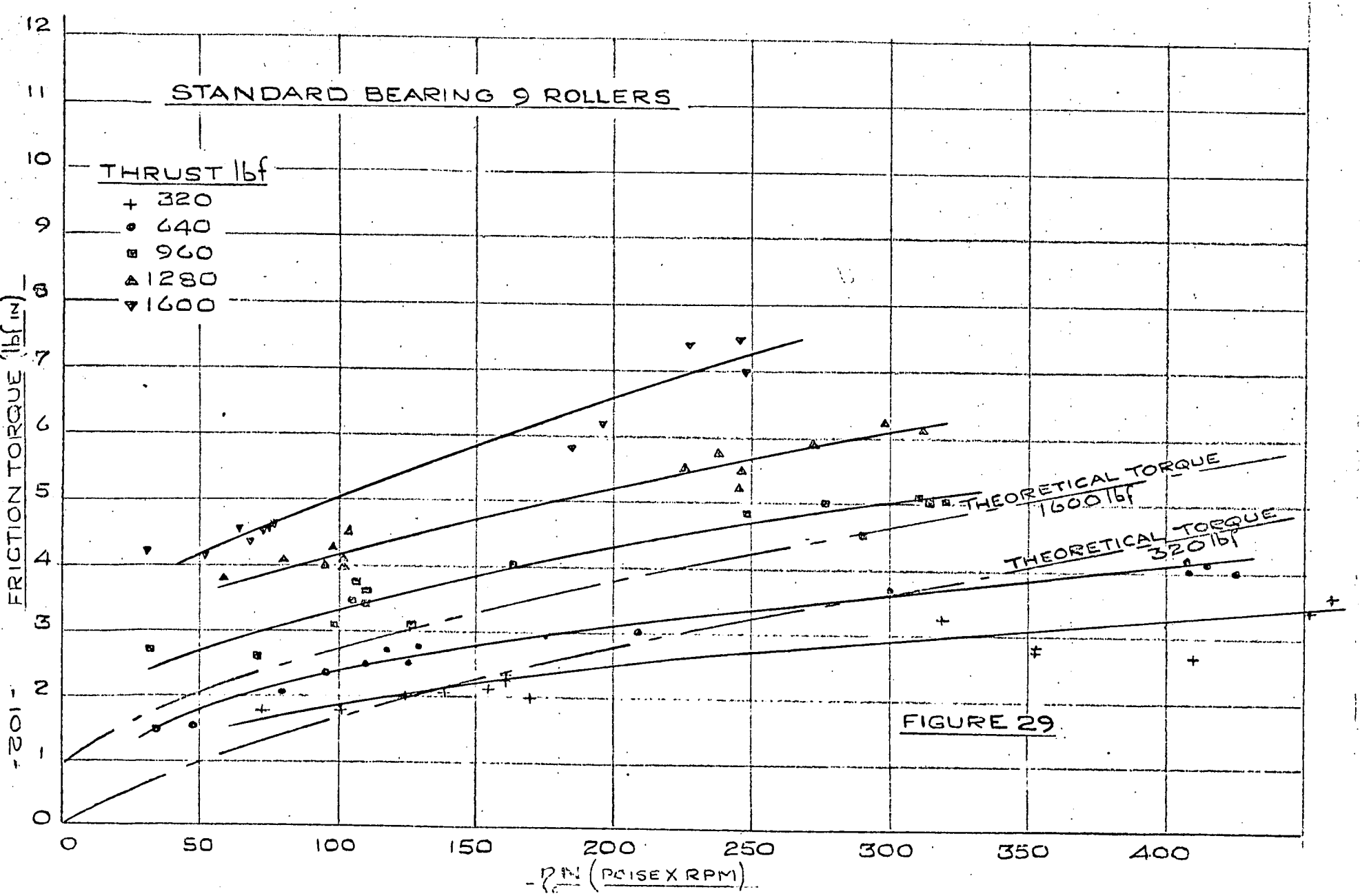
STANDARD BEARING 9 ROLLERS
THRUST lbf
320
640
960
1280
1600
THEORETICAL TORQUE 1600 lbf
THEORETICAL TORQUE 320 lbf
FRICTION TORQUE (lbf in)
RN (POISE X RPM)
0
1
2
3
4
5
6
7
8
9
10
11
12
0
50
100
150
200
250
300
350
400

FIGURE 29

with the temperature, which in turn depended upon the speed and load. The experimental points tend to cluster into two groups, one obtained using HVI 55 oil and the other using HVI 165, even though a wide range of speeds was used. The effect is most marked at higher loads. It would only have been possible to obtain points spanning the full range by using a third test oil with an intermediate viscosity

Although presenting a difficulty to the experimenter, it is of interest from the design point of view, that with a given lubricant in a machine, running under constant load, the bearing friction torque will vary little over a wide range of speeds. For example, the five points at the lower end of the torque curve for the Steep angled bearing running with 4480 lbf thrust, were obtained using HVI 55 oil over a speed range from 124 to 1474 r.p.m.

The friction forces in a tapered roller bearing are due to :

(a) Viscous rolling friction, T_V

(b) Elastic hysteresis friction, T_E

(c) Sliding friction at the race contacts.

(d) Sliding at the lip of the inner race.

(e) Gross oil churning losses.

(f) Cage friction.

In order to avoid oil churning the oil supply was maintained at a minimal value throughout the tests. The supply was cut periodically and it was noted that no change in reaction torque occurred until the temperature began to rise. Neglecting churning and cage losses, the torque due to the sum total of the hysteresis, viscous rolling and sliding friction at the outer race must be equal to that due to the hysteresis, sliding friction at the inner race and the sliding friction at the lip. The hysteresis and viscous rolling losses at both races are of the same order of magnitude, so that it is probable that the torque due to sliding at the lip is transmitted to the outer race largely by sliding.

On Figures 25 to 29, in addition to the experimental friction torque curves, the theoretical curves have also been plotted for the highest and lowest loads shown on the figure. These curves represent the sum of T_V and T_E at the outer race, assuming that each roller takes an equal share of the load.

In general the experimental and theoretical curves have a similar form and there is reasonable agreement at the lower loads. As the load increases, it is clear that sources of friction other than the two considered become significant. It may be instructive to assess the magnitude of the effect of the slip at the outer race surface on the friction torque.

We may calculate the slip required to account for the difference between the experimental curve and the sum of T_v and T_E for the Steep angled bearing running at $\eta_o N = 200$ (r.p.m. poise) under a thrust of 4480 lbf. The discrepancy between the experimental and theoretical figures is near its greatest value under these conditions and is equal to 4.5 lbf in. Further, lubrication will be fully elastohydrodynamic.

The film thickness h may be obtained directly from Figure 19.

$$h \text{ at } \eta_o N = 200 \text{ is } 10.5\ \mu\text{in}$$

Now $$W = \frac{2.135T}{10^8}$$

$$= \frac{9.55}{10^5}$$

The integral J may be taken from Figure 24 for this value of W.

From the graph $J = 1.5 \times 10^5$

for the Steep angled bearing

$$\frac{Reo}{h} = 3.2 \times 10^4$$

Hence, from equation 7.7

$$Fs = V \eta_o (4.8 \times 10^9)$$

Speed does not appear in the equation, so that it is

difficult to ascribe an appropriate value to η_o.

For example, at an inner race speed of 222 r.p.m. the value of η_o was 1.0 poise, whilst at 583 r.p.m. η_o was only 0.3 poise, $\eta_o N$ being 222 and 195 (r.p.m. poise) respectively. We will take η_o as 0.5 poise to avoid underestimating v.

$$v = \frac{Fs}{2.4 \times 10^9} \quad cm/s$$

where Fs is expressed in dynes.

We may calculate the value of the force Fs acting at the mean radius of the outer race (BL) required to account for a friction torque of 4.5 lbf in.

$$Fs = 3.6 \times 10^5 \text{ dynes/cm}$$

$$\text{Hence,} \quad v = 1.5 \times 10^{-4} \text{ cm/s}$$

The surface velocity of a roller at the outer race at 300 r.p.m. is 77 cm/s, so that the slip required to produce the friction torque is 2×10^{-6} of the surface velocity. It is clear that slip of this order could not be detected by the apparatus used.

As may be seen in Figures 25 to 29, the discrepancy between the experimental and theoretical friction torque increases with load and increases slightly with $\eta_o N$. The integral J increases sharply for values of W from 10^{-5} to 10^{-4}, so that little slip

is required at high loads to account for the friction torque.

Dowson and Higginson (19) have shown that for parallel roller bearings with unloaded lips, the conditions which favour slip are high speed, low load and small roller diameter. However, there is a good measure of agreement between the experimental and theoretical curves at low loads and high speeds where conditions are conducive to slip. Hence, although slip at the races may have occurred without detection, it seems unlikely that its presence alone could satisfactorily explain the discrepancy.

Before examining conditions at the lip, some consideration should be given to the curves for low loads. The 320 lbf thrust curves in the case of the Standard bearing and the bearing with 9 rollers drops below the theoretical curves. A load of 320 lbf was applied to the Steep angled bearing but the results were erratic and the bearing noisy, much of the noise coming from the cage. It was clear that all rollers were not fully in contact. These results were discarded. It seems reasonable that similar but less extreme conditions existed at low thrust loads with the other two bearings. A check was made of the bearing tolerances.

8.2. Examination of effects of maldistribution of roller loading.

A dimensional check was made on a sample of 18 rollers taken, at random, from several Standard Bearings and also on a further sample of 18 rollers from a single bearing. Both samples were measured using an S.I.P. gauge measuring machine with a discrimination of 1×10^{-5} in.

The rollers were placed on a specially designed conical stand, machined at an angle to match the end thrust face of a roller. In each case the diameter was measured at an arbitrarily fixed height above the stand.

An analysis of the measurements (see Appendix 2) showed that the two samples had the following means and standard deviations.

Sample from several bearings	Sample from a single bearing
$\bar{x} = 0.63294$ in.	$\bar{x} = 0.63290$ in.
$s = 6.705 \times 10^{-5}$ in.	$s = 4.413 \times 10^{-5}$ in.

The Student's t test was applied to examine the significance of the difference of the means. This indicated a significant difference between the two samples at rather less than the 5 per cent level and was considered as evidence that the rollers of a single bearing had been matched. It may also be noted that the standard deviation of the roller diameters from the single bearing

is less than that for the other sample. Had the result of the t-test been other-wise it was intended to lump the two samples together and test for normality. A Chi-squared "Goodness of Fit" test on the lumped sample resulted, as was expected, in a poor fit with a value of Chi-squared for 2 degrees of freedom, in excess of 30. The small number of rollers from a single bearing precluded a meaningful test of normality being made on this sample alone; however, the histogram was generally of the correct shape.

The stiffness of a bearing assembly may be calculated using the working approximation given by Dowson and Higginson (19). This relationship assumes elastic races with rigid backing and is said to be accurate to within 5 per cent. Care was taken in the design of the race mountings to provide rigidity. The relationship, whilst derived for cylindrical rollers, is independent of roller radius and may be applied directly to tapered rollers.

If δ is the sum total deflection of the rollers and the two races,

$$\delta = 17.5\ wk$$

where $_w$ is the load per unit length of contact (lbf). Pi and Po may be assumed to be equal and K is an elastic constant.

$$K = \frac{2}{\pi E'}$$

i.e. $K = 1.93 \times 10^{-8}$ in^2/lbf for steel

For the Standard Bearing,

$$\delta = 1.56 \frac{T}{n} 10^{-6} \text{ in} \qquad 8.1$$

where T is the thrust in lbf and n the number of rollers in engagement.

If a bearing is loaded by a gradually increasing load, the flexibility in the rig will allow the races to seat first on the three largest rollers. Continued loading will pick up the smaller rollers in turn.

Figure 30, shows the relationship between thrust and deflection for different numbers of rollers in a Standard Bearing. The radial lines from the origin are labelled from 3 to 18 rollers and have been plotted using Equation 8.1. The sizes of rollers have been measured along the abscissa and ordinates taken to points of intersection with appropriate radial lines to give a curve representing bearing stiffness. The curve marked A was plotted from the measured dimensions of the rollers of a single bearing. The curve marked B is given for comparison and assumes that the roller sizes in a bearing are normally distributed. Such an assumption, based on a small sample of 18 rollers, is statistically indefensible.

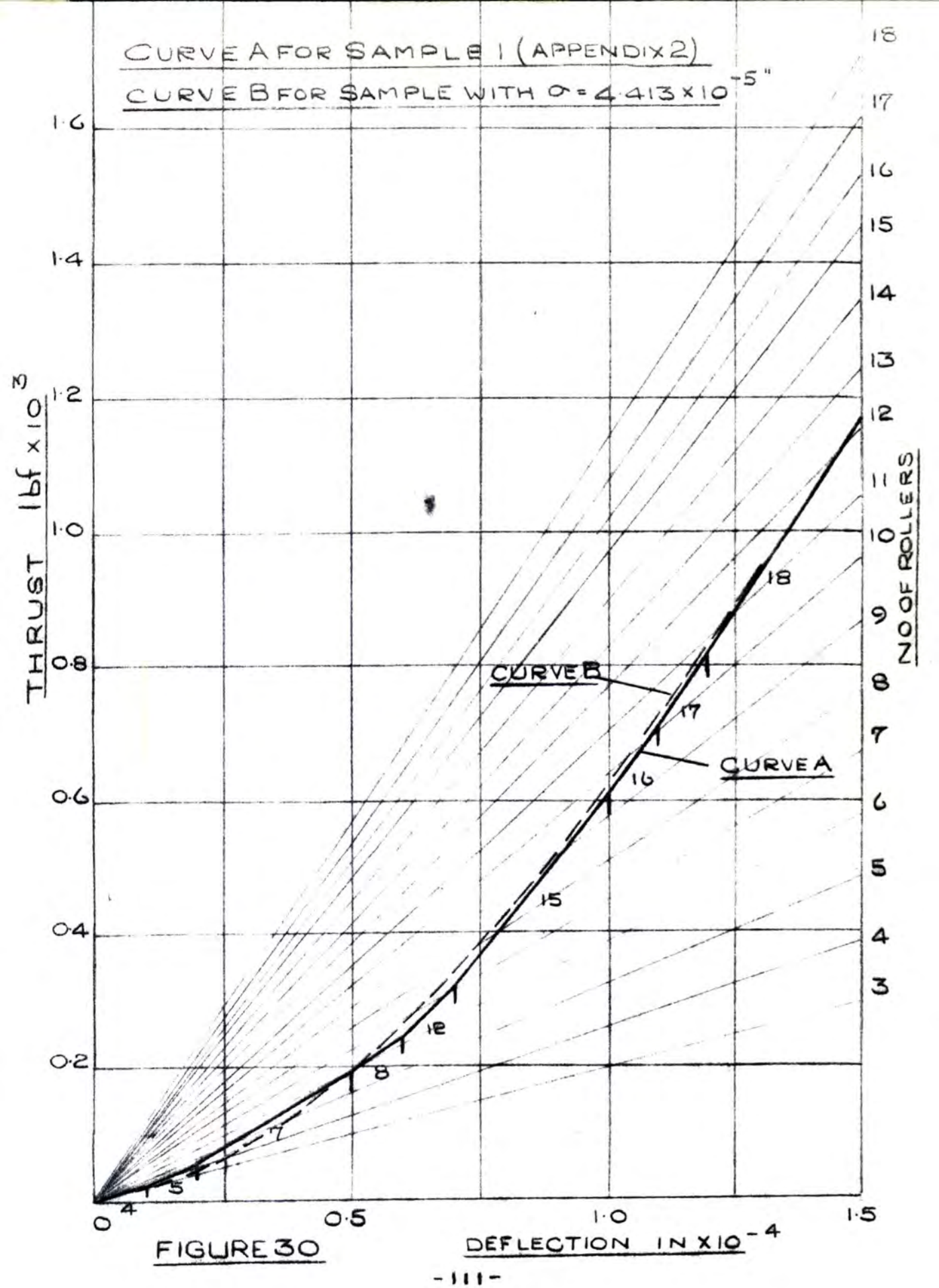
CURVE A FOR SAMPLE 1 (APPENDIX 2)
CURVE B FOR SAMPLE WITH σ = 4·413 × 10⁻⁵"
THRUST lbf × 10³
NO OF ROLLERS
DEFLECTION IN X10⁻⁴
CURVE B
CURVE A
1·6
1·4
1·2
1·0
0·8
0·6
0·4
0·2
0
0·4
0·5
1·0
1·5
18
17
16
15
14
13
12
11
10
9
8
7
6
5
4
3
5
7
8
12
15
16
17
18

FIGURE 30

However, it is of interest to note how well the two curves agree.

Clearly, from Figure 30, a considerable load may well be required to bring all the rollers into action and even then the loading will be unevenly distributed. It would seem entirely reasonable to expect the friction load curves at lower loads to fall below those predicted by the previously stated theoretical considerations, which assume equal load sharing.

In addition to the dimensional effects explored above, there are inevitably small errors in concentricity of the races with the bore and outer diameter and also in the roundness of the races. A Standard Bearing was tested on an OMT roundness measuring machine. The inner race was found to be concentric and round to within 1×10^{-4} in., whilst the outer race was concentric with the outer diameter to within 2×10^{-4} in, and round to within 5×10^{-5} in.

8.3. Effects of uneven loading of the rollers on the theoretical torque curves.

To illustrate the effect that the uneven loading of the rollers has on the friction torque curves, two revised theoretical curves for the Standard bearing have been calculated. Two loads have been chosen, the first at a low thrust of 320 lbf and the second at a comparatively heavy thrust of 3200 lbf.

We have already noted in equation 8.1, that the deflection of a roller and its races is directly proportional to the load. Hence, if the total load is divided amongst the rollers in proportion to the deflections taken from Figure 30, we may calculate the contribution to the total friction torque made by each individual roller.

For the Standard bearing the hysteresis torque for an individual roller, Ti, is given by:

$$Ti = \frac{4.61\ L^{\frac{3}{2}}}{10^5} \quad \text{lbf. in.}$$

where L is the thrust load on the roller in question in lbf. The sum total of all such contributions gives the revised hysteresis torque for the bearing.

A check was made on the value of W for the lightest loaded roller when the total load on the bearing was 3200 lbf. This roller carried an individual load of 39.6 lbf., and W was found

to be:

$$W = \frac{8.56}{10^5}$$

It was reasonable to assume, therefore, that all the rollers were operating in the elastohydrodynamic range and further, that the torque due to viscous forces would not be effected by the uneven distribution of load and would remain unchanged.

At the lower thrust load of 320 lbf. the situation is more complex. Only twelve rollers are in engagement and one of these is barely running under elastohydrodynamic conditions. So that whilst the hysteresis torque is increased due to the uneven distribution of the load, the viscous torque is reduced in proportion to the number of rollers actually under load.

On Figure 31, the experimental friction torque curves for thrust loads of 320 lbf. and 3200 lbf. have been reproduced. The curves shown in broken lines and marked A' and B' are the theoretical curves for 3200 lbf. and 320 lbf. thrust respectively, assuming a uniform distribution of load amongst the rollers. The curves shown in full line and marked A and B, are the revised theoretical curves for 3200 lbf. and 320 lbf. thrust respectively, taking into account the uneven loading of the rollers. It will be seen that in the case of the lower load, the curves almost

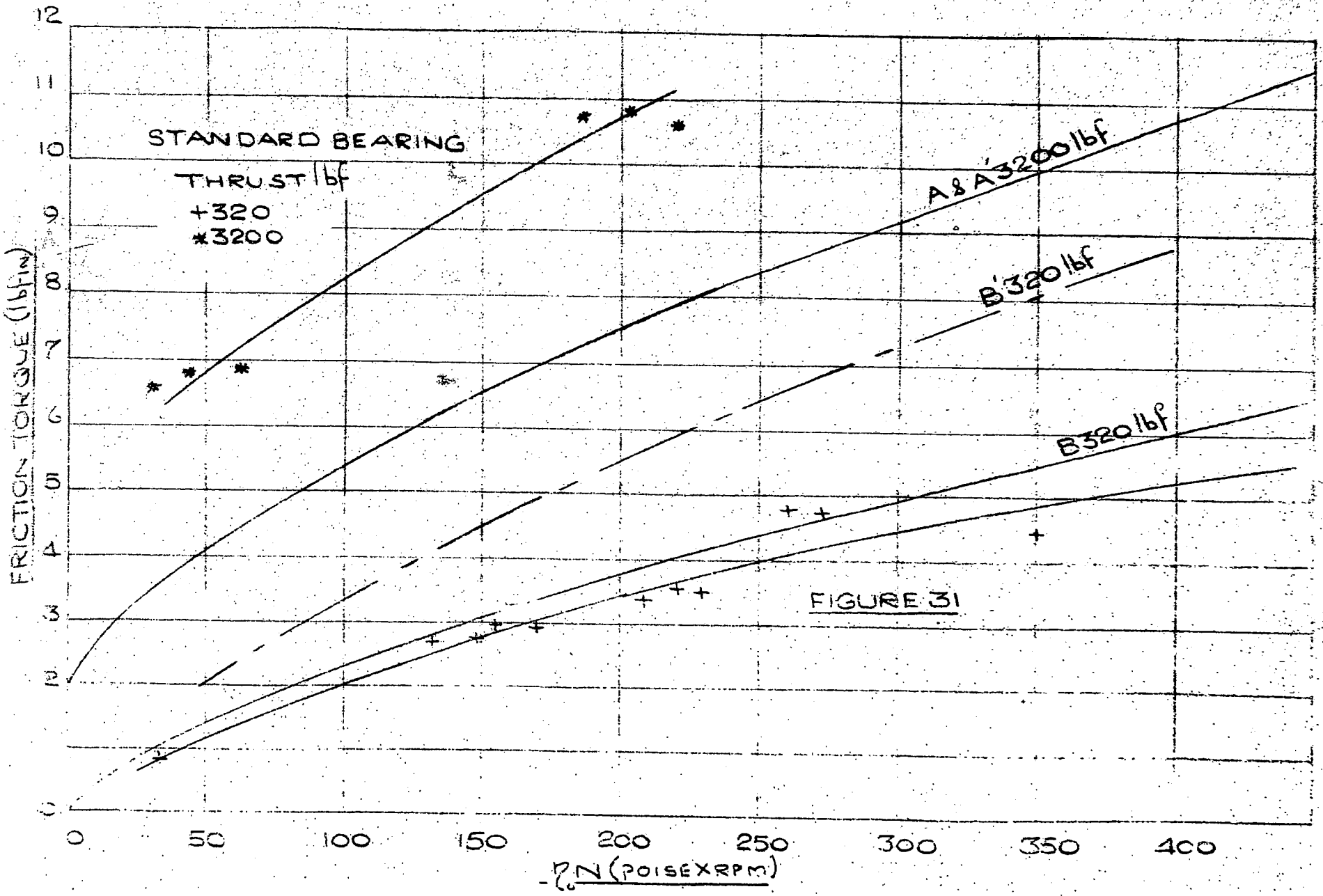
STANDARD BEARING
THRUST lbf
+320
*3200
A & A' 3200 lbf
B' 320 lbf
B 320 lbf
FRICTION TORQUE (lbf in)
μN (POISE X RPM)
0
50
100
150
200
250
300
350
400
1
2
3
4
5
6
7
8
9
10
11
12

FIGURE 31

theoretical curve is unaltered.
coincide. At the high load the ~~curves coincide.~~ It has already been stated that the lip forces are expected to increase with load, so that the remaining torque over and above that accounted for by hysteresis and viscous forces was expected to be greater at the higher loads.

8.4. Effect on bearing life of maldistribution of load.

The effect, on bearing life, of the uneven distribution of load amongst the roller is complex, and as far as is known no published work on the subject is available.

Practical bearing life formulae are based on statistical data gained from extensive tests performed by the manufacturers on complete bearings and are now standardised by the I.S.O. From the nature of their derivation it is assumed that any uneven loading, due to dimensional tolerances, is automatically taken into account.

Recent work on single cylindrical and toroidal rollers by McKelvey and Moyer (20) confirms that the 90% survival life, L_{10} based on the Weibull distribution may be represented by the familiar equation,

$$L_{10} = K p_o^{-6.66}$$

where p_o is the maximum Hertzian pressure and K is a factor determined from bearing tests.

Bearing fatigue failures often show damage on the races along circles of stress concentration, where the ends of rollers run on the races. In special applications, where cost is not of primary importance, superblending of the roller end radii may be adopted

to minimise the dog-bone effect at the contact. Crowned rollers and or races provide an alternative solution. When these features are present it is probable that the maximum pressure occurs near the centre of the track.

Because of the magnitude of the exponent in the life-stress relationship, it seems reasonable to suppose that, at the higher loads, when all rollers are in engagement, the cumulative fatigue life of a bearing with uniformly loaded rollers would exceed that of one in which the load was unevenly distributed. The frequency of stressing of a point on a race would be the same for both cases.

At low loads, where some of the rollers are free, the frequency of stressing is reduced; this further complicates matters. However, as such loads are small, these conditions are less likely to be of interest as far as bearing failure is concerned.

A detailed review of the state of knowledge on fatigue in rolling contacts is given by K.L. Johnson (26). It is clear that there is much yet to be done before the influence of the lubricant film and surface finish on fatigue is fully understood.

8.5. Frictional forces at the bearing lip.

We will now return to consider conditions at the lip of a bearing.

After completing the lubricated test runs, an attempt was made to clean the bearing so as to run dry. The test cell was filled with trichloroeythelene, drained, filled with benzene and drained. Surprisingly, after this treatment lasting over a period of a week or more, on running without any further lubrication, a full 10 mv was present across the races even with a substantial load on the bearing. The film could, of course, have broken down by increasing the load and speed. However, it is interesting to note yet again, how small a quantity of lubricant is required to maintain a film and how tenaciously it adheres to the metal. The test bearings were stripped, washed in hot detergent and dried in acetone. After this treatment, no trace of a film remained. A number of short runs were made using the Steep angled bearings in a dry state. It was observed that the torque measurements were very erratic and much greater than those for the same loads and speeds but with a lubricant supply. Further, the increase was greater as the load increased and at all speeds and loads the bearings were noisy. Conditions were too unsteady to allow more than a few readings to be taken.

If the total lubricated frictional resistance is due in the main, to hysteresis and fluid losses at the rolling surfaces, it might be expected that the dry rolling friction alone would be less than the total lubricated friction. As this is not so, the difference, and much larger contribution, must be attributed to the dry sliding friction occuring at the lip. The very fact that this contribution is so greatly reduced in the lubricated case, is strong evidence of satisfactory lubrication at the lip during most normal running conditions.

Although the results of the electrical measurements taken will be fully discussed in the following section, it is appropriate to mention here that evidence of the existance of a film at the lip was sought by measuring the electrical contact resistance using a bearing with an insulated lip as described in Section 4.6 and shown in Figure 10.

Measurements of electrical resistance were made across pairs of the three contacts in turn. If the contacts are regarded as ohmic resistances, then the total resistance will be the sum of those at the individual contacts in series. The method has limited usefulness because of the non-linear nature of the relationship between film thickness and resistance. If one of a pair of films is well established, the resistance at that film

will be very large indeed and a small resistance in series due to substantial metalic contact at the other would not effect the total by a detectable amount. However, in the low speed range, where partial contact leads to manageable resistance, the indications given by the method are of interest.

Three simultaneous equations are obtained, from which the resistance at each contact may be calculated. In all cases evidence showed the presence of a partial film at the lip of the same order of resistance as those at the two rolling contacts. A surprising result was, that the resistance at the inner race contact was higher than that at the outer race.

It was realised that a much improved method of investigating this particular aspect would be to arrange an electrical contact to an individual roller; this was not possible on the present rig without undertaking major modifications.

Conditions at the lip were not understood, nor was sufficient information available for a realistic analysis to be made. It was expected that any viscous losses would, in some manner, be proportional to ηN. As conditions were probably not elastohydrodynamic, it was also thought that they would depend inversely upon film thickness and load. In all cases the experimental curves show a discrepancy from the theoretical curves which increases strongly

with load but only slightly with increasing values of ηN. That is to say, better agreement may be obtained by including a further term which depends on the load only.

A recent paper by Iko and Orte (21) reports that a considerable amount of research is proceeding into the nature of the lubrication at the flanges of cylindrical roller bearings under axial load. It has been found that irrespective of its initial form, the flange assumes a specific form after being run-in and that this depends upon the initial shape of the roller ends. It also seems that whilst the initial surface finish of the flange has little influence of the axial load carrying capacity, the surface finish of the roller ends is of importance.

Recent tests on cylindrical roller bearings have also shown that the scale factor in bearings of different sizes is unimportant and that a hyperbolic relationship between specific pressure on the flange and sliding speed may be used as a criterion of axial load carrying capacity.

8.6. Effects of bearing geometry on friction torque.

It has already been noted that the experimental friction torque curves show the same trends as the theoretical curves within the limits already discussed.

A comparison of the curves for the Standard bearing with 18 and with 9 rollers, shows that the 9 roller bearing has the advantage of low frictional torque at high values of ηN and at low loads as predicted by the theory, and that the advantage is reduced as the load increases.

The frictional torque of the Steep angled bearing is marginally less than that for the Standard bearing for all values of ηN, the difference being more marked as the load increases. Again, this agrees with the theory. It should be remembered that the Steep angled bearing has 16 rollers whilst the Standard bearing has 18.

The viscous rolling losses are several times the magnitude of the hysteresis losses within the range of practical thrust loads. Hence, it would seem that for bearings operating at substantial values of ηN, the number of rollers should be reduced to the minimum possible, consistent with an adequate load carrying capacity and life.

The geometry of the Steep angled bearing, was of course,

chosen by the designer to be more suitable for higher thrust loads than that of the Standard bearing. The advantages to be gained by using this geometry are limited only by the speed at which the inertia forces, both normal to the race and at the lip, become excessive. We have already seen that the effect of high speed is to increase these forces but that the gyroscopic effect is minimal. Even if the friction at the lip accounted for the whole of the difference between the experimental and theoretical curves, its magnitude was still quite modest compared with the viscous rolling friction.

A design study, taking into account the effects of elastohydrodynamic lubrication would be of interest, and might reveal that an optimum configuration would require fewer and larger rollers than are common in present practice. Because of the reduced friction torque such an arrangement could possibly be suitable at higher speeds than have hitherto been considered reasonable with the Steep angled geometry.

Although it is apparently paradoxical to consider the use of larger rollers in high speed applications, it should be noted that for a bearing with a rotating inner and stationary outer race the inertia forces are not simply dependent upon roller size. From equation 3.3, it may be seen that, for a given outer diameter

of bearing, an increase in roller size implies an increase in the angled β, hence a decrease in cage velocity and, of course, the inertia forces decrease as the square of a reducation in cage velocity. Attention to the detailed design of the lip would clearly be rewarding, for although the cage speed ω_c and roller speed ω_r would decrease for a given inner race velocity, the sliding velocity at the lip would remain substantially constant.

8.7. Electrical voltage measurements.

In Figures 32, 33 and 34, the time-average voltage measurements, taken across the two races of each bearing, are plotted against the theoretical film thickness at the outer race, calculated using equation 6.6.

As explained in Chapter 4, the surface temperature of the outer race of each bearing was assessed by extrapolation of the thermocouple readings. The viscosities appropriate to these temperatures were taken from Figure 16 and the mean used in the film thickness calculations. The difference between the temperatures of the two outer races was greater in the case of the runs with the Standard bearing than with either the nine roller or the Steep angled bearing. As was discussed earlier, a heat shield was introduced after the tests on the Standard bearing and this effectively reduced the difference. In all cases the difference increased as the speed and general temperature level increased, but on the other hand the percentage difference in viscosity reduced slightly as the temperature increased. However, this effect may explain some of the scatter, particularly in the case of the Standard bearing. In all cases, the points which show the greatest deviation from the curves, particularly at the higher film thicknesses, were generally those for higher speeds and temperatures. A number of

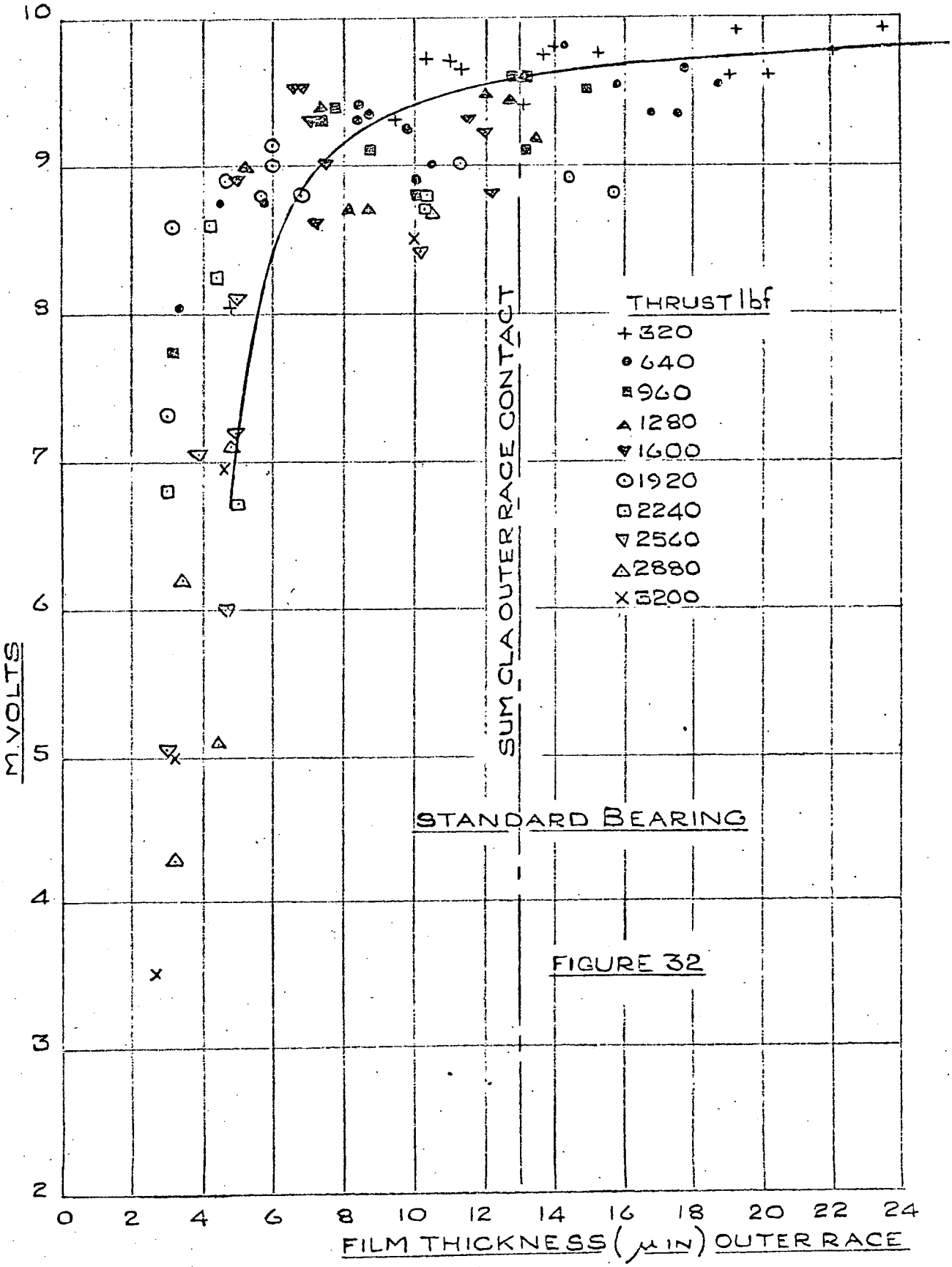
10
9
8
7
6
5
4
3
2
M.VOLTS
0
2
4
6
8
10
12
14
16
18
20
22
24
FILM THICKNESS (μ IN) OUTER RACE
SUM CLA OUTER RACE CONTACT
THRUST lbf
+ 320
• 640
▪ 960
▲ 1280
▼ 1600
⊙ 1920
⊡ 2240
▽ 2560
△ 2880
× 3200
STANDARD BEARING

FIGURE 32

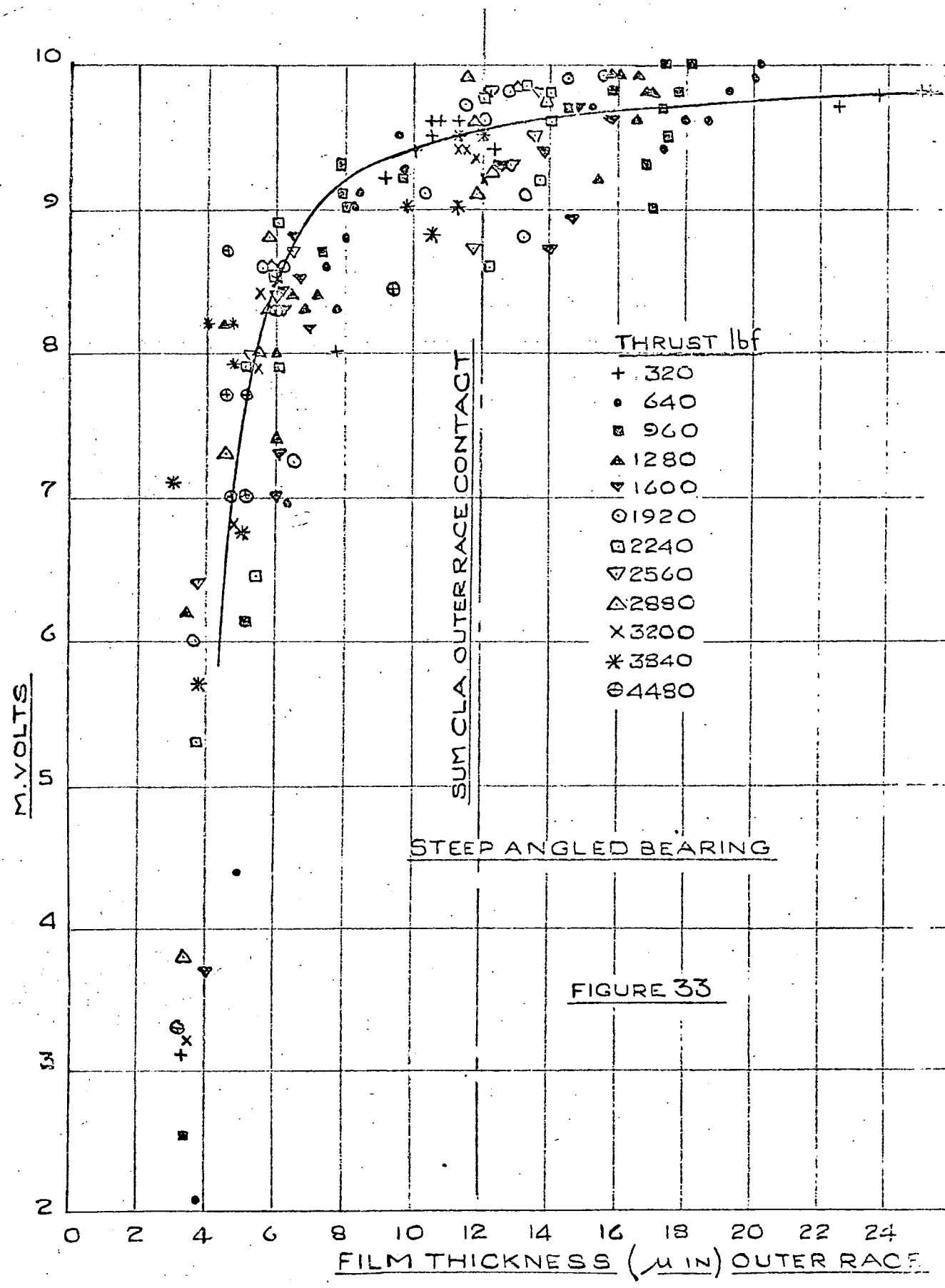
M. VOLTS
10
9
8
7
6
5
4
3
2
0
2
4
6
8
10
12
14
16
18
20
22
24
FILM THICKNESS (μ IN) OUTER RACE
SUM CLA OUTER RACE CONTACT
THRUST lbf
+ 320
• 640
▪ 960
▲ 1280
▼ 1600
⊙ 1920
⊡ 2240
▽ 2560
△ 2880
× 3200
✳ 3840
⊕ 4480
STEEP ANGLED BEARING

FIGURE 33

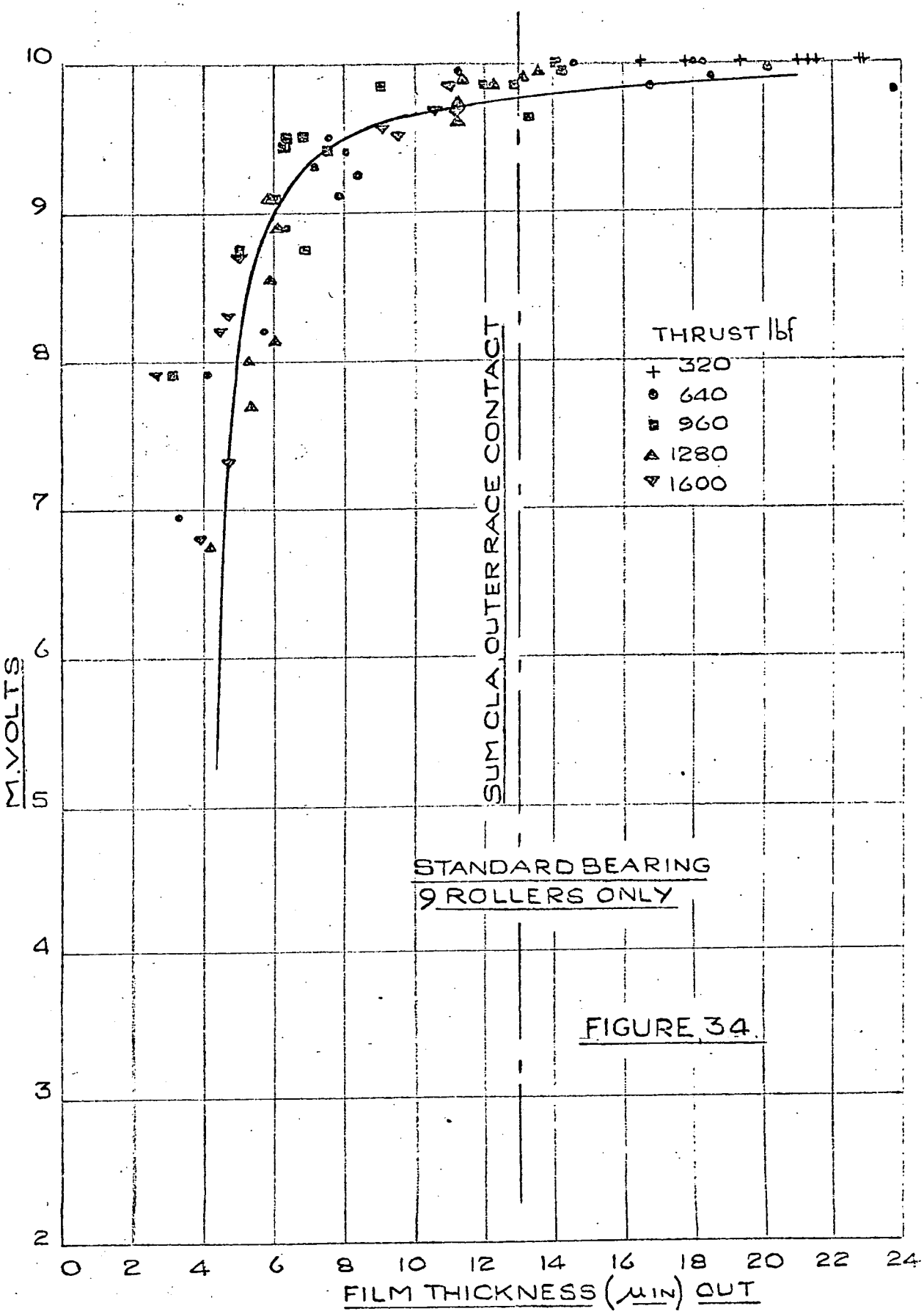
10
9
8
7
6
5
4
3
2
M.VOLTS
0 2 4 6 8 10 12 14 16 18 20 22 24
FILM THICKNESS (μIN) OUT
SUM CLA, OUTER RACE CONTACT
THRUST lbf
+ 320
● 640
■ 960
▲ 1280
▼ 1600
STANDARD BEARING
9 ROLLERS ONLY

FIGURE 34

results taken under unsteady conditions at temperatures above $80^{o}C$, have been discarded.

The points taken at each value of thrust are indicated, the symbols being consistent for the three figures. The curves have not been continued to low values of voltage because of the anomaly, already pointed out by Poon and Haines (22), of using a theoretical elastohydrodynamic film thickness in a region where a great deal of asperity contact is taking place. Further, as may be clearly seen in the Photograph in Figure 12a, the frequency of contact is so great that in equation 4.1, can no longer be considered small nor the relationship between the voltage and the no-contact time assumed to be linear.

As with the friction torque results, the experimental points at each load tend to gather around two areas. Generally, the points at the lower film thicknesses were obtained using HVI 55 oil whilst the HVI 165 oil resulted in higher film thicknesses. An attempt was made to reduce the scatter of the results by multiplying the voltages by a figure proportional to the Hertzian width, i.e. $w^{\frac{1}{2}}$; it being argued that if the film behaved as an ohmic resistance, then for a given resistivity, the voltage would depend not only upon film thickness but also upon the area of contact. Garnell and Higginson (2) applied this method of

standardisation to their results for cylindrical roller bearings under radial loads and found that it improved correlation. In the present case it was not found to be helpful and was discarded. Higginson (23) has suggested that asperities which do not come into contact before reaching the high pressure zone are unlikely to do so later. If this is so, it would seem unlikely that a simple relationship between resistance and Hertzian width could be expected.

On each figure, a line has been drawn indicating the sum of the C.L.A. surface finish values for the outer race contact. It is clear, that in each case, when the film thickness exceeds this value the voltage drop approaches 10 mv and the resistance of the film is very large indeed. Although, as already stated, the low voltage readings are unreliable as a measure of no-contact time, it is of interest to note that the curves do not appear to approach zero film thickness. That is to say, that at zero voltage, a theoretical film still seems to exist. In this respect the results are similar to those obtained by Poon and Haines (22), who defined this point as the lower threshold point of elastohydrodynamic lubrication (point B). In the present work speeds below 125 r.p.m. could not be obtained, so that the region close to zero voltage was not investigated. It may be pertinent to mention at this stage, that after a shut down of the rig it was

observed that a film still existed as indicated by the milli-volt meter. The load was always reduced to about 300 lbf thrust prior to shut down. The film persisted for long periods of time under this loading unless a further load was applied to squeeze the lubricant out of the contact.

The curves drawn in Figures 32, 33 and 34 have not been fitted in a statistical sense. If the contact film is regarded as an ohmic resistance, then the voltage vs. film thickness curves would be expected to follow a law of the form;

$$V = \frac{R_s}{R_1 + 201\ R_s}$$

where V is the ratio of the time average voltage to the applied voltage and R is the film resistance.

If v is the time average voltage across the film, then the following approximate relationship holds (Appendix 2)

$$v = \frac{R_s}{100\ R_s + 10^5} \qquad 8.2$$

A relationship between film thickness and the resistance R_s was not known. However, a series of curves were drawn with contact voltages as ordinates against a number of alternative absicca, each relating film thickness to resistance to a different scale. By moving the origin to the right, curves giving a reasonable fit with the experimental data were obtained. Figure 35 shows Equation 8.2 plotted to four alternative scales.

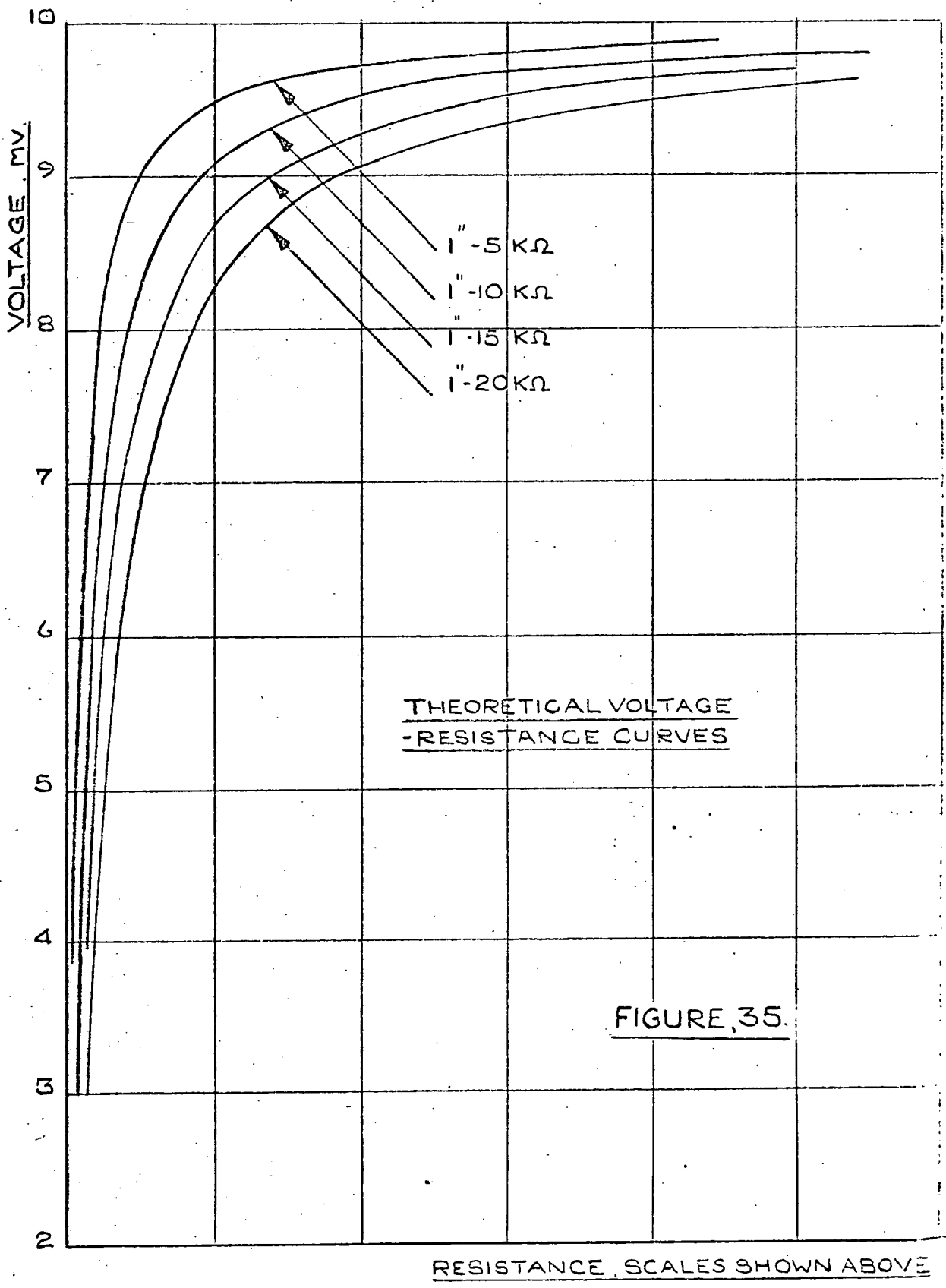
VOLTAGE, MV.
10
9
8
7
6
5
4
3
2
1"-5 KΩ
1"-10 KΩ
1"-15 KΩ
1"-20 KΩ
THEORETICAL VOLTAGE
-RESISTANCE CURVES
RESISTANCE, SCALES SHOWN ABOVE

FIGURE, 35.

The similarity between these curves and the general trend of the experimental results is striking.

It is not suggested here that a simple relationship between film thickness and resistance exists. Indeed many workers have discussed the complexities involved and it is generally agreed, that as a means of assessing film thickness, the resistance method is unsatisfactory. Crook has drawn attention to the temperature effects on the resistivity and to the effects of small particles of metallic debris (24). If we accept the figure for the resistivity of mineral oil of 10^{12} ohms/cm suggested by Lane and Hughes (25), then for the Standard bearing with a thrust load of 2240 lbf, a film thickness of 10 μin. at each race, and assuming the passage of current through contacts of Hertzian width, then the resistance expected would be approximately 70 MΩ as shown in Appendix 3, whereas the experimental value was of the order of 70 KΩ.

8.8. Oscilloscope traces.

Throughout the tests contact conditions were monitored on an oscilloscope. Typical photographs taken of the oscilloscope screen are presented in Figure 12. Although the traces yield no quantitative information it was found helpful to have a responsive visual check on the state of contact, particularly whilst changes in the variables were being made. In all the photographs a base line at zero voltage is shown and the graticule is to a vertical scale of 2mv per division. The time bases for photographs a, b and c are to a scale of 2ms/cm whilst that for photograph d is 0.2ms/cm.

Although the resistance method is basically an on-off arrangement, it may be noted from the photographs that only rarely does the measured voltage reach the extreme values of zero and 10mv. It seems that contacts and interruptions overlap before the extreme voltages are reached and the general level of the trace tends to follow the voltmeter readings. Photograph d has a faster time scale and shows an isolated contact where the voltage drops almost to zero. The transit time across the Hertzian width for the Standard bearing, with a thrust load of 2240 lbf, running at 1000 rpm is 0.1ms. If contacts follow each other with this order of frequency it is hardly surprising that the capacity of the circuit has a smoothing effect on the trace.

8.9. Electrical measurements on bearing with insulated lip.

As already described, resistance readings were taken across the inner and outer races, across the inner race and the lip and also across the outer race and the lip. The results have a limited value, but at conditions of considerable contact they do indicate the presence of a film at the lip.

The following result is typical and was obtained with a Steep angled bearing at 285 rpm with a load of 320 lbf thrust. The lubricant was HVI 55 and the outer race surface temperature 28°C.

Contact	Voltage mv
Lip to outer	6.0
Lip to inner	6.4
Inner to outer	2.3

If the contacts are regarded as simple resistances in series, the following simultaneous equations may be formed;

$$R + R_o = 6.0$$

$$R + R_i = 6.4$$

$$R_i + R_o = 2.3$$

where R , R_o and R_i are the resistances of the contacts at the lip, the outer race and the inner race respectively.

Solving gives;

$$R = 5.05 \text{ units}$$

$$R_i = 1.35 \text{ units}$$

$$R_o = 0.95 \text{ units}$$

Similar results were obtained at low loads in several cases.

The results are surprising. Theoretically conditions at the outer race are more conducive to the formation of a film than those at the inner race. The equivalent radius of curvature is greater whilst the entraining velocity is the same in both cases.

As the thrust load is low it is possible that the smaller rollers are being driven by the cage and are rolling freely on the outer race being forced radially outwards by centrifugal force. If this is so, some of the rollers could be out of contact with the inner race, hence the number of contact resistances in parallel at the inner race would be fewer than at the outer race. This may explain the higher voltage drop at the inner race.

The resistance across the lip is much greater than at either rolling contact. Hence, it appears that a satisfactory film exists at the lip even at low rotational speeds.

Concluding remarks and suggestions for further work.

From the rigid body analysis of the tapered roller bearing it was seen that the inertia effects give rise to forces on the lip of the bearing and also to a gyroscopic couple. The couple is small and even at high rotational speeds does not seriously disturb the even distribution of the loads at the race contacts. The lip forces are small but nevertheless are of the same order of magnitude as those arising from reasonable external loads.

Equations for film thickness have been derived for both the bearings used in this investigation. These were based on the theoretical work of Dowson and Higginson. Curves have been presented showing the relationship between thrust, ηN and film thickness covering the commercial range of these parameters.

Theoretical values of friction torque have been computed on the assumption that the principal sources of torque are due to viscous rolling traction and to metallic hysteresis at the contacts. The experimental torque curves agree reasonably well with the theoretical curves in the middle load range, but are lower than the theoretical curves at low load and higher at high load.

A calculation of the magnitude of slip required at the outer race to account for the maximum discrepancy between the

theoretical and experimental curves at the higher loads revealed that an unmeasurably small amount of slip could well be responsible for the difference. Slip was never detected on the rig, even at the lightest loads and highest speeds.

However, a difference between the curves at low loads could not be accounted for by slip. Measurements of the rollers from several bearings gave an indication of the range of dimensional differences in a set of rollers. Applying the relationship derived by Dowson and Higginson it was possible to calculate the deflections and hence the thrust loads required to bring a number of rollers into engagement and further, to proportion the uneven distribution of load amongst the rollers.

At low loads some of the rollers were completely free of load. So that whilst the hysteresis torque increased under these conditions, the viscous torque was reduced and the total theoretical torque curve was found to be in good agreement with the experimental curve.

At higher loads all rollers were running in the elastohydrodynamic range, so that the rolling viscous torque remained constant as for a uniform distribution of loading whilst the hysteresis torque was considerably increased. Agreement between the theoretical and the experimental curves was imppoved by taking this effect into account. The remaining difference, at the higher loads was

most probably due to friction forces at the lip.

Although the mechanism of the lubrication at the lip was not understood, nor indeed was it thoroughly investigated, it was clear from a comparison between the total friction torque obtained with a lubricated and a dry bearing, that under normal running conditions, a satisfactory film existed at the lip.

The electrical measurements indicated the presence of a fully developed oil film at the race contacts under most running conditions.

When the theoretical film thickness was in excess of the sum total of the surface roughness C.L.A. values, the resistance across the races became very high and the voltage approached its open-circuit value. At conditions which resulted in a smaller film thickness, asperity contacts were clearly detectable on the oscilloscope.

After some 200 hours running with each bearing, no damage, either electrical or mechanical, was detected on any of the rollers or races. Indeed, a check on the C.L.A. surface finish values revealed no change after running from the original values.

Suggestions for further work.

1. Further work on conditions obtaining at the lip of tapered roller bearings would be of value, and would also be relevant to parallel roller bearings subjected to axial loads.

2. There appears to be little basic reason why tapered roller bearings should not be used in applications requiring high rotational speeds. Further design and experimental work on high speed applications would be of the greatest interest and particularly relevant to turbine and compressor design.

3. The present investigation has been limited to thrust loads only. It would be useful to extend the work to combined thrust and journal loads, as most applications involve such combinations.

4. Further work on the effects of uneven distribution of load, film thickness and surface finish on bearing life would clearly be desirable.

5. Some limitations of the present rig have been revealed and modifications would be desirable before further work was undertaken. The main limitation is in the cooling of the rig bearings to allow high speed running. The design of the key drive was not entirely satisfactory but could be simply improved.

Appendix 1.

References.

1. Archard, J.F. 'Experimental studies of elastohydrodynamic lubrication'. Inst. Mech. Engrs. Symposium on elastohydrodynamic lubrication. September 1965. Paper, R2.

2. Garnell, P. and Higginson, G.R. 'The mechanics of roller bearings'. Symposium on elastohydrodynamic lubrication. September, 1965. Paper, 16.

3. Garnell, P. 'Further investigations of the mechanics of roller bearings'. Proc. Inst. Mech. Engrs. 1966-67, 181, (Pt. 1), 16. Paper 1.

4. Dowson, D. and Higginson, G.R. 'A numerical solution to the elastohydrodynamic problem'. J. Mech. Enging.Sci. 1959, 1, No. 1, 6.

5. Frenkel, M.S. 'Ball and taper roller bearings'. J.R. Ae. S. December, 1952, p. 199-236.

6. Smith, C.F. 'Some aspects of the performance of high-speed lightly loaded cylindrical roller bearings'. Proc. Inst. Mech. Engrs. 1962. V176. No. 22.

7. Archard, J.F. and Kirk, M.T. 'Lubrication at point contacts'. Proc. R. Soc. 1961. A.V. 261. P 543-544.

8. Dowson, D. and Higginson, G.R. 'Elastohydrodynamic lubrication'. 1966 Pergamon Press. Ch. 9.

9. Furey, M.J. 'Metallic contact and friction between sliding surfaces'. A.S.L.E. 1961 (No. 4)1.

10. Tallian, T.E. McCool, J.I., and Sibley, L.B. 'Partial elastohydrodynamic lubrication in rolling contact'. Proc. Inst. Mech. Engrs. Symposium on elastohydrodynamic lubrication. September, 1965. Paper, 14.

11. Tallian, T.E. McCool, J.I., Chin, Y.P. and Brady, E. 'Influence of lubrication on endurance of rolling contacts'. Progress Report, 6. U.S. Navy Contract No. N.O.w. -61-0716-c.

12. Ref. 11, Progress Report, 5.

13. Palmgren, A. 'Ball and Roller Bearing Engineering'. S.K.F. Industries. 3rd Ed. 331. p. 88.

14. Dowson, D. and Whitaker, A.V. 'The isothermal lubrication of cylinders'. A.S.L.E. preprint 64. LC-22. Washington Conference. 1964.

15. Pai, S.I. (1956), 'Viscous Flow Theory'. Van Nostrand Co., Ltd.,

16. Dowson, D,. Higginson, G.R. and Whitaker, A.V. 'Elastohydrodynamic lubrication: a survey of isothermal solutions'. J. Mech. Eng. Sci. 1962. V4, p. 121-126.

17. Bowden, F.P. and Tabor, D. 'The friction and lubrication of solids'. Pt. II, 1964. Oxford University Press.

18. Greenwood, J.A. Ph.D. Thesis, University of Cambridge. 1958.

19. Dowson, D. and Higginson, G.R. 'Theory of roller-bearing lubrication and deformation'. Inst. Mech. Eng. Symposium on elastohydrodynamic lubrication. 1963. Paper, 19.

20. McKelvey, R.E. and Moyer, C.A. 'Critical maximum compressive stress and fatigue life'. Symposium on fatigue in rolling contact. March, 1963. I.Mech.E. Paper, 1.

21. Iko, O and Orte, S. 'Axial load carrying capacity of cylindrical roller bearings'. S.K.F. The Ball Bearing Journal. No. 151, 1967.

22. Poon, S.Y. and Haines, D.J. 'Frictional behaviour of lubricated rolling-contact elements'. Proc. Inst. Mech. Engrs. 1966-67, 181 (P1) 16, Paper, 3.

23. Christensen, H. 'Nature of metallic contact in mixed lubrication'. (Discussion, Higginson, G.R.) Symposium on elastohydrodynamic lubrication. 1963, Paper, 12.

24. Crook, A.W. 'Simulated geartooth contacts'. Proc. Inst. Mech. Eng. (1957). 171, 187-214.

25. Lane, T.B. and Hughes, J.R. 'A study of the oil film formation in gears by electrical resistance measurements'. Brit. Jour. Appl. Phys. (1952) 3, 315-18.

26. Johnson, K.L. 'Correlation of theory and experiment in research on fatigue in rolling contact'. Symposium on fatigue in rolling contact. 1964. Paper 14.

Appendix 2.

Tabulated measurements made on two samples of rollers, using an S.I.P. gauge measuring machine.

The diameter x was measured in each case at a fixed height above the ground end of the roller.

$$x = 0.63290 + \frac{t}{10^5} \text{ in.}$$

In the case of Sample 1, all the rollers were taken from a single bearing. Sample 2 was made up of rollers taken at random from several bearings.

Sample 1.	Sample 2.
t in.	t in.
+ 4	+ 9
- 7	+ 2
- 8	+ 1
+ 8	+ 9
+ 2	+ 9
- 6	- 3
- 2	+ 6
+ 3	- 3
- 3	+ 1
- 3	+ 13
- 3	+ 5
- 2	+ 4
+ 2	+ 14
+ 4	- 1
- 2	+ 9
+ 7	- 3
- 2	- 3
- 1	- 2

Total number of rollers in each sample = 18.

Sample 1.

Mean value of x = 0.63290 in.

Standard deviation of sample = 4.413×10^{-5} in.

Sample 2.

Mean value of x = 0.63294 in.

Standard deviation of sample = 6.705×10^{-5} in.

---

t-test on difference of means of the two samples.

Estimated standard deviation of the population = 5.841×10^{-5} in.

Standard error of difference of means = 1.947×10^{-5} in.

Difference of means = 4.0×10^{-5} in.

$t = 2.05$

Degree of freedom = (36 - 2) = 34

The probability of this difference between the means occurring by chance is less than 5%.

Appendix 3.

Relationship between the voltage across the bearing and the total film resistance.

The circuit is shown in Figure 9. Let R_3 be the contact resistance, whilst R_2 and R_1 are the shunt and series resistances respectively. v is the voltage across the film and V is the ratio of v to the supply voltage,

$$R_1 = 200\ K\Omega$$

$$R_2 = 1\ K\Omega$$

If the total resistance of the circuit is R_t, then;

$$R_t = R_1 + \frac{R_2 R_3}{R_3 + R_2}$$

If i_2 and i_3 are the currents passing through R_2 and R_3 respectively and i_1 is the current passing through R_1.

$$v = i_2 R_2 = i_3 R_3$$

and,

$$i_1 = i_2 + i_3$$

$$i_1 = \frac{v}{R_2} + \frac{v}{R_3}$$

$$i_1 = v\,\frac{(R_3 + R_2)}{R_2 R_3}$$

also,

$$V = \frac{R_2 R_3}{R_t(R_3 + R_2)}$$

$$\frac{1}{V} = \frac{R_1}{R_2} + \frac{R_1}{R_3} + 1$$

Now as $\frac{R_1}{R_2} = 200$ and $R_1 = 200\ K\Omega$

$$V = \frac{1}{201 + \frac{200 \times 10^3}{R^3}}$$

Then, the voltage across the film is given by,

$$v = \frac{2.01}{201 + \frac{200 \times 10^3}{R^3}}$$

or more conveniently,

$$v \simeq \frac{R_s}{100R_s + 10^5}$$

Appendix 4.

Calculation of film resistance.

If the resistivity ρ for oil is 10^{12} ohms/cm. and the Hertzian width 2b is given by,

$$2b = 8\left(\frac{wRe}{2\pi E'}\right)^{\frac{1}{2}}$$

Then for a thrust of 2240 lbf, the Hertzian width for the Standard bearing is,

$$2b = \frac{7.8}{10^3} \text{ in}$$

For a contact length l of 0.790 in and 18 rollers, the total contact area A is 0.111 in^2.

Now the total resistance R is given by,

$$R = \rho \frac{l}{A}$$

$$R = 3.54 \times 10^7 \Omega$$

and for two films,

$$R = 70 \text{ M } \Omega$$